

INFORMATION TO USERS

This manuscript has been reproduced from the microfilm master. UMI films the text directly from the original or copy submitted. Thus, some thesis and dissertation copies are in typewriter face, while others may be from any type of computer printer.

The quality of this reproduction is dependent upon the quality of the copy submitted. Broken or indistinct print, colored or poor quality illustrations and photographs, print bleedthrough, substandard margins, and improper alignment can adversely affect reproduction.

In the unlikely event that the author did not send UMI a complete manuscript and there are missing pages, these will be noted. Also, if unauthorized copyright material had to be removed, a note will indicate the deletion.

Oversize materials (e.g., maps, drawings, charts) are reproduced by sectioning the original, beginning at the upper left-hand corner and continuing from left to right in equal sections with small overlaps.

ProQuest Information and Learning
300 North Zeeb Road, Ann Arbor, MI 48106-1346 USA
800-521-0600

UMI[®]

CRYSTALLIZATION BEHAVIOR AND KINETICS OF POLYOLEFINS

By
Cristian LUNGU

A Thesis Submitted to the Faculty of Graduate Studies and Research in Partial
Fulfillment of the Requirements for the Degree of Master of Engineering

Department of Chemical Engineering
McGill University
Montreal

December, 2000



**National Library
of Canada**

**Acquisitions and
Bibliographic Services**

**395 Wellington Street
Ottawa ON K1A 0N4
Canada**

**Bibliothèque nationale
du Canada**

**Acquisitions et
services bibliographiques**

**395, rue Wellington
Ottawa ON K1A 0N4
Canada**

Your file Votre référence

Our file Notre référence

The author has granted a non-exclusive licence allowing the National Library of Canada to reproduce, loan, distribute or sell copies of this thesis in microform, paper or electronic formats.

The author retains ownership of the copyright in this thesis. Neither the thesis nor substantial extracts from it may be printed or otherwise reproduced without the author's permission.

L'auteur a accordé une licence non exclusive permettant à la Bibliothèque nationale du Canada de reproduire, prêter, distribuer ou vendre des copies de cette thèse sous la forme de microfiche/film, de reproduction sur papier ou sur format électronique.

L'auteur conserve la propriété du droit d'auteur qui protège cette thèse. Ni la thèse ni des extraits substantiels de celle-ci ne doivent être imprimés ou autrement reproduits sans son autorisation.

0-612-70242-1

Canada

ABSTRACT

In order to understand crystallization behavior and to predict polymer resin properties, crystallization kinetics and morphology studies are performed. Thermal analysis of sixteen polyethylene and polypropylene resins was carried out, using Differential Scanning Calorimetry (DSC) to study the crystallization kinetics and mechanism of crystallization. Attention is given to different polyethylene grades, particularly linear low-density polyethylenes (LLDPE) manufactured with Ziegler-Natta and metallocene catalysts. The polymers are obtained with different monomers (1-butene, 1-hexene or 1-octene). Some polymers are based on gas phase polymerization, while others are based on solution polymerization. The isothermal crystallization data were treated to account for transients and to compensate for instrument errors. The data were fitted to the Avrami and Tobin equations, and the corresponding kinetic parameters are reported. The non-isothermal data were fitted to the Ziabicki equation, in order to determine the relevant parameters. Subsequently, the non-isothermal data were compared to the predictions of the Nakamura equation, with good agreement. An effort was made to compare the isothermal and non-isothermal crystallization behavior of the various resins to evaluate the effect of co-monomer and catalyst type. The results indicate significant differences among the resins, and reveal the utility of the DSC as a tool for distinguishing the characteristics of the various resins.

RÉSUMÉ

Afin de comprendre le comportement des polymères face à la cristallisation et de prévoir leurs propriétés, nous avons effectué des études de cinétique et de morphologie de la cristallisation. Nous avons fait l'analyse thermique de seize polyéthylènes et polypropylènes en utilisant la calorimétrie à balayage différentiel (CBD) afin d'étudier la cinétique et le mécanisme de la cristallisation. Nous avons étudié différentes catégories de polyéthylènes, notamment les polyéthylènes basse densité linéaire produites en utilisant les catalyseurs Ziegler-Natta et métallocène. Les polymères sont obtenus en employant différents monomères (1-butène, 1-hexène ou 1-octène). Certains polymères sont basés sur la polymérisation en phase gazeuse, alors que d'autres sont basés sur la polymérisation en solution. Les données de la cristallisation isotherme ont été traitées de façon à tenir compte des effets transitoires et à compenser les erreurs dues à l'instrument. Nous les avons introduites dans les équations d'Avrami et de Tobin et présentons les paramètres cinétiques correspondants. Les données non-isothermes ont été introduites dans l'équation de Ziabicki afin de déterminer les paramètres pertinents. Par la suite, nous avons comparé les données non-isothermes avec les estimations de l'équation de Nakamura, en obtenant une bonne concordance. Nous avons comparé le comportement de diverses résines face à la cristallisation isotherme et non-isotherme afin d'évaluer l'incidence du type de co-monomère et de catalyseur. Les résultats indiquent qu'il existe des différences significatives entre les résines et démontrent l'utilité de la CBD comme outil servant à distinguer les caractéristiques de diverses résines.

ACKNOWLEDGEMENTS

Part of my gratitude and sincere appreciation goes to my research supervisor Prof. Dr M. R. Kamal without whom this project would not have been possible. He made me believe and trust my resources, kindly directed, and guided me, stimulating my interest in the field of polymer science and engineering.

I would like to express my appreciation to Dr M. Samara and Dr H. Tao for their permanent presence, advice and comments, when needed, and to all my colleagues for their help in various aspects.

I am indebted to Nova Chemicals Co. and Montell as the main suppliers of the materials used in this present study.

Also, I extend my gratefulness to the financial support received from the Ministère de l'Éducation du Québec, and McGill University, Department of Chemical Engineering in the form of teaching and research assistantships.

Finally, I would like to express my love to my wife, Michaela, for her patience, support and constant encouragement.

TABLE OF CONTENTS

ABSTRACT	ii
ACKNOWLEDGEMENT	iv
LIST OF FIGURES	viii
LIST OF TABLES	xi
TABLE OF CONTENTS	v
1 INTRODUCTION	1
2 GENERAL BACKGROUND	4
2.1. POLYOLEFINS TECHNOLOGY.....	4
2.1.1. <i>Titanium, Chromium, and Metallocene Based Catalysts</i>	4
2.1.2. <i>Technology Features</i>	7
2.2. POLYOLEFINS STRUCTURES AND PROPERTIES.....	7
2.3. POLYMER MORPHOLOGY. THERMODYNAMICS AND MOLECULAR KINETICS.....	9
2.3.1. <i>Polymeric Crystals</i>	11
2.3.2. <i>Structure and Order in Polymeric Materials</i>	12
2.3.3. <i>The Crystallization Process</i>	14
2.3.4. <i>Thermodynamics of Crystallization</i>	15
2.3.4.1. <i>Nucleation</i>	16
2.3.4.2. <i>Crystal Growth</i>	19
2.3.5. <i>Molecular Weight Influence and Melting Point</i>	20
2.4. CRYSTALLIZATION KINETICS.....	21
2.4.1. <i>Avrami Isothermal Model</i>	22
2.4.2. <i>Tobin Isothermal Model</i>	23
2.4.3. <i>Ozawa Isothermal Model</i>	24
2.4.4. <i>Malkin Isothermal Model</i>	24
2.4.5. <i>Nakamura Non-Isothermal Model</i>	25
2.4.6. <i>Ziabicki (Non)-Isothermal Model</i>	27
2.4.7. <i>Formulation of the Cooling Function, $K(T)$</i>	28
3 SCOPE AND OBJECTIVES	29

4 EXPERIMENTAL	31
4.1. RESINS PROPERTIES	31
4.2. PYRIS-1 DSC APPARATUS	32
4.2.1. <i>Baseline, Temperature, Heat Flow and Furnace Calibration</i>	34
4.2.2. <i>Sample Preparation and Instrument Set-Up</i>	35
4.2.3. <i>Method Editor Page or Experiment Design</i>	36
4.2.4. <i>Experimental Run</i>	36
4.2.5. <i>Data Analysis Using SigmaPlot Program</i>	36
4.3. EXPERIMENTAL PROCEDURE	37
4.3.1. <i>Non-Isothermal Experiments</i>	37
4.3.2. <i>Isothermal Experiments</i>	39
5 DATA ANALYSIS	41
5.1. ISOTHERMAL CRYSTALLIZATION EXPERIMENTS	41
5.1.1. <i>Transient Response</i>	44
5.1.2. <i>Induction Time</i>	45
5.1.3. <i>Overall Crystallization Rate</i>	47
5.2 NON-ISOTHERMAL CRYSTALLIZATION EXPERIMENTS	48
6 RESULTS AND DISCUSSION	51
6.1. ISOTHERMAL CRYSTALLIZATION KINETICS	51
6.1.1. <i>Heating and Cooling Experiments</i>	52
6.1.2. <i>Isothermal Kinetic Parameters</i>	53
6.2. NON-ISOTHERMAL CRYSTALLIZATION	58
6.3. INTRA-GROUP ISOTHERMAL AND NON-ISOTHERMAL COMPARISON	62
6.4. INTER-GROUP ISOTHERMAL AND NON-ISOTHERMAL COMPARISON	68
6.5. MELTING BEHAVIOR AND EQUILIBRIUM MELTING TEMPERATURE	70
6.6. SUMMARY	73

7 SUMMARY, CONCLUSIONS AND FURTHER WORK	78
7.1. SUMMARY AND CONCLUSIONS.....	78
7.2. RECOMMENDATIONS FOR FURTHER WORK.....	80
8 REFERENCES	81
APPENDIX 1 Resins Physical Properties	87
APPENDIX 2 Compression Molding Experimental Procedure	89
APPENDIX 3 Plots of Isothermal DSC Exotherms	92
APPENDIX 4 Heat of Fusion, Heat of Crystallization and Peak Melting Temperature Values at Different Cooling Rates (Non-Isothermal Experiments)	97
APPENDIX 5 Heat of Fusion and Peak Melting Temperature Values at Different Cooling Rates (Isothermal Experiments)	102
APPENDIX 6 Experimental Values of the Avrami and Tobin Parameters (n, K), Heat of Crystallization and Induction Time (Linear and Non-Linear Regression). NLR – r^2 – Parameter Values for Selected Isothermal Temperatures	107
APPENDIX 7 Non Isothermal Simulation. Kinetic Data	113
APPENDIX 8 Plots of Relative Crystallinity as a Function of Temperature. Non-Isothermal Simulation for Selected Resins	115
APPENDIX 9 Plots of Normalized Heat Flow (Q^*) and Heat of Crystallization (H_c) versus Time (Non-Isothermal. Intra-Group Study)	120
APPENDIX 10 Plots of $\text{Log}\{-\text{Ln}(1-X)\}$ vs. $\text{Log } T$ for Selected Resins E, G, H, and F. First and Second Run at similar Isothermal Temperature	123

LIST OF FIGURES

<i>Figure 2.1:</i>	Generic Structure of a Metallocene Catalyst (M: transition metal of groups 4b, 5b or 6b; R: hydrocarbyl, alkylidene, halogen radicals; S: hydrogen, hydrocarbyl radicals; B: alkylene, alkyl radicals, heteroatom groups).....	6
<i>Figure 2.2:</i>	The Crystal Lamellae.....	10
<i>Figure 2.3:</i>	Typical Conformation of a Spherulite.....	10
<i>Figure 2.4:</i>	Cooling of a Liquid Polymer below its Melting Temperature. (Crystallizing particles –spherulites- appear at random in the liquid and grow with time. Impinging –overlapping- particles and the gradual exclusion of liquid volume for the appearance of new nuclei can be noticed. The release rate of latent heat of crystallization must be less than the rate of heat removal from the polymer for the growth to continue.)... 14	14
<i>Figure 2.5:</i>	Number of Spherulites in Isotactic Polypropylene as a function of time and Different Crystallization Temperatures.....	17
<i>Figure 2.6:</i>	Sketch of two possible Growth Morphologies leading to Spherical Symmetry.....	18
<i>Figure 2.7:</i>	(a) Dependence of Spherulitic Growth Rate on Temperature for Different Molecular Weight Fractions of a Polymer. (b) Effect of Nucleation density on Overall Crystallization Rate.....	20
<i>Figure 4.1:</i>	Schematic Representation of a DSC.....	33
<i>Figure 4.2:</i>	Non-Isothermal Thermogram at Selected Cooling Rate 20°C/min.).....	38
<i>Figure 4.3:</i>	Non-Isothermal Experiments for LLDPE B (BUT/Gas/ZN). (Legend: (i) cooling rate (°C/min.), (ii) heat of crystallization H_c (J/g), and (iii) the onset crystallization temperature (°C)).....	38
<i>Figure 4.4:</i>	Isothermal Thermogram at 88°C for Resin E (Cooling Rate: 100°C/min.).....	39
<i>Figure 4.5:</i>	Typical Crystallization Peak.....	40
<i>Figure 5.1:</i>	Plot of $\log\{-\ln[1-x(t)]\}$ vs. $\log t$ for Isothermal Crystallization at selected Temperatures (°C) for LLDPE A (HEX/Gas/Z-N).....	43

<i>Figure 5.2:</i>	Normalized Heat Flow versus Time during Isothermal Crystallization for LLDPE A (HEX/Gas/Z-N) at selected Temperatures ($^{\circ}\text{C}$). (Constant significance: (i) isothermal temperature ($^{\circ}\text{C}$), (ii) heat of crystallization H_c , (J/g), and (iii) induction time (sec.)).....	43
<i>Figure 5.3:</i>	Transient Effect in a DSC Isotherm.....	44
<i>Figure 5.4:</i>	Typical Melting Plot used to determine the Heat of Fusion using a DSC.	45
<i>Figure 5.5:</i>	Schematic Diagram of the Crystallization Process as a function of time..	46
<i>Figure 5.6:</i>	Normalized Heat Flow (Endo Up) vs. Temperature during Non-Isothermal Crystallization for LLDPE A (HEX/Gas/Z-N) at Different Cooling.....	48
<i>Figure 6.1:</i>	DSC Endotherms for Linear/Low-Density Polyethylene.....	52
<i>Figure 6.2:</i>	DSC Isotherms for Selected Resins at Various Isothermal Crystallization Temperatures ($^{\circ}\text{C}$).....	57
<i>Figure 6.3:</i>	Non-Isothermal DSC Thermograms for LLDPE A, C, D, and E at Various Cooling Rates (Legend: (i) Cooling Rate ($^{\circ}\text{C}/\text{min}$), (ii) Heat of Crystallization (J/g), (iii) On-Set Temperature of Crystallization ($^{\circ}\text{C}$))...	60
<i>Figure 6.4:</i>	Non-Isothermal DSC Thermograms for LLDPE B and H and LDPE F and K at Various Cooling Rates (Legend: (i) Cooling Rate ($^{\circ}\text{C}/\text{min}$), (ii) Heat of Crystallization (J/g), (iii) On-Set Temperature of Crystallization ($^{\circ}\text{C}$)).	61
<i>Figure 6.5:</i>	Non-Isothermal DSC Isotherms for LLDPE G, I, J and L at Various Cooling Rates (Legend: (i) Cooling Rate ($^{\circ}\text{C}/\text{min}$), (ii) Heat of Crystallization (J/g), (iii) On-Set Temperature of Crystallization ($^{\circ}\text{C}$))...	61
<i>Figure 6.6:</i>	Non-Isothermal DSC Thermograms for LLDPE M, HDPE 2908, PP-1, and PP-2 at Various Cooling Rates (Legend: (i) Cooling Rate ($^{\circ}\text{C}/\text{min}$), (ii) Heat of Crystallization (J/g), (iii) On-Set Temperature of Crystallization ($^{\circ}\text{C}$)).....	62
<i>Figure 6.7:</i>	Intra-Group Isothermal Study for LLDPE B and H. Left Plots-Rate and Heat of Crystallization vs. Time at the maximum rate (MR) and similar isothermal temperatures. Right Plots-Rate and Heat of Crystallization at the maximum rate and similar supercooling above and below the maximum rate.....	64
<i>Figure 6.8:</i>	Normalized Heat Flow vs. Time for LLDPE B and H. (Intra-Group Non-Isothermal).....	64

Figure 6.9: Intra-Group Isothermal Study for LLDPE A, C, and M. Left Plots-Rate and Heat of Crystallization vs. Time at the maximum rate (MR) and similar isothermal temperatures. Right plots-Rate and Heat of Crystallization at the maximum rate and similar supercooling above and below the maximum rate.....65

Figure 6.10: Intra-Group Isothermal Study for LLDPE D and E. Left plots-Rate and Heat of Crystallization vs. Time at the maximum rate (MR) and similar isothermal temperatures. Right plots-Rate and Heat of Crystallization at the maximum rate and similar supercooling above and below the maximum rate.....66

Figure 6.11: Intra-Group Isothermal Study for LLDPE G and L. Left Plots-Rate and Heat of Crystallization vs. Time at the maximum rate (MR) and similar isothermal temperatures. Right Plots-Rate and Heat of Crystallization at the maximum rate and similar supercooling.....67

Figure 6.12: Intra-Group Isothermal Study for LLDPE I and J. Left plots-Rate and Heat of Crystallization vs. Time at the maximum rate (MR) and similar isothermal temperatures. Right plots-Rate and Heat of Crystallization at the maximum rate and similar supercooling above and below the maximum rate.....67

Figure 6.13: Inter-Group Isothermal and Non-Isothermal Analysis. Rate and Heat of Crystallization vs. Time (LLDPE B, A, and L).....69

Figure 6.14: Inter-Group Isothermal and Non-Isothermal Analysis. Rate and Heat of Crystallization vs. Time (LLDPE E and J).....69

Figure 6.15: Equilibrium Melting Temperatures as a function of Crystallization Temperature.....71

LIST OF TABLES

<i>Table 1.1:</i>	Classification and Density of Polyolefins.....	2
<i>Table 2.1:</i>	General Catalyst Characteristics.....	5
<i>Table 2.2:</i>	Theoretical Values of n and the Isothermal Rate Constant k for Different Morphologies and Nucleation Mechanisms.....	28
<i>Table 4.1:</i>	Resins Physical Properties.....	32
<i>Table 4.2:</i>	Thermal Conductivity of Some Gaseous Substances.....	33
<i>Table 5.1</i>	Different Values of Avrami Exponent and their Interpretation.....	48
<i>Table 6.1</i>	Heat of Fusion and Peak Melting Temperature of Compression Molded Samples.(First Melting; Heating Rate: 10°C/min.).....	53
<i>Table 6.2:</i>	Physical Properties for LLDPE B and H (Butene).....	63
<i>Table 6.3:</i>	Physical Properties of LLDPE A,C,D,E, and M (Hexene).....	65
<i>Table 6.4:</i>	Physical Properties of LLDPE G, I, J, and L (Octene).....	68
<i>Table 6.5:</i>	Physical Properties of LLDPE B, A, and L.....	70
<i>Table 6.6:</i>	Physical Properties of LLDPE E and J.....	70
<i>Table 6.7:</i>	Thermodynamic Equilibrium Melting Points For Polyethylenes and Polypropylenes Samples.....	72

CHAPTER 1

INTRODUCTION

Polymer crystallization can be regarded as a self-organization process in which a hierarchy of various patterns on various length scales are formed, ranging from crystallite stems on the nanometer scale up to spherulites of the size of some hundreds of microns.¹ Thermodynamic laws are obeyed when crystallization occurs, like in any other transformation, but whether crystallization takes place, and at what speed, is dictated by the kinetics of the process. Presently, studies are oriented towards the inherent dynamic character of polymer crystallization, since real processing conditions can be simulated in this case. The aim is to improve our general understanding of crystallization behavior of polymers.

The global thermoplastic market has grown consistently, accounting at present for approximately 10% of the world chemical industry.² More than half of the global production, almost two-thirds, consists of polyolefins. Generally speaking, polyolefin technology may be divided into low- pressure or high-pressure processes. Resin properties, Molecular Weight (MW), Molecular Weight distributions (MWD), density and others are dictated by the type of catalyst and reactor conditions employed. The manufacturing process is based on free radical polymerization at 200-300°C, and pressures between 0.1 and 0.3 GN/m², in tubular or stirred autoclave type reactors.² Commercially, end products are used for film and packaging, industrial liners, heavy-duty bags, lamination films, and cable and wire.

The present study deals with the crystallization kinetics of polyethylene resins obtained by different manufacturing processes.

Polyethylene has the simplest structural unit (i.e. the ethylene unit). In this particular case, the structural unit is also the repeating unit.



The second type of polymer used in this study is polypropylene. A methyl group replaces one of the hydrogen atoms (α - substitution).



The n -value has a significant importance, if one is concerned about the physical state and properties of the end material.³

There are a variety of industrial processes for polyethylene production^{2,4-6} offering a wide range of properties and end uses.^{4,7,8} The products are divided according to their density, as shown in Table 1.1.

Table 1.1. Classification and Density of Polyolefins

Polyethylene Type	Macromolecular Classification	Density Range(g/cm ³)
LDPE	Homopolymer	0.910-0.925
MDPE	Homopolymer	0.926-0.940
LLDPE	Copolymer	0.910-0.940
VLDPE	Copolymer	0.890-0.915
HDPE	Copolymer	0.941-0.959
HDPE	Homopolymer	0.960 and higher
HMWPE	Homopolymer	0.947-0.955
UHMWPE	Homopolymer	0.940
Polypropylene	Homopolymer	0.904-0.906

LLDPE (Linear Low-Density Polyethylene) differs from the high-density (HDPE) and low-density polyethylene (LDPE) by the type of chain branching and the type of comonomer used in polymerization.

The present text is divided into seven chapters. The second chapter provides the general background, and consists of a general literature review, that leads to the phenomenon of crystallization and its kinetics. The methods that represent the basis for thermal analysis are briefly presented in Chapter 3. Chapter 4 is dedicated to the experimental procedure and presents a detailed methodology for one who intends to follow a similar investigation. Chapter 5 contains the results of the crystallization kinetics study, and

comparison between the experimental data and kinetic models is also given. The results and the discussion are presented in Chapter 6. Suggestions for further work and general conclusions are given in Chapter 7. A list of references for further consultation is provided. The detailed data are tabulated for all 16 resins in the Appendices.

CHAPTER 2

GENERAL BACKGROUND

This chapter provides general background relating to the polymerization techniques usually employed in polyolefin manufacture in addition to a brief discussion of their molecular structure and crystallization behavior.

2.1. Polyolefins Technology

In 1933, Fawcett and Gibson⁹ at Imperial Chemical Industries (ICI) introduced a high-pressure process for polyethylene manufacture. Using oxygen as an initiator, the end product was a branched polyethylene, low-density polyethylene, LDPE (or high-pressure polyethylene, HPPE). In the early 1950s, Ziegler observed the positive influence of organometallic compounds on polyethylene manufacture, with a low-pressure route, and thus, the high-density polyethylene (HDPE) made its appearance. Later, Natta using Ziegler technology improved the process and applied it to the production of polypropylene. This led to the development and extension of Ziegler-Natta catalysts for polyolefin production.

2.1.1. Titanium, Chromium and Metallocene Based Catalysts.

The properties of the most commonly used catalysts are listed in Table 2.1.⁹ The group developed by Phillips Petroleum Chemicals are used to produce more than 60% of the market production of LDPE.

Table 2.1 General Catalyst Characteristics

Catalyst Type (common name)	Transition Metal	Features
Ziegler	Titanium (Ti)	-Relatively narrow molecular weight distribution -Hydrogen is used to control molecular weight -Aluminum alkyl co-catalysts required
Phillips	Chromium (Cr)	-Relatively broad molecular weight distribution -Hydrogen is not used for molecular weight control -Do not give isotactic polymers

Bohm¹⁰, Keii *et al.*¹¹, and Ivanchev *et al.*¹² using different types of Ziegler-Natta catalysts explained the efficiency of these reactions. For a TiCl₄ and MgO based catalyst, the active sites of titanium were increased from about 1% in the first generation catalyst, to 7-39% in a magnesium containing system. The polyethylene thus obtained has a much narrower molecular weight distribution ($M_w/M_n \cong 3-4$ versus 8-16), although some specific conditions, which will influence the reaction parameters, are to be considered. Bohm¹⁰ made a significant study concerning this third generation of catalysts.

Phillips Petroleum Chemicals improved the technology of polyethylene polymerization by developing a chromium-based catalyst. The structure has a bis(triphenylsilyl)chromate base $[\Phi_3\text{SiO}_3]_2\text{CrO}_2$. Shida¹³ and co-workers presented a comprehensive report regarding this system.

Hogan and Banks¹⁴ from Phillips Petroleum Chemicals discovered the first chromium-based catalysts. Groenveld¹⁵ studied kinetics of ethylene polymerization in the temperature range between -48°C and 202°C. He found the highest productivity at two temperatures -2°C and 142°C. Usually, polyethylene resins obtained using Ti/Cr based catalysts exhibit a relatively high melt index and shear response, and a broader molecular weight. An extensive report has been presented by Lesnikova¹⁶, in which different interpretations for the deposition mode of the chromate onto the support solution media used were considered.

The discovery of Metallocene catalysts by Kaminsky and Sim¹⁷ in the early 1980s enabled the synthesis of many kinds of stereoregular, and partially regular, homopolymers and copolymers. In this category, organometallic coordination compounds

represent the base structure, in which one or two cyclopentadienyl rings are bonded through a central metal atom by a π -bond, equally distributed over all five-carbon atoms in the ring. A schematic representation is shown in Figure 2.1. It was found that the alum(in)oxane stabilizes the anion in Metallocene systems and, at the same time, acts toward the production of cationic active sites. Ethylene was the first olefin to be polymerized using bicyclopentadienyl or tricyclopentadienyl zirconium derivatives.¹⁷

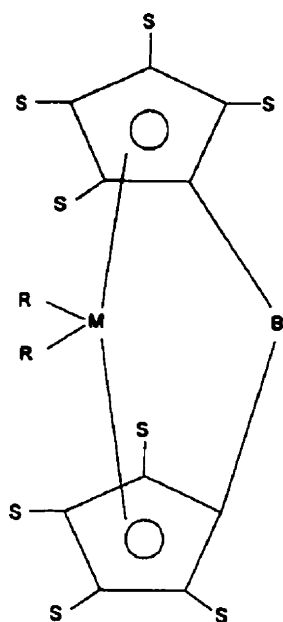


Figure 2.1 Generic Structure of a Metallocene Catalyst (M: transition metal of groups 4b, 5b or 6b; R: hydrocarbyl, alkylidene, halogen radicals; S: hydrogen, hydrocarbyl radicals; B: alkylene, alkyl radicals, heteroatom groups)

The activity of the Metallocene was increased using an alum(in)oxane obtained in a reaction of an alkylaluminum with water. Fierro *et al.*¹⁸ have revealed the nature of the catalyst system that is used to obtain a wide range of product densities, in the case of polypropylene.

2.1.2. Technology Features.¹⁹

In the autoclave reactor process, LDPE is obtained by polymerizing ethylene monomer using oxygen or peroxides as initiators. The polymer density obtained is between 0.915 and 0.925 gm/cm³ at a conversion of 15-20%. A telogen such as butene-1, normally added to the feed stream, is used to control the molecular weight. A low temperature

process gives a broad MWD, whereas with a high uniform temperature and high initiator concentrations, the molecular weight distribution is narrow. If it is combined with a low-pressure process, long chain branching is grafted onto the backbone. A temperature increase leads to an increased percentage of chain reactions, lowering the MW. A pressure increase may enhance the chain growth reactions resulting in a higher density value.

In the tubular reactor process, the reaction steps are almost the same as in the autoclave process. Density, chain branching, MW and MWD are controlled using a telogen. Final product density may be in the range of 0.918 to 0.930 g/cm³. Ziegler-Natta catalysts enhance the production of LLDPE. If previously the pressure was an important parameter in controlling the density, now the amount and type of α -olefin co-monomer in the feed stream is responsible for the density distribution. Also, temperature variation influences the MW, and the catalytic system influences the MWD. Molecular hydrogen is used usually as a MW and MWD modifier.

2.2. Polyolefin Structures and Properties. ^{2,4-8}

Among all the properties of polyolefins, density is the most important. Polyethylene densities are in the range of 0.890-0.980 g/cm³. Amorphous PE density is lower, being equal to 0.850 g/cm³. The reason is the relative content of long-chain branching (LCB), which varies in length from 20 to thousands of carbon atoms, and short-chain branching (SCB), which varies from 5 to 10 carbon atoms. LCB and SCB influence density, MW, MWD, the degree of crystallinity, lamellar thickness and melt rheology. Branching is usually expressed as the number of methylene groups per thousand carbon atoms. Due to the broad MWD in the case of LDPE, there is a broad interval over which melting occurs.

High LCB implies, for a given melt index, improved mechanical properties, broader MWD, higher flow resistance and the possibility of entanglements that will affect the processability. Because of LCB, LDPE has enhanced melt strength and elasticity, important for use in blown films, shrink films and extrusion coating processes. However,

melt strength is sensitive to extension. During film blowing, melt strength could be exceeded if the die is poorly designed.

Individual crystallite entities are about 10-30nm wide in LDPE films, forming spherulites, which are almost equal in dimension to the wavelength of light. In commercial LDPE films, LCB plays an important role. The higher the degree of LCB, the smaller will be the molecular size, and the lower will be the capacity to form crystalline aggregates. Thus, melt elasticity, viscosity and the translucence of LDPE film are greatly reduced.

LLDPE is a copolymer of ethylene with α -olefins, acting as co-monomer, usually propylene, butene-1, pentene-1, hexene-1 or octene-1. Its density ranges between 0.900 and 0.945 g/cm³. The VLDPE (very low-density polyethylene) has a density range between 0.890 g/cm³ and 0.915 g/cm³, with a similar structure. The advantages of LLDPE arise from its specific properties.

HDPE is closely packed, as can be seen from its higher density in the range of 0.960-0.980 g/cm³, with crystallinity as high as 95%, and melting point around 138.5°C. Commercial versions have small amounts of butene-1, hexene-1, and octene-1 (in proportion of 1-3%), few SCB, and a melt index in the range of 5 to 15. The morphology of solid HDPE is determined by the relative magnitudes of crystalline nucleation and growth rates, which are both so high that it is almost impossible to quench HDPE to manipulate optical properties. It is possible to lower crystallization rate, by increasing molecular weight. While this improves impact strength, it reduces yield strength, stiffness and hardness.

Polypropylene is used in plastics and fiber applications. It contains a methyl group that adds some properties, not available in polyethylene. Tacticity can be controlled by the choice of catalyst. The isotactic form, which may be crystallized, is usually found in combination with the amorphous atactic polypropylene. The end product is a thermoplastic elastomer. Presently, most of the processed polypropylene on the market is

in the isotactic form. Recently, the use of metallocene catalysts has led to the possibility of obtaining syndiotactic polypropylene.

2.3. Polymer Crystallization and Morphology.

There are mainly two important groups of polymers. Firstly, amorphous polymers that have no order with respect to their internal arrangement. Their constituent chains are tangled up in various ways. Secondly, semi-crystalline polymers, where the molecules respect a neat and quite orderly fashion in their distribution, bounded together by means of secondary interactions. Roughly, a distinction can be made between the two types by plotting the specific volume against temperature. For the first case, there is only the glass transition temperature, T_g , separating the glassy and rubbery phases. For the second case, there is the T_g and also the melting temperature, T_m , associated with the crystalline fraction of the polymer.²⁰

From another point of view, for crystallization to occur in a polymer, the requirement is the presence of a regular chain structure, combined with a high mobility of chains at the melting temperature. This means that the polymer has a higher capability to orient itself, thus rendering a structure with a high percent crystallinity. A main issue is the number of branches along the chain, which is strongly related to the industrial method of polymerization. For instance HDPE obtained by free radical polymerization has 0.1 to 5 branches/100 C atoms, while other grades have 0 to 0.5 branches/100 C atoms.²¹ Another important factor is the steric isomerism and stereo-regularity, which influence the mechanism of crystallization and hence the properties of the end product. The stereo-regularity is related to the regular substitution in the main chain (i.e. for polypropylene), while the steric isomerism concerns the spatial arrangement of the substituents. These can be classified further as isotactic, atactic, and syndiotactic (regular alternation).

Mandelkern²² and Keller²³ studied the mechanism of crystallization and the crystal growth of various polymers from dilute solutions. They were able to measure the dimensions of crystal lamella and they find a thickness of the order of 100Å. The

dimension, which is much smaller than the average length of a regular chain (10^5\AA), leads to the conclusion that the

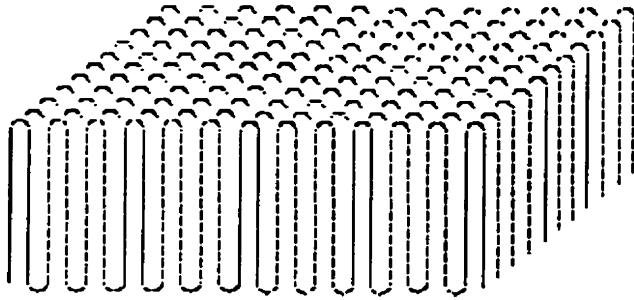


Figure 2.2. The Crystal Lamella.

polymer chain has to be folded in order to be confined in lamellae, as observed in Figure 2.2. The length of folding is in fact controlled by the crystallization temperature, namely the degree of supercooling. Of course, the size and the shape of such crystallites are significantly different, when one tries to produce them from the bulk material instead of a dilute solution. X-ray diffraction studies revealed higher conglomerates known as spherulites (Figure 2.3), and the relationship and interaction between them is not so easy to explain. Fibrils are the main components of a spherulite and exhibit a radial growth

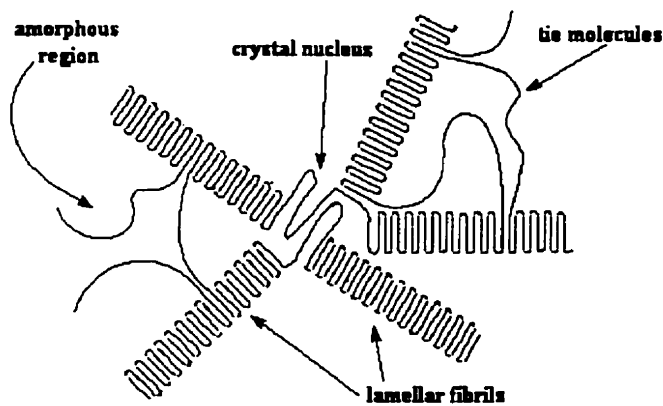


Figure 2.3. Typical Conformation of a Spherulite.

from the center. The fibrils themselves are made up from crystallites, where the chains are folded at right angles to the fibril length. Between fibrils, one may find the amorphous material that was rejected during the crystallization process.²⁴

The spherulite size varies between a few microns and an upper limit of millimeters. The spatial and size distributions are functions of process parameters, mainly affecting nucleation and growth. Under special conditions, such as very slow cooling rates, and a temperature very close to the melting temperature, crystallization can produce extended polymer chains. This means that there is reduced or no sign of folding.²⁵ This theory holds also in the case of high-pressure crystallization (~5,000atm.) of polyethylene melts²⁶ or highly oriented polyethylene of very high modulus.²⁷

2.3.1. Polymeric Crystals.

Many theories and mechanisms have been proposed to explain the formation of polymer crystals and crystallization kinetics.^{6,24,34,44} It is commonly accepted that, when crystallized from melt, molecular trajectory is similar to a random coil rather than an adjacent re-entry folding of the molecule, as in the case of solution grown crystals. Also, it is suggested that the molecule exits and re-enters several crystals, this behavior being dictated by the crystallization temperature.

The progress made takes into consideration the existence of three steps²⁸, depending on the relative rates of secondary nucleation and surface spreading. The third step is specific for long chain molecules, whereas the first two have been observed in atomic solids. For polymers with higher crystallinity, an important feature is that the skeletal structure of the superstructural crystalline aggregates (such as spherulites) is determined by a small number of leading and dominant lamellae. This behavior, observed for polymers with low-crystallinity, leads to crystallinity development behind the growth front.

2.3.2. Structure and Order in Polymeric Materials.

In comparison with non-covalently bonded materials (e.g. metals), polymers differ in their behavior above melting. The covalent bond remains intact, and only secondary bonding forces suffer from disruption. Thus, the total entropy is associated with the conformational entropy of the polymer chain. The maximum entropy involves a highly

disordered state which, in our case, may be interpreted as a randomly coiled molecule, with high internal mobility.

Molecular flexibility is related to chemical structure, which determines the degree of molecular rigidity. The structural units give flexibility to the backbone (the polymer "skeleton"), which, in the case of polyethylene, are only aliphatic units (-CH₂-). High flexibility occurs even at ambient temperature. The chain can change its shape, if the kinetic energy is adequate to overcome the internal potential energy for rotation about a backbone bond.

The end product of a polymerization reaction may result in two ordered forms, isotactic and syndiotactic, or totally random, atactic. Potentially crystallizable polymers are usually isotactic and syndiotactic. The structural units are arranged in a regular symmetric fashion. In atactic polymers, there is no symmetry, and thus, they are resistant to crystallization. Although, there is a certain level of crystallinity attainable, higher levels cannot be achieved.²⁹

As was previously mentioned, the crystallization process may be affected, in the last instance, by the process history. Secondary factors may induce side reactions, and the general result could affect the backbone structure, sometimes by disrupting the regularity of the chain. This produces a higher degree of non-crystalline material that can be regarded as amorphous. Each defective unit that is rejected, takes with it a little portion of the crystallizable chain. This fact may be observed if one compares two samples of PE, one of low density and another one of high density. During the polymerization processes, the chain end of a radical can turn around and react with itself forming an intermediate radical ring with a butyl branch. In a typical LDPE, there are 15 short branches per thousand carbon atoms. The result may be observed in the maximum attainable crystallinity percentages being around 50 for LDPE and as high as 90 (under normal circumstances) for HDPE. When a chain end of a long molecule reacts with another one, or with an atom within the same molecule, long chain branches are generated. The influence on the crystallization is low, but it may affect the diffusion rates of the polymer chain. Present industrial processes attempt to avoid these side effects by using Ziegler-

Natta and Metallocene catalysts. An unexpected behavior was observed in the case of LDPE. Branches tend to concentrate in the shortest molecules. Therefore, the polymer looks like a mixture of HMW (high-molecular weight) molecules and branched LMW (low-molecular weight) chains. Upon crystallization, these two different species tend to fractionate.

In relation to molecular weight, chain mobility and crystallization degree, two essential conclusions can be drawn. Firstly, the mobility of higher molecules, as they move past one another is lower as they are “sucked” into the growing crystal. Secondly, a long molecule may be knotted or experience higher entanglement and, thus, elastic forces will resist the crystallization process. In reality, commonly used polymers are in fact copolymers. This leads to two phases (with low miscibility), in which the two molecular species behave as homopolymers.

2.3.3. The Crystallization Process.

Crystallization can be defined as a process of phase transformation described, at a phenomenological level, by the general kinetic equation of the following form:

$$X = X(t, T). \quad (2.1)$$

X is a measure of the extent or degree of crystallization, and it is defined as the time and temperature dependant ratio of the crystallized mass to the original polymer mass, where t is the time elapsed from the onset of crystallization, and T is the absolute temperature.

As illustrated in Fig. 2.4, the fraction, $X = X(t, T)$, is defined as:

$$X = \frac{\text{mass of crystallized part}}{\text{total mass of polymer}} = \frac{\rho_c \sum V_i(t)}{\rho_l V_0} \quad \text{for } i = 0 \text{ to } n,$$

$$\begin{array}{ll} \text{at } t = 0 & \sum V_i(0) = 0 \quad \text{thus } X = 0, \\ \text{at } t = \infty & \sum V_i(\infty) = V_0 \rho_l / \rho_c \quad X = 1. \end{array} \quad (2.2)$$

V_0 is the total volume of molten polymer, n is the number of crystallizing particles, V_i is the volume of each particle, and ρ_c and ρ_l are the particle and liquid densities,

respectively. For polymers, in general and in contrast to metals, the crystalline density depends on the temperature of crystallization and other factors, and may change with time and distance along the spherulite radius during crystallization.³⁰ Thus, the difference between the degree of crystallization, as defined above, and the degree of crystallinity, which is the more frequently measured quantity, is understandable.

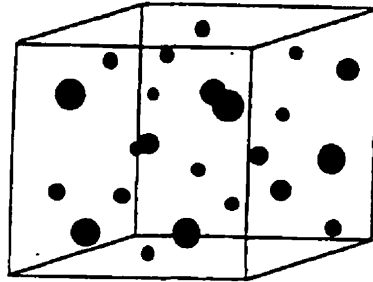


Fig. 2.4. Cooling of a Liquid Polymer below its Melting Temperature. (Crystallizing particles - spherulites- appear at random in the liquid and grow with time. Impinging -overlapping- particles and the gradual exclusion of liquid volume for the appearance of new nuclei can be noticed. The release rate of latent heat of crystallization must be less than the rate of heat removal from the polymer for the growth to continue.)

Usually it is assumed that the process of crystallization obeys the principle of additivity. The principle is based on the assumption that the instantaneous rate of transformation is a function of temperature and the amount transformed only, and it is not dependent on the thermal history of the transformation.³¹ In this case the transformation rate can be written in the form:

$$\frac{dX}{dt} = \frac{h(T)}{g(X)} \quad (2.3)$$

where $h(T)$ is a function of temperature only, and $g(X)$ is a function of the amount transformed only. Both functions are obtained from the classical theories of nucleation and growth and describe the microscopic kinetics of crystallization. At a macroscopic level, the crystallization kinetics refers to the geometrical and spatial aspects of the process of growth, and it aims to obtain a solution to the general equation (2.1), and to quantify the transformation.

2.3.4. *Thermodynamics of Crystallization.*

Kinetics relates forces to the motion of masses in a given system. In polymer crystallization, the forces are internal. They are generated by the excess of thermodynamic free energy in the system. The motion refers to the transport of the molecules from the disordered liquid phase (i.e. melt or solution) to the ordered solid phase (i.e. crystal), and to the rotation and rearrangement of the molecules at the surface of the crystal.

The phase transformation can be induced by different means, when a polymeric system is analyzed. It is usually described in terms of nucleation and subsequent growth of a new phase within the existing one. Usually, a change in the thermodynamic state of the system leads to the onset of crystallization, for example, by lowering the temperature below a critical value, by supersaturation of the solution through evaporation, or by an increase in hydrostatic pressure. Turnbull and Fisher³² extended to polymers the classical thermodynamic concept of nucleation developed by J. W. Gibbs. According to their theory, in the absence of an existing solid, fluctuations in the supercooled melt can overcome the Gibbs free energy barrier to nucleation. Phase transformation begins as soon as the free energy of crystallization becomes negative. In the early stages, however, the initial process begins with the formation of sub-critical nuclei of the new phase by way of positive free energy of crystallization. To become stable, they must grow spontaneously to the critical size with an associated critical free energy. In some particular cases, the critical equilibrium nucleus size is not achieved immediately at a supercooled state, and the new phase can appear only after an “incubation period”.

The Gibbs free energy of a system, G , is given by:

$$G = H - TS \quad (2.4)$$

In the case of crystallization, change takes place without any volume constraint and without any compositional or chemical changes during the process. The only thermodynamic quantity causing the transformation is the lowering of temperature below the equilibrium melting temperature, T_m . Thus, the change in Gibbs free energy is given by:

$$\Delta G = (H_{crystal} - H_{melt}) - T (S_{crystal} - S_{melt}) = \Delta H - T\Delta S \quad (2.5)$$

To a first approximation, the change in enthalpy, ΔH , is equal to the latent heat of fusion, and ΔS is equal to the entropy of the melt (the entropy of the crystal being much smaller by comparison). At the melting temperature, by definition, $\Delta H = T_m \Delta S$. Below this value, the system will spontaneously seek to minimize its free energy by undergoing crystallization, if certain necessary conditions are satisfied. These conditions relate to the process of crystallization that involves two independent phenomena: (i) nucleation, and (ii) crystal growth.

2.3.4.1. Nucleation.

The value of ΔG , defined in Eq. (2.5), increases monotonically with increasing size of the embryo above the equilibrium melting temperature. Below T_m , this function changes to one with a maximum, defined by:

$$\frac{d(\Delta G)}{dr} = 0 \quad (2.6)$$

where r is the radius of the embryo. This maximum represents the activation energy barrier that has to be overcome in order to form a stable nucleus which will grow.³³ At the molecular level for a smooth crystal surface, a new layer can be grown after secondary nucleation, a process similar to primary nucleation, but with a lower free enthalpy barrier since the surface area that must be created is smaller. The change in the free energy of the growing crystal can be described by³⁴:

$$\Delta G'' = \Delta G_c + \sum \gamma A \quad (2.7)$$

where γ represents the specific surface energy and A is the corresponding surface area and the summation is carried out over all crystal surfaces.

For polymer crystallization, there are three physical mechanisms: (i) spontaneous homogeneous nucleation that occurs (rarely) in a supercooled homogeneous melt, (ii) orientation induced nucleation caused by alignment of macromolecules and spontaneous nucleation, and (iii) heterogeneous nucleation on the surface of a foreign phase. The last

one always occurs at lower supercooling than does the homogeneous nucleation. The heterogeneities are known as nucleation catalysts or nucleating agents.

Hoffman, Davis and Lauritzen²⁰ using the Turnbull and Fisher³² theory, described the rate of nucleation, N , in polymers using the following equation:

$$N = N_0 = \exp\left(-\frac{U^*}{R(T - T_g - C_2)}\right) \exp\left(-\frac{\Delta G^*}{k_B T} f(\Theta)\right), \quad (2.8)$$

$$\text{with } \Delta G^* = \frac{\beta \sigma_e \sigma^2 T_m^2}{(\Delta h f(T))^2 \Delta T^2}, \quad f(\Theta) = \frac{(2 + \cos \Theta)(1 - \cos \Theta)^2}{4}, \quad f(T) = \frac{2T}{T_m + T}, \quad (2.9)$$

where σ is the crystal growth face surface energy, σ_e is the crystal end (fold) surface energy, Δh is the heat of fusion per unit volume, ΔT is the supercooling, and $\beta = 32$ is a geometrical constant. R is the gas constant, k_B is the Boltzmann constant, T_g is the glass transition temperature, and $(T_g - C_2)$ is the Gibbs-Di Marzio "equilibrium" glass transition temperature with $C_2 = 50^\circ\text{C}$ (usually treated as an adjustable parameter). U^* is the activation barrier to transport molecules from the melt to the crystal surface. Experimentally derived values of U^* range from 6 to 25 kJ/mol.

In the case of homogeneous nucleation, the function $f(\Theta)$ assumes a value of 1 ($\Theta = 180^\circ$). For heterogeneous nucleation, the wetting contact angle is $0 < \Theta < 180^\circ$, and

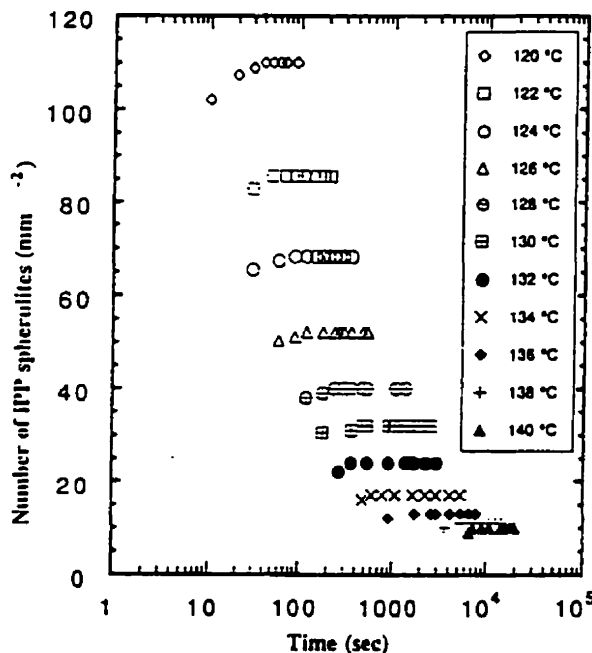


Fig. 2.5. Number of Spherulites in isotactic Polypropylene (iPP) as a function of time and Different Crystallization Temperatures.

therefore $0 < f(\Theta) < 1$. The function, $f(T)$, is an approximate correction factor that takes into account the fact that the heat of fusion changes with supercooling.^{20,35,36} As illustrated in Fig. 2.5, the number of nuclei is very sensitive to crystallization temperature, T_c . For strain induced nucleation, Yeh and Hong³⁷, derived an equation based on the premise that the difference in free energy between oriented melt and crystal is raised with respect to that in quiescent crystallization by the difference in entropy between the two melt states, $\Delta S' = (S_{melt} - S_{oriented, melt})$. For the high temperature region, i.e. for $T > (T_m + T_g)/2$, the enhancement of nucleation rates is given by:

$$\frac{N^0}{N} = \exp \left[\frac{\beta \sigma_e \sigma^2}{k_B T} \left(\frac{T_m^2}{\Delta h^2 \Delta T^2} - \left(\frac{\Delta h \Delta T}{T_m} + T \Delta S' \right)^{-2} \right) \right], \quad (2.10)$$

$$\text{with } \Delta S' = \frac{k_B \bar{N}}{2} \left(\frac{24 \bar{n}}{\pi} \right)^{0.5} (\lambda - 1), \quad (2.11)$$

where N^0 is the nucleation rate in the oriented state, N is the nucleation rate in the unoriented state, \bar{N} is the number of network chains per unit volume, \bar{n} is the number of statistical segments per network chain, and λ is the stretch ratio. Due to probably experimental difficulties, experimental measurement of enhanced nucleation under flow stress conditions has been reported in few cases only.^{38,39}

2.3.4.2. Crystal Growth.

For most polymers that exhibit high crystallinity, a spherulitic microstructure can be observed upon crystallization from the melt. In Fig. 2.6, two basic types of spherulitic morphologies are shown.

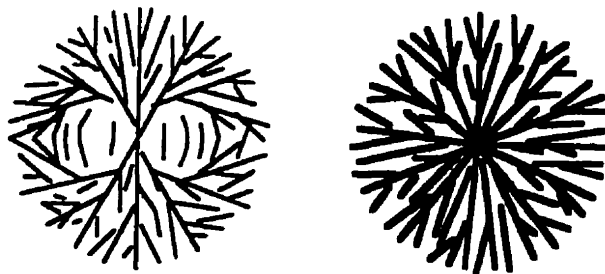


Fig. 2.6. Sketch of two possible growth morphologies leading to spherical symmetry.

The first one has a central nucleus from which crystalline lamellae initiate, with a more or less radial growing pattern in all directions. The different crystal lamellae are nucleated separately and independent of each other. The symmetry extends from the center. The second model is a development of one single lamellae crystal by continuous branching and fanning out, until a spherical shape is obtained. In the center, a unidirectional growth (parallel lamellae) that undergoes a so-called sheaf stage can be observed.

Hoffman *et al.*⁴⁰, Wunderlich⁴¹ and Bassett⁴² derived the following equation for the spherulite growth rate, using the molecular theory of growth:

$$G = G_0 \exp\left(-\frac{U^*}{R(T - T_g - C_2)}\right) \exp\left(-\frac{\beta b \sigma \sigma_e T_m}{k_B T (\Delta h_f(T)) \Delta T}\right), \quad (2.12)$$

where all the quantities have the same meaning as in Eqs. (2.8) and (2.9), except for b which is the thickness of the molecular layer added at each pass of crystal growth (of the order of 0.4nm), and β , which can assume two values (4 or 2), depending on whether the growth is in regimes I or III, or regime II, respectively.⁴⁰ Experimental measurement of spherulite radius growth rate versus time of crystallization at various crystallization temperatures showed a decrease of the rate with increasing temperature.

2.3.5. Molecular Weight Influence and Melting Point.^{28,29}

It is generally accepted that increasing molecular weight causes a decrease in the rate of crystal growth (Figure 2.7.). It is also possible that molecular fractionation occurs as a result of major differences in melting point and mobility.

One explanation was introduced by Wunderlich and Mehta.⁴³ The basic concept considers that when the nucleus grow beyond its critical size, it reaches a point at which its energy of formation becomes zero and ultimately negative, reaching thus the stability point. Hence, it is possible that dissolution occurs, which is caused by molecular fractionation under appropriate conditions. To eliminate this behavior, low rates of crystallization and low supercooling are required.

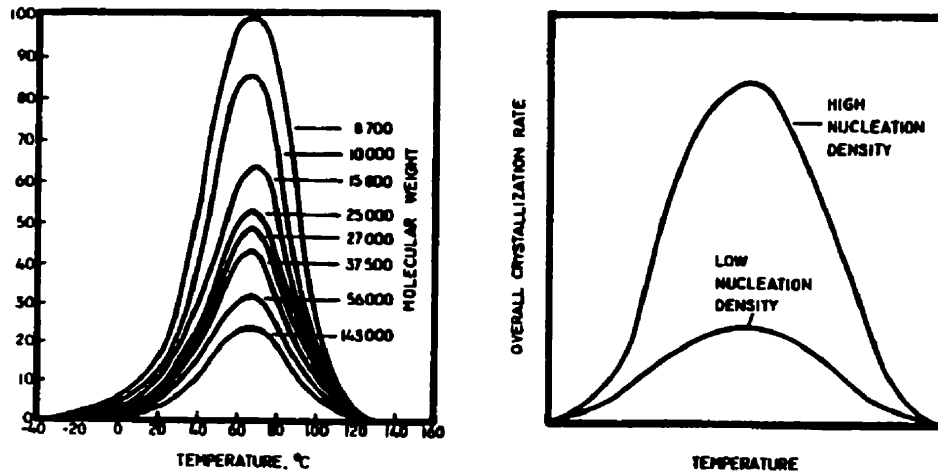


Figure 2.7. (a) Dependence of Spherulitic Growth Rate on Temperature for Different Molecular Weight Fractions of a Polymer. (b) Effect of Nucleation Density on Overall Crystallization Rate.

Different melting point values have been observed for polymer crystals with different thickness, due to crystallization temperature. For a polymer crystal, the most basic and essential parameter is its melting point, which is the necessary temperature to melt an infinitely thick crystal. Earliest techniques involve small angle X-ray scattering (SAXS) and demonstrate that thickness is strongly dependent upon crystallinity. Hence, there will be always a distribution of thickness.

In the case of PE solution growth crystals, it was observed that the grown crystals are thickened by successively adding lamellar layers forming thus a spiral terraced structure with its axis along the c-axis direction.^{43,44}

2.4. Crystallization Kinetics.

The rates of nucleation and growth (or the overall crystallization rates) vary among polymers. Factors like chemical structure, molecular weight, molecular weight distribution, temperature and pressure play a significant role in polymer behavior. Several models have been employed to describe polymer crystallization kinetics. Among the most commonly used are the Avrami⁴⁵, Tobin⁴⁶, Ozawa⁴⁷ and Malkin⁴⁸ models for isothermal

crystallization, and the Nakamura⁴⁹ and Ziabicki⁵⁰ models for non-isothermal crystallization.

The literature offers some critical descriptive comparisons between the Avrami and Tobin models for the isothermal crystallization data of poly(ethylene terephthalate) (PET), poly(phenylene sulfide) (PPS)⁵¹, medium-density polyethylene (MDPE)⁵² and poly(oxymethylene) (POM)⁵³. For the Avrami and Malkin models, comparisons of the isothermal data were analyzed and critically observed for polyethylene (PE), isotactic polypropylene (iPP), PET, poly(propylene oxide) (PPO) and polyurethane (PU)⁴⁸. An analysis of all three models, Avrami, Tobin and Malkin has not yet been given.

According to the theory, semicrystalline materials exhibit two main independent crystallization processes upon cooling. The overall crystallization is the sum of primary and secondary crystallization. The first is a macroscopic development of crystallinity as a result of two consecutive microscopic mechanisms: primary nucleation and secondary nucleation (i.e. subsequent crystal growth). The second is mainly related to the crystallization of the interfibrillar melt, rejected and trapped between the fibrillar structure formed during the growth of crystalline aggregates (e.g. axialites, spherulites, etc.).^{54,55} An important remark that has to be made is that, if the crystallization time becomes very long, other types of secondary crystallization (i.e. crystal perfection and crystal thickening) may become significant enough to increase the value of the ultimate absolute crystallinity.

2.4.1. Avrami Isothermal Model.

The Avrami equation describes the overall kinetics of crystallization, including nucleation and growth as:

$$\chi(t) / \chi_{\infty} = \Theta(t) = 1 - \exp(-kt^n) \quad (2.13)$$

where k is the Avrami crystallization rate constant and n is the Avrami exponent of time; $\chi(t)/\chi_{\infty}$ is the relative degree of crystallinity, changing from 0 at the beginning of crystallization to 1 at the end (although only a portion of the material has actually

crystallized). The k and n constants, as mentioned, are typical for a given crystalline morphology and type of nucleation under imposed crystallization conditions.⁵³ If required in the analysis, the rate of evolution of the heat of crystallization as a function of time and the relative extent of crystallization $\Theta(t)$, can be related one to another using the following equation:

$$\Theta(t) = \frac{\int_0^t \left(\frac{dH_c}{dt} \right) dt}{\Delta H_c} \quad (2.14)$$

where t defines an arbitrary time period during the isothermal crystallization process, dH_c is the enthalpy of crystallization released during an infinitesimal time period, dt , and ΔH_c is the overall enthalpy of crystallization for each specific crystallization temperature T_c .

The analysis of the experimental data has led to a general conclusion concerning the applicability of the Avrami equation. The model is appropriate for the early stages of crystallization. In the search for a simple characterization parameter, the crystallization half-time, $t_{1/2}$, equation was introduced. The expression is in the form of Eq. 2.15 and represents the time at which half of the conversion has taken place. The crystallization half-time, $t_{1/2}$, is a convenient measure for the speed of crystallization.

$$t_{1/2} = \left(\frac{\ln 2}{k(T)} \right)^{1/n} \quad (2.15)$$

Since Avrami's introductory theory, relating to the solidification of molten phases with the purpose of describing the macroscopic evolution of the crystallinity under quiescent isothermal conditions, a number of mathematical models have been proposed over the years. It is worth mentioning that Avrami's work prevailed over Kolmogoroff⁵⁶, Johnson and Mehl⁵⁷ and Evans⁵⁸ models. The newest mathematical models, some based on different approaches (i.e. Tobin and Malkin models), are summarized in later sections for both isothermal and non-isothermal crystallization kinetics. Presently, three of the four models presented are used to describe the kinetics of crystallization at constant temperature from quiescent crystallization data.

2.4.2. Tobin Isothermal Model.

For heterogeneous nucleation and growth, Tobin⁴⁶ expressed the degree of crystallinity by a non-linear integral equation for which the zeroth-order expression is:

$$\frac{\chi(t)}{1 - \chi(t)} = kt^n \quad (2.16)$$

In its original form, nonlinear Volterra integral equation, the zeroth-order expression is:

$$\Theta(t) = \frac{k_T t^{n_T}}{1 + k_T t^{n_T}} \quad (2.17)$$

where $\Theta(t)$ is the relative crystallinity as a function of time, k_T is the Tobin crystallization rate constant, and n_T is the Tobin exponent which is not necessarily an integer, as in the Avrami model, and it is governed by different types of nucleation and growth mechanisms.⁵¹⁻⁵³ By taking into account growth site impingement, Tobin's model allows a better fit than the Avrami equation for long periods of time.

Rabesiaka and Kovacs⁵⁹ applied a similar model ending up with good results for the fitting of their dilatometric data for PE for a $\Theta(t)$ up to 0.9.

2.4.3. Ozawa Isothermal Model.

Ozawa⁴⁷ extended the Avrami⁴⁵ isothermal model to the non-isothermal case by assuming a constant cooling rate. In this respect, the following equation was proposed:

$$\frac{\chi(T)}{\chi_\infty} = 1 - \exp\left(\frac{-K(T)}{|\dot{\lambda}|^{n_O}}\right) \quad (2.18)$$

where χ_∞ is the crystallinity at the end of the crystallization process, $\chi(T)$ is the crystallinity at temperature T, $K(T)$ is named as the cooling function of non-isothermal crystallization at temperature T (strongly dependent upon nucleation and growth rates) and n_O is the Ozawa index (known as the Avrami exponent and takes values between 1 and 4).⁶⁰

Following the same approach as in the Avrami theory, by taking twice the logarithm of both sides of Eq. 2.18 at constant temperatures, it follows that:

$$\ln \left[- \ln \left(1 - \frac{\chi(T)}{\chi_{\infty}} \right) \right] = \ln [K(T)] + n \ln |\lambda^{-1}| \quad (2.19)$$

By plotting the term on the left-hand side versus $\ln |\lambda^{-1}|$, a straight line is obtained if the theory is valid. Calculating the slope and the intercept, values for n and $K(T)$ are obtained, respectively.

Lopez and Wilkes⁶¹ favored this approach, considering that the model weaknesses (secondary crystallization and chain folding are neglected) are less important under non-isothermal conditions. The slow secondary crystallization as well the fold length factor are practically absent at fast and continuous cooling.

2.4.4. Malkin Isothermal Model.

Considering that the Avrami kinetic model is valid only for the single stage crystallization processes (primary crystallization), Malkin *et al.*⁴⁸ developed a new macrokinetic model that describes the overall crystallization rate, as a summation of the rate at which the degree of crystallinity varies as a result of emergence of primary nuclei, and the rate of variation in the degree of crystallinity as a result of crystal growth. The linear function expression is:

$$\Theta(t) = 1 - \frac{C_0 + 1}{C_0 + \exp(C_1 t)} \quad (2.20)$$

where $\theta(t)$ is the relative degree of crystallinity as a function of time. The constant C_0 relates directly to the ratio of the linear growth rate, G , to the nucleation rate, N , (i.e. $C_0 \propto G/N$) and C_1 relates directly to the overall crystallization rate (i.e. $C_1 = aN + bG$, where a and b are specific constants). Furthermore, both C_0 and C_1 , are temperature dependent. The constants in Eq. 2.20 can be determined using the kinetic parameters from the Avrami analysis, k_a and n_a , respectively. Their mathematical expressions are:

$$C_0 = 4^{n_a} - 4 \quad (2.21)$$

$$C_1 = \ln(4^{n_s} - 2) \left(\frac{k_s}{\ln(2)} \right)^{\frac{1}{n_s}} \quad (2.22)$$

The advantage of the macrokinetic model is its better fit of the experimental data for the entire range of degrees of conversion, mainly in the regions of limiting degrees of conversion (at $\theta \rightarrow 0$ and $\theta \rightarrow 1$).

2.4.5. Nakamura Non-Isothermal Model.

A good understanding of conventional polymer processing requires a series of tests under non-isothermal conditions. In this case, a temperature difference in the sample is defined as a balance between the heat generated by the system and heat lost due to continuous supercooling.

A simplification in DSC measurements is possible by decreasing the temperature at a constant rate. The process may be considered in this case quasi-isothermal. Nakamura *et al.*⁴⁹ proposed Eq. 2.23 as the non-isothermal kinetic expression, where $K(T)$ is related to the crystallization rate constant from Avrami's equation with n having the same significance. By considering the effect of impingement with adjacent crystals on growth rates, Nakamura developed the following modification to the Avrami equation for non-isothermal kinetics:

$$\chi(t) = 1 - \exp[-(\int_0^t K(t) dt)^n] \quad (2.23)$$

where $K(T)$ is the non-isothermal crystallization rate constant. It is related to the isothermal crystallization rate by the following relationship:

$$K(T) = [k(T)]^{1/n} = \frac{(\ln 2)^{1/n}}{t_{1/2}} \quad (2.24)$$

where $1/t_{1/2}$ is a temperature dependent overall rate of crystallization, and n is the Avrami index from the isothermal experiments. The crystallization half time can be expressed using Eq. 2.25 below, known as the Hoffman-Lauritzen²⁰ expression, in which it is assumed that the number of nucleation sites is independent of temperature and all sites

are activated at the same time. The relationship describes the overall rate of crystallization as a function of temperature:

$$\left(\frac{1}{t_{1/2}} \right) = \left(\frac{1}{t_{1/2}} \right)_0 \exp \left(- \frac{U^* / R}{T - T_\infty} \right) \exp \left(- \frac{K_g}{T \cdot \Delta T \cdot f} \right) \quad (2.25)$$

where T is the crystallization temperature, R is the universal gas constant, $\Delta T = T_m^0 - T$ is the supercooling, and $f = 2T / (T + T_m^0)$ is a correction factor accounting for the reduction of the latent heat of fusion as the temperature is decreased, T_m^0 being the equilibrium melting point. The $(1 / t_{1/2})_0$ term is a pre-exponential factor in which all terms are temperature independent. Both $(t_{1/2})_0$ and K_g can be obtained from Eq. 2.25 using universal values for U^* (an optimal value for a large number of polymers and corresponds to almost 50% relative crystallinity) and T_∞ . This is achieved by plotting the logarithm of the rate constant versus temperature and using non-linear regression.

Differentiation of Eq. 2.23 leads to the more often used form of the Nakamura equation mainly in process modeling:

$$\frac{d\Theta}{dt} = nK(T)(1 - \Theta) [- \ln(1 - \Theta)]^{n-1/n} \quad (2.26)$$

Because Eq. 2.23 neglects the induction time for nucleation, this leads to an over-prediction of crystallinity, limiting thus its application. Non-isothermal induction times can be calculated from isothermal induction time, using the following equation proposed by Sifleet *et al.*⁶²:

$$\bar{t} = \int_0^{t_f} \frac{dt}{t_i(T)} = 1 \quad (2.27)$$

where $t_i(T)$ is the isothermal induction time as a function of temperature. The dimensionless induction time index, \bar{t} , reaches unity by integration and the upper limit of integration is taken as the non-isothermal induction time t_f . Usually the non-isothermal processes are regarded as a succession of infinitesimal isothermal steps.

2.4.6. Ziabicki (Non)-Isothermal Model.

Ziabicki derived an empirical mathematical relationship, for the temperature dependence of the crystallization half times:

$$\left(\frac{1}{t_{1/2}} \right) = \frac{1}{(t_{1/2})_{\max}} \exp \left[- 4 \ln(2) \frac{(T - T_{\max})^2}{D^2} \right] \quad (2.28)$$

where $(1/t_{1/2})_{\max}$, T_{\max} and D can be determined from the experimental data and describe, respectively, the time when the crystallization reaches 50% of its maximum value, the temperature where the maximum rate is achieved, and the temperature interval (mid-width) of the bell-shaped plot of the rate (k) versus temperature.

In this work, the Ziabicki Eq.(2.28) was used as follows. Using the experimental values for $t_{1/2}$, knowing thus the crystallization process rate at 50% crystallinity, and employing a nonlinear multivariable regression computer program, $(t_{1/2})_{\max}$, T_{\max} and D can be determined. The best fit will be described by the value of the parameter, r^2 , closest to unity. From the experimental data, $t_{1/2}$ and $(t_{1/2})_{\max}$ or $t_{1/2}$ and T_{\max} can be used as known values. The unknown (variable) parameters will be given by the following sets: T_{\max} and D or k_{\max} and D , respectively. The other method consists of using one constant and three variables as output, namely $t_{1/2\max}$, T_{\max} and D . The results are tabulated in Appendix 8.

2.4.7. Formulation of the Cooling Function, $K(T)$.

Different approaches and steps were made towards the simplification of the kinetic equations. Hammami and Mehrota⁶³ transformed Ozawa's equation into:

$$\frac{\chi(T)}{\chi_{\infty}} = 1 - \exp \left[- \Psi(T) \cdot t^n \right] \quad (2.29)$$

where t denotes the time required to cool the sample melt from the equilibrium melting temperature T_m^0 to T , ΔT is the degree of supercooling, and the function Ψ is given by:

$$\Psi(T) = \frac{K(T)}{(\Delta T)^n} \quad (2.30)$$

The resemblance with the Avrami equation is obvious:

$$\frac{\chi(t)}{\chi_{\infty}} = 1 - \exp(-k \cdot t^n) \quad (2.31)$$

where k is the overall isothermal rate constant.

According to Elias,⁶⁴ theoretically derived expressions for k for different crystallization mechanisms are presented in Table 2.2.

Table 2.2. Theoretical Values of n and the Isothermal Rate Constant k for Different Morphologies and Nucleation Mechanisms.

Crystal Growth	Nucleation Mode	Avrami Exponent (n)	Isothermal Rate Constant (k)
Rod	Heterogeneous	1	NGA
	Homogeneous	2	$N^*GA/2$
Disc	Heterogeneous	2	πG^2ND
	Homogeneous	3	π / G^2N^*D
Sphere	Heterogeneous	3	$4\pi/3NG^3$
	Homogeneous	4	$\pi/3N^*G^3$

Constant significance: A is constant area, D is thickness, and G is linear growth rate, N is nucleation density and N^* is nucleation rate.

Also at a given temperature, one can see that $\Psi(T)$ is constant and the relative crystallinity is only time dependent as in the Avrami equation. Thus, the similarities between Eqs. 2.29 and 2.31 suggest that the cooling function is related to the overall rate of crystallization.⁶⁵

CHAPTER 3

SCOPE AND OBJECTIVES

One of the most complex subjects in polymer physics concerns the morphology and crystallization kinetics of polymers. Films represent the highest percentage of the polyethylene produced from industrial processes. Their properties are dictated by two factors: firstly, by the polymerization process (such as gas, solution, or suspension polymerization using a Metallocene or Ziegler-Natta catalysts), and secondly, by processing considerations. Both influence the characteristics of the polymer resins. These factors will affect the morphology and the crystallinity of the products. In the study of crystallization kinetics, a series of experimental techniques were developed, such as calorimetry, light-microscopy, X-ray diffraction and dilatometry.

The present study is dedicated to the investigation of the crystallization behavior of sixteen resins, using differential scanning calorimetry. It represents a part of a more general research project, in progress in our polymer-processing group. Eleven of the analyzed resins are linear-low-density polyethylene (LLDPE), which are special heteropolymers with different co-monomers such as butene, hexene and octene, two are low-density polyethylene (LDPE), one a high-density polyethylene (HDPE), a commercial injection-molding grade, and two are polypropylenes (PP-1 and PP-2). The physical properties provided by the suppliers of the resins are tabulated in Appendix 1.

The main objectives of the present study are: (i) to perform isothermal crystallization experiments to study the kinetics of the sixteen resins using a DSC apparatus, (ii) to perform non-isothermal crystallization experiments, for the resins, at different controlled cooling rates, and (iii) to fit experimental data to the crystallization kinetic models employed.

It should be emphasized that the main objective of the study is to obtain the crystallization data using the DSC, so that the results may be employed, by others, in the development of models (e.g. film blowing) and in understanding morphological development during the solidification of various resins. While an effort is made to fit models and to evaluate the effects of structural factors, the main objective is to produce the data and to ensure their accuracy. The detailed quantitative and theoretical analysis of the results is beyond the scope of this work. These aspects are currently under study by other members of the group.

CHAPTER 4

EXPERIMENTAL

In this chapter, the resins used in the present study as well as the apparatus with which the experimental data were collected are presented. The detailed experimental procedure used for operating the Differential Scanning Calorimeter (DSC) and the instrument operational principles are described.

4.1. Resins Properties.

The polyethylene resins used in the present study (supplied by Nova Chemicals Inc.) were experimental linear low-density polyethylene (LLDPE), low-density polyethylene (LDPE), and a commercial grade of high-density polyethylene (HDPE, Sclair 2908). The two polypropylenes (PP) examined were manufactured by Montell.

Different types of co-monomers were used in the manufacture of the L(L)DPE resins, and different techniques of polymerization were employed as described in Chapter 2, i.e. mainly using gas and solution techniques. In comparison with the commonly used multi-site catalysts, that give rather a complex mixture of branched polyethylene with a molar mass-dependent degree of branching, single-site catalysts produce generally uniform copolymers with narrow Molecular Weight Distribution (MWD) and molar mass-independent uniform co-monomer incorporation.⁶⁶ Table 4.1 lists some physical properties of the polymer resins used, such as density, melt index, number-average molecular weight, M_n , weight-average molecular weight, M_w , polydispersity, M_w/M_n , co-monomer content, Co-me, and co-monomer type, Como, as well as the polymerization technique used in manufacture.

Table 4.1 Resins Physical Properties

Resin Code	Como	Med	Cat	Co-me %	Mn (g/mol)	Mw (g/mol)	Mw/Mn	Density (g/cm ³)	Melt Index
1-B	BUT	Gas	ZN	4.03	24200	98700	4.1	0.9194	0.94
2-H	BUT	Sol	ZN	3.80	24900	120000	4.8	0.9190	0.75
3-A	HEX	Gas	ZN	3.94	30000	111000	3.7	0.9208	0.9
4-C	HEX	Sol	ZN	3.77	36000	111300	3.1	0.9234	0.85
5-D	HEX	Gas	Met	3.08	44000	98000	2.2	0.9192	1
6-E	HEX	Gas	Met	2.56	43000	94000	2.2	0.9194	1.03
7-M	HEX	-	-	4.50	20600	74200	3.64	0.9192	-
8-G	OCT	Sol	ZN	3.20	17000	106000	6.2	0.9200	1
9-I	OCT	Sol	Met	5.00	22000	53000	2.4	0.9070	6.5
10-J	OCT	Sol	Met	3.20	38000	70000	1.8	0.9180	1.8
11-L	OCT	Sol	ZN	2.80	25900	114000	4.4	0.9212	0.63
12-F	LDPE	Gas	-	-	12000	88000	7.3	0.9190	2.3
13-K	LDPE	Gas	-	-	16000	66200	4.1	0.9203	2.31
14	HDPE	-	-	-	22300	74500	3.3	0.961	7.4
15	PP-1	-	-	-	-	-	-	-	-
16	PP-2	-	-	-	-	-	-	-	-

4.2. Pyris-1 DSC Apparatus.

The latest version of the Perkin-Elmer Differential Scanning Calorimeter (DSC) for thermal analysis, which is used in this study, is the Pyris-1 DSC apparatus (Figure 4.1). In this model, the temperature and heat controller, that regulates digital data output, is now built into the apparatus, and the operational software to monitor temperature and regulate heat flow is more user-friendly. This allows quick optimization of design of experiments, and more efficient handling of recorded data for mathematical and physical analysis.

First of all, the flow of dry nitrogen (X-dry N₂) into the main furnace chamber has to be regulated and metered properly to avoid moisture settling on the sample and pan holders, which would affect the heat flow between the furnace and the pan holders. In some cases, water vapor or gases may be generated due to a chemical reaction. The gas pressure has to be regulated (between 20 and 40psi) to an optimum value, depending on the nature of

the sample, the maximum temperature used during the experiment, the gas heat transfer coefficient, cooling agent nature, and heating and cooling rates of the sample.

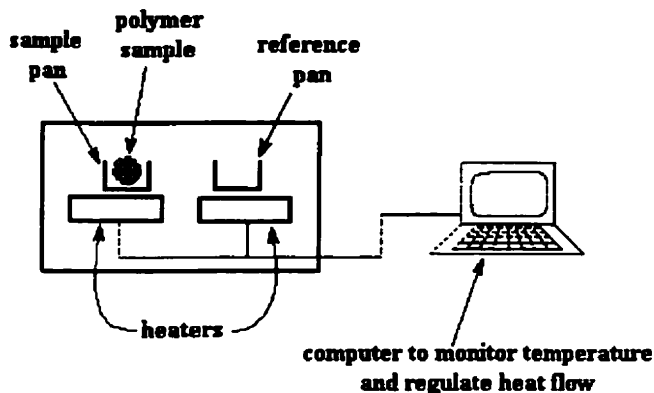


Figure 4.1 Schematic Representation of a DSC

The nitrogen gas stream cools the holders and thus can take with it an amount of heat generated during a heating step, and in this case, readings can be lower than expected. However, differences can be made small and added to the overall error.⁶⁷ The influence of the type of gas used as purge, depends on its thermal conductivity (see Table 4.2), and the heat transfer.⁶⁸ The DSC apparatus has default device settings which would detect when the combination of test conditions chosen is inappropriate (for instance, wrong cooling media and purge gas flow rate), which will protect the system against malfunction and damage.

Table 4.2. Thermal Conductivity of Some Gaseous Substances

Gas @ 1 atm	Thermal conductivity @ 373 K/(10 ⁻² J/smK)
Helium	17.77
Nitrogen	3.09
Air	3.17
Carbon Dioxide	2.23

A nitrogen source is also needed to ensure a “gas “ shield over the sample holders when the main chamber cover is opened to handle the sample and reference pans. This prevents moisture deposition inside the holders, or any foreign particles from reaching inside the instrument, thus protecting the furnace and the thermocouples. The pressure of the gas

can be regulated in the range 9-15psi., and a medium level is recommended, which was found to be sufficient; this becomes active when the button on the instrumental panel is turned to "ON".

4.2.1. Baseline, Temperature, Heat Flow and Furnace Calibration.

For experimental accuracy, the calibration is a crucial step in thermal analysis. The first step consists of assessing the manual baseline, without which any further steps cannot be made. The purpose is to adjust the heat flow and to reduce the imbalance between the sample and the reference pan holders. Three numbers are defined in order to describe the manual baseline settings for the Pyris-1 DSC (two if one uses the DSC-7, for instance, slope and baseline). The signal is observed on a scale that has the heat flow on the ordinate axis. The abscissa has the temperature interval or range of interest. A straight line that has a slope less than $3\text{mW}/^\circ\text{C}$ is acceptable.

In the process of plotting the manual baseline at the beginning of the program, the imbalance is due to the onset of the actual step in the run. The instrument performs an "equilibration step" before the program is launched, which consists of 10 readings at 10 second intervals of the heat flow and temperature values. If the recorded values are within the prescribed range set at the initial state, i.e. 0.01mW for the heat flow, and 0.01°C for the temperature, the program is initiated, otherwise it waits until one of the conditions is met. By increasing the rate of heating/cooling, a higher imbalance would be detected at the beginning of the process. To stabilize the process, a longer period is required, and thus the prediction of the "flat line" is improbable for a long-range temperature interval.

The next step is the temperature calibration. To ensure minimum error, the lag compensation has to be performed first. To determine lag-compensation, an Indium sample of $5 \pm 0.5\text{mg}$ is heated at rates of 5 and $20^\circ\text{C}/\text{min}$, from 120°C to 180°C . The lag compensation value is given by the following formula:

$$LC\# = \frac{OT_2 - OT_1}{T_2 - T_1} \quad (4.1)$$

where OT_2 and OT_1 represent the temperatures at onset of melting for the two heating rates T_2 and T_1 used. Due to the higher temperature gradient signal of T_2 , the onset of melting, will be at a higher value than for T_1 .

The lag-compensation obtained is now used in the temperature calibration that involves the use of the same Indium sample that is heated at a rate of 10°C from 120°C to 180°C . The onset values for the temperature and heat of melting (J/g) are recorded. To check that the test was correctly conducted, the calibration procedure is repeated after a 5-10 minutes pause, and the values obtained should match the prescribed ones for Indium of 156.6°C for the onset of melting, and 28.45J/g for the heat of fusion. The reference pan that is used with the Indium sample should have the same weight as that to be used with the sample in the thermal analysis experiment. A Sartorius electronic precision balance was used for weight measurements to within the required range of $\pm 0.01\text{mg}$. The heating rate used for the temperature calibration must be the same as the heating rate used for the thermal analysis of the polymer sample.

For the furnace calibration, the user has to define the temperature interval or range of interest before the procedure can be started. The instrument reads the heat flow values in mW for a determined time at the specified limits, and returns at the end the prescribed value within the range of error.

4.2.2. Sample Preparation and Instrument Set-Up.

To perform a reliable experiment, sample preparation and handling are important. Care was taken in sample encapsulation (crimping) and deposition into the sample pan holders. Particular attention was paid in weighing the sample to the required accuracy using a high precision balance. Procedures were followed to ensure proper compression molding of the polymer sheets from which the samples were cut.

To obtain the best results, the instrument manual baseline was checked daily before use, in order to ensure that it was within prescribed limits. A “not balanced” baseline can increase the difficulty in manipulating the raw data.

Using ice and water as the cooling agent, equilibration and stabilization of the system was required which took about 40-60 minutes for the heat flow reading to become stable. The duration of experiments was not allowed to exceed more than about 3 hours, because the ice melts and the overall temperature is increased, which will affect the true experimental data.

4.2.3. Method Editor Page or Experiment Design.

This step contains the procedure that will be performed during the actual run. Before the program is started, there are two options for data collection, time interval in seconds or the number of points under which data values are recorded. Time increment was chosen for the experiments, and was 0.033 minutes or approximately 2 seconds. The end condition can be specified to be different from the initial load temperature.

4.2.4. Experimental Run.

The aim of the thermal analysis procedure is to measure the heat flowing in and out of the sample. To eliminate the heat absorbed and released by the aluminum pan sample holders an experimental baseline has to be obtained under the same conditions as the actual run. By superimposing the baseline and experimental plots, the true heat flow for the sample is obtained. The trend of the transformation obtained is dictated by the phase change that occurs in the sample. Small imperfections observed can be related to the size and weight of the sample.

4.2.5. Data Analysis Using SigmaPlot Program.

Raw data from each experiment are obtained in the form of temperature/time and normalized heat flow/heat flow values. The data were analyzed using SigmaPlot5 software program. The area under each thermogram was obtained to determine the heat of fusion and the heat of crystallization. Depending on the data obtained, a suitable form of the generalized Simpson's rule was used for numerical integration. Heat of fusion and

heat of crystallization numerical values were thus obtained. Plots of the Avrami⁴⁵ equation along with the regression equations should be obtained in order to obtain the Avrami parameters. Due to the fact that polymeric substances cannot attain 100% crystallinity, Avrami's final expression is:

$$\Theta(t) = \chi(t) / \chi_{\infty} = \{1 - \exp(-kt^n)\} \quad (4.2)$$

where Θ denotes weight % crystallinity at time t , $\chi(t)$ is the absolute crystallinity at time t , χ_{∞} is the ultimate absolute crystallinity and k is the isothermal crystallization rate constant. Taking twice the logarithm of Equation 4.2 yields:

$$\log\{-\ln(1 - \chi(t) / \chi_{\infty})\} = \log k + n \ln t \quad (4.3)$$

and from the graphical representation of $\log\{-\ln(1 - \chi(t) / \chi_{\infty})\}$ versus $\log t$, the parameters, n and k can be determined from the intercept and the slope of the distribution, respectively.

4.3. Experimental Procedure.

The use of aluminum pans in the DSC limits the maximum temperature to 600°C. Because polyethylene degrades above 250°C⁶⁹, and processing conditions are normally in the range 180-200°C, the maximum temperature used in isothermal experiments was 230°C to avoid thermal degradation. Similar conditions were used for polypropylene.

4.3.1. Non-Isothermal Experiments.

Non-isothermal cooling scans, at different rates, for each resin were conducted. This enables the assessment of the temperature interval of interest. The rates employed were 1, 2.5, 5, 10, 20, and 40°C/min, and in some cases 0.5°C/min. Each resin sample was first kept at 50°C for five minutes (step 1, Fig. 4.2) and then heated at 10°C/min to 180°C (step 2; first melting), well above its expected melting temperature. It was held there for 5 minutes (step 3) to erase previous thermal history. Then, cooling to 50°C was performed at all of the rates given above (step 4), for each individual resin. The heating part of the

cycle was repeated at 10°C/min, at the end of cooling, to obtain the second heat of fusion (step 5 and 6; second melting). For each cooling rate, a different sample was used.

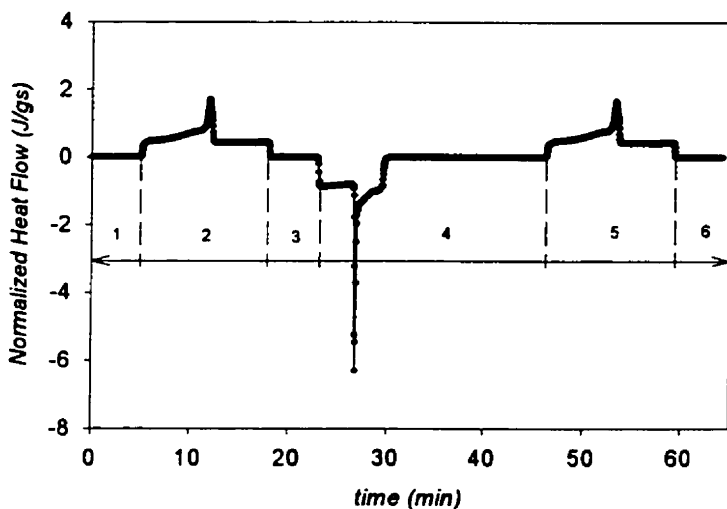


Figure 4.2. Non-Isothermal Thermogram at Selected Cooling Rate (20°C/min.).

Typical data for six cooling rates are shown in Figure 4.3 for LLDPE B (the crystallization interval only; step 4). The heats of fusion (for the first and second melting) and crystallization were determined and are tabulated in Appendix 4. The experimental melting temperature was recorded, and the on-set temperature of crystallization for a rate of 0°C/min was determined, by extrapolation, using non-linear regression.

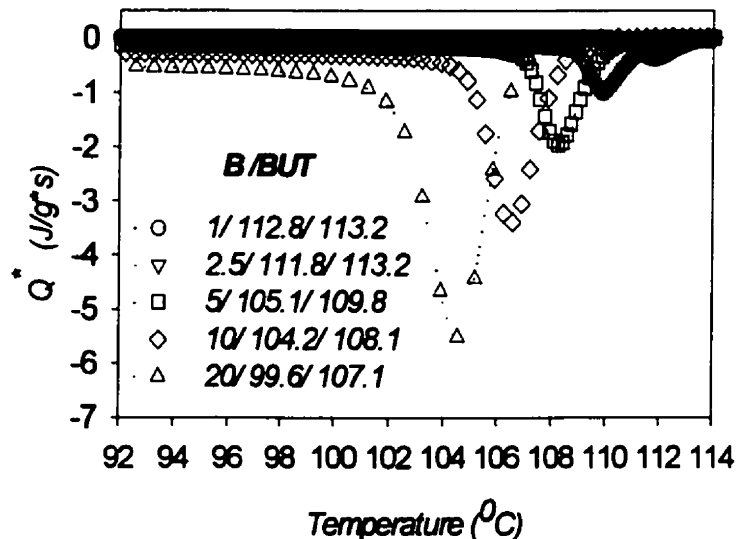


Figure 4.3. Non-Isothermal Experiments for LLDPE B (BUT/Gas/ZN). (Parameters Indicated- Legend: (i) cooling rate (°C/min.), (ii) heat of crystallization H_c , (J/g), and (iii) the on-set crystallization temperature (°C)).

4.3.2. Isothermal Experiments.

Using the data obtained, as shown in Figure 4.3, the temperature range over which the isothermal experiments should be conducted was identified. The temperature where the highest crystallization rate was observed, during the non-isothermal experiments, was chosen as a reference. Isothermal experiments were conducted at temperatures on each side of this reference temperature. A range of 16-20°C was used for this investigation. The heat of fusion and heat of crystallization were measured and are tabulated in Appendix 5. For each isothermal temperature, a different sample was used for the investigation.

The general procedure used in the analysis of the polymer samples to study isothermal crystallization behavior and kinetics is described below.⁶²

The first three steps are similar in both isothermal and non-isothermal experiments. Starting at 50°C, there is an initial isothermal holding (step 1, Fig. 4.4) for 5 minutes at

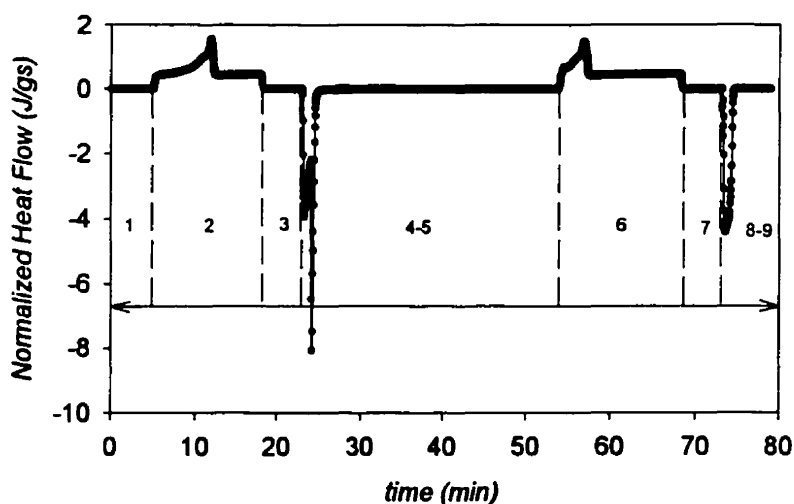


Figure 4.4. Isothermal Thermogram at 88°C for Resin E (Cooling Rate:100°C/min.)

the set load temperature. This period is required to bring the sample, initially at room temperature, to the apparatus temperature. The next step consists of a thermal scan, heating from 50°C to 180°C at a rate of 10°C/min (step 2). A holding time (step 3) of 5 minutes at 180°C was used to erase the previous thermal history of the sample that

occurred during pellet preparation, and consequently during compression molding of the sample sheet material. Subsequently, the sample is cooled rapidly, at 100°C/min. until it reaches the selected isothermal crystallization temperature. The sample is held at that isothermal temperature for 15 to 120 minutes (when the crystallization temperature approaches the melting temperature higher holding periods are required) until the crystallization is complete, as indicated by the termination of the heat flow increase on the instrument panel (step 4-5). The value of the heat flow remains constant when the ultimate crystallization is achieved. At this point the sample is heated again at a rate of 10°C/min to 230°C (step 6) and held for five minutes to erase previous thermal history (step 7). From this temperature, cooling was carried out again at the same rate (100°C/min.) but to the final temperature of $T_f = T_{iso} + 50$. Usually, this final temperature

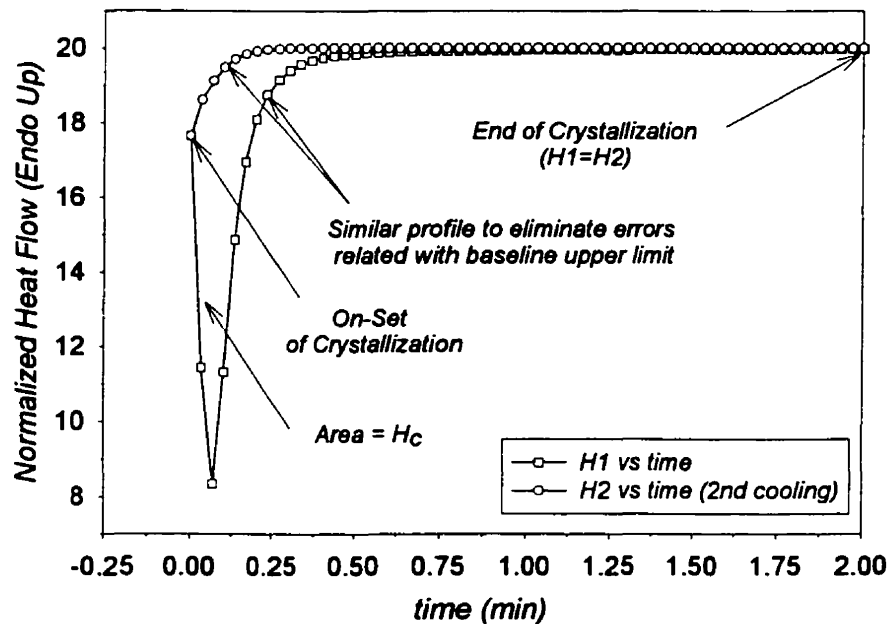


Figure 4.5. Typical crystallization peak (H1-first heating; H2-second heating, after crystallization).

is higher than the experimental melting temperature, and, as expected, no crystallization occurs. By superimposing the two plots (Fig. 4.5), the area corresponding to the “true” crystallinity can be more easily identified, and errors due to baseline assessment are minimized. This procedure also provides an approach to eliminate transient and heat transfer effects.

CHAPTER 5

DATA ANALYSIS

In this chapter, the procedures employed to analyze the experimental data are described. The steps required to retrieve the kinetic parameters from the isothermal experiments are presented first. Also, the estimation of the experimental heats of fusion before and after the crystallization is explained. Finally, the use of isothermal kinetic parameters in the analysis of the non-isothermal experiments is discussed.

5.1. Isothermal Crystallization Experiments.

The crystallization of polymers is strongly related to nucleation and growth. Both phenomena are polymer architecture dependent. This means that the structural conformation will affect the type of nucleation and crystallization kinetics, in addition to the crystallinity and morphology of the material.⁷⁰

Isothermal crystallization can be defined as controlled crystallization at a specific temperature, below the polymer melting temperature. The duration of crystallization depends on polymer type and the temperature at which the investigation is conducted. From several minutes, one can reach several hours, weeks or up to months. The literature indicates higher rates of crystallization for polymers with regular chains.⁷¹ This has been confirmed by experiments involving crystallization from solution.⁷²

The crystallization heat evolved is monitored with the DSC, and the fraction crystallinity can be determined by employing one of the following relationships⁷³:

Definitions of Crystallinity (χ_c)

<i>Based on</i>	<i>Definition</i>
Specific volume (v)	$\chi_c = \frac{v_a - v}{v_a - v_c}$
Specific Heat (c_p)	$\chi_c = \frac{c_p^a - c_p}{c_p^a - c_p^c}$
Specific Enthalpy (h)	$\chi_c = \frac{h_a - h}{h_a - h_c}$
Specific Enthalpy of Fusion (Δh_m)	$\chi_c = \frac{\Delta h_m}{\Delta h_m^c}$
Infrared Mass Extinction Coefficient (ϵ)	$\chi_c = \frac{\epsilon_\lambda}{\epsilon_\lambda^{(c)}} = 1 - \frac{\epsilon_\lambda}{\epsilon_\lambda^{(a)}}$
X-ray Scattering Intensity (I – area under selected peak)	$\chi_c = \frac{I_c}{I_c + I_a} \approx 1 - \frac{I_a}{(I_a)_{melt}}$
NMR	$\frac{\chi_c}{1 - \chi_c} = \frac{Area_{BroadComp}}{Area_{NarrowComp}}$

In the above, c refers to the crystalline phase and a to the amorphous phase. When no subscript is used, reference is made to the sample under consideration. According to Avrami⁴⁵, as previously mentioned, the evolution of the crystallization process can be expressed by the equation:

$$\chi(t) = 1 - \exp(-kt^n) \quad (5.1)$$

where $\chi(t)$ is the fraction of the material transformed at time t ; n , and k are constants. The parameter n is an integer that depends on the mechanism of nucleation and the form of the crystal. On the other hand, k , the rate constant, is linked with the nucleation and growth parameters, i.e. for spherulitic growth, $n=3$ and $k = \frac{4}{3}\pi v^3 N \rho^*$, where ρ^* is the

relative density $\frac{\rho_c}{\rho}$, v is the rate of crystal growth, and N is the number of nuclei (predetermined in this case by constant number of nuclei per cm^3).

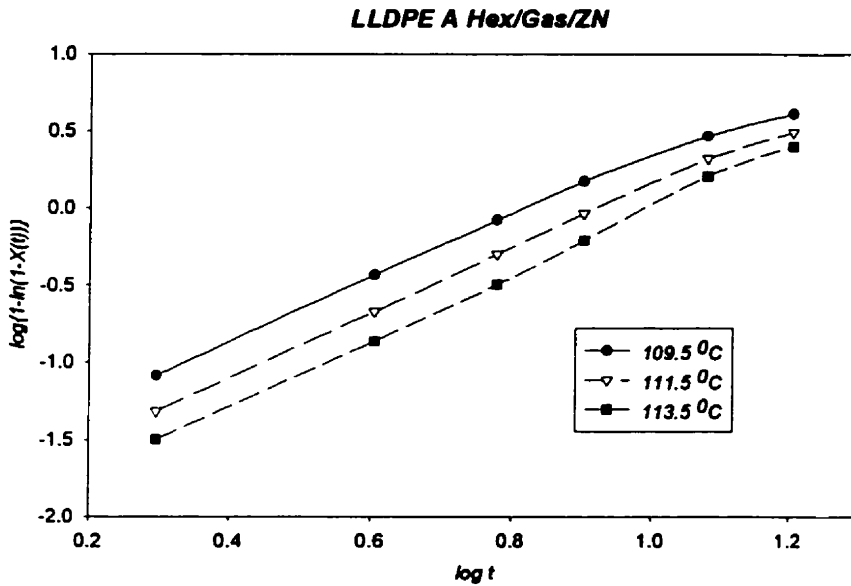


Figure 5.1. Plot of $\log\{-\ln[1-x(t)]\}$ versus $\log t$ for Isothermal Crystallization at selected Temperatures ($^{\circ}\text{C}$) for LLDPE A (HEX/Gas/Z-N).

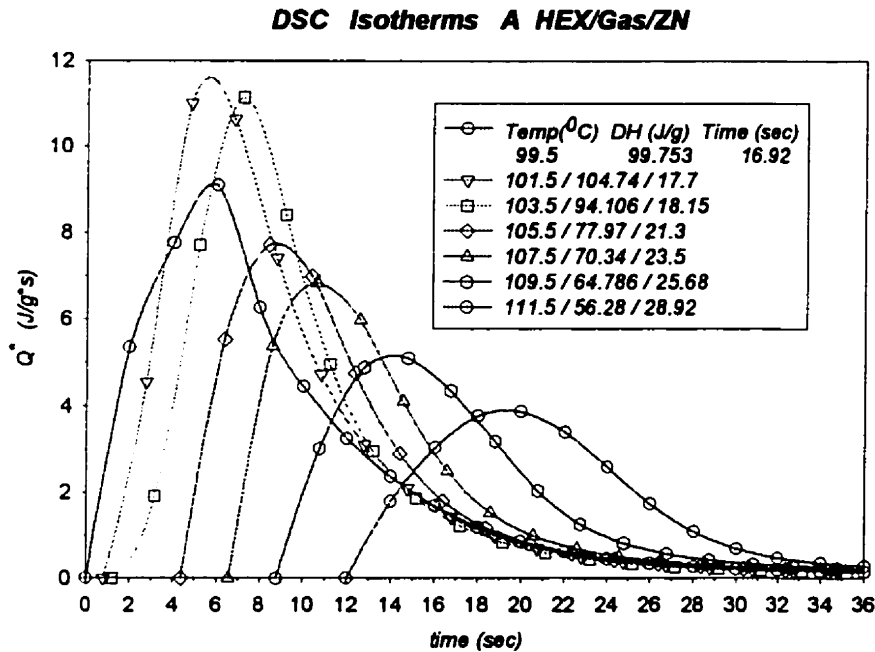


Figure 5.2. Normalized Heat Flow versus Time during Isothermal Crystallization for LLDPE A (HEX/Gas/Z-N) at selected Temperatures ($^{\circ}\text{C}$). (Indicated Parameters: (i) isothermal temperature ($^{\circ}\text{C}$), (ii) heat of crystallization H_c (J/g), and (iii) induction time (sec.)).

In Fig. 5.1, a typical plot of the crystallization data, using the Avrami equation (in its logarithmic form, Eq. 4.3) is shown. From the plot, the Avrami exponent is obtained from

the slope, and the intercept gives the value of the rate constant, k , for which the Arrhenius expression is:

$$k = A \exp(-E / RT) \quad (5.2)$$

where A is the pre-exponential factor and E is the activation energy of the crystallization process. In our study, the values were determined by non-linear regression using Sigma Plot software.

Figure 5.2, shows typical DSC isotherms for resin A. The detailed experimental isothermal plots for all the resins are given in Appendix 3. In Figure 5.2, it can be seen that the maximum crystallization rate occurs at 101.5°C.

5.1.1. Transient Response.

Due to the fact that, during DSC measurements, the heat cannot be released fast enough to match the programmed temperature, the system exhibits a transient response (Figure 5.3) as it approaches the true isothermal state.

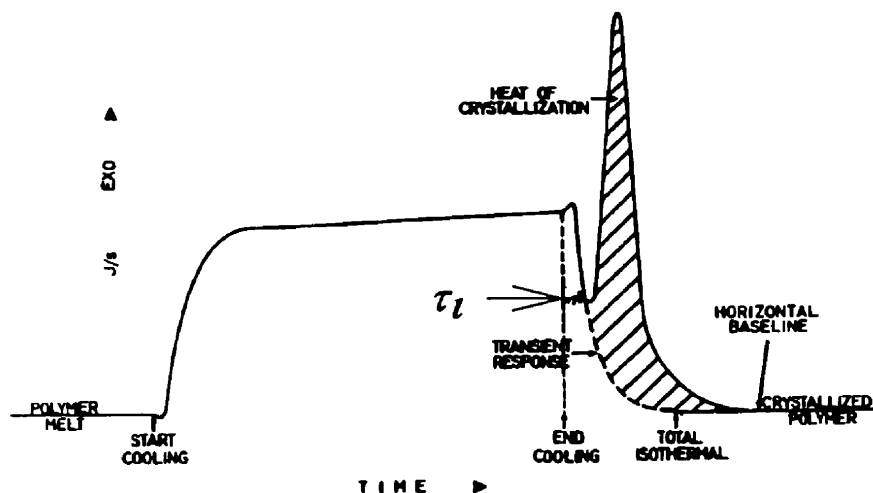


Figure 5.3
Transient Effect in
a DSC Isotherm

In order to correct for this situation and for any possible crystallization before reaching the isothermal crystallization temperature, the sample is remelted and cooled again at the same rate, as described in section 4.3.2 and Figure 4.5. Thus, a reference baseline for the exotherm is constructed as shown in Figure 5.3.⁵² The shaded area equals the crystallinity obtained in the isothermal crystallization.

The transient response manifests itself whenever a specific step of the program is started. This can be interpreted as an imbalance, which is strongly influenced by the size of the parameters used in the thermal investigation. For instance, a higher rate of cooling or heating will induce a higher imbalance. For an endothermic process such as melting, a typical plot is presented in Figure 5.4, where the heating rate used was 10°C/min.

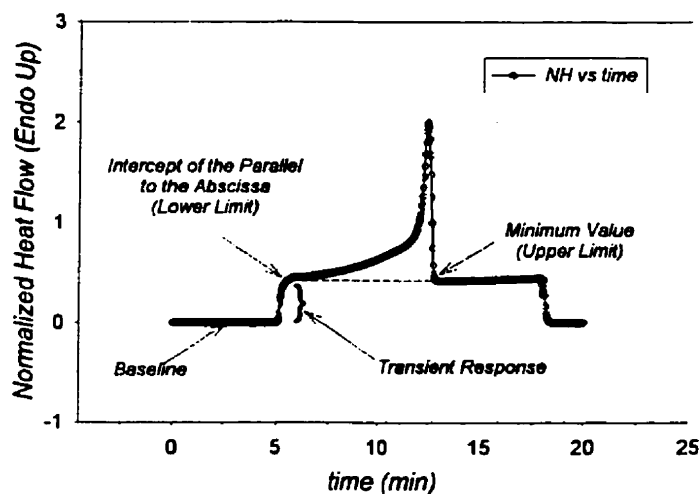


Figure 5.4 Typical Melting Plot used to determine the Heat of Fusion using a DSC.

To obtain the experimental latent heat of fusion, one has to choose carefully the limits of the integration. The limits for the integration were chosen first on the horizontal line to the right hand side of the peak. Then, a line parallel to the abscissa was drawn from that limit. The intersection with the rising profile, on the left, was set as the left limit. The integration was carried out using Simpson's rule for 1, 2, ... , N-1, N points.

5.1.2. Induction Time.

As the polymer is cooled from the melt, crystallization develops as a result of random fluctuations of order of the polymer chains.⁷⁴⁻⁷⁷ During cooling, the polymer experiences a non-isothermal step.^{78,79} The rate employed will affect the nature of the nucleation process. For polyethylene^{80,81}, homogeneous nucleation is considered to take place at rates higher than 55°C/min.

The time period before the initial signs of evolution of heat of crystallization are detected is known as the “(apparent) induction time”⁸², τ_i , or crystallization start time, τ_{st} , as indicated in Figure.5.5. The introduction of the concept of the “incubation time”⁸³, as shown in Fig.5.5, provide some clarification of the meaning of the induction time. The “incubation time” (τ'_i) is up to the point where the signal deviates from zero value. It is considered that from this point, the crystallizing particles are visible under an optical microscope⁷⁷. The “induction time” is the limit from where measurable crystallization occurs. Thus, to be more precise, we can say that the “incubation time” represents the period required, at a supercooled state, to reach the equilibrium nucleus dimension, and the induction time is the time required to reach the steady-state of nucleation. The period of crystallization is given by the following equation⁸⁴:

$$\tau_{end} = 2(\tau_{0.5} - \tau_{st}) + \tau_i \quad (5.3)$$

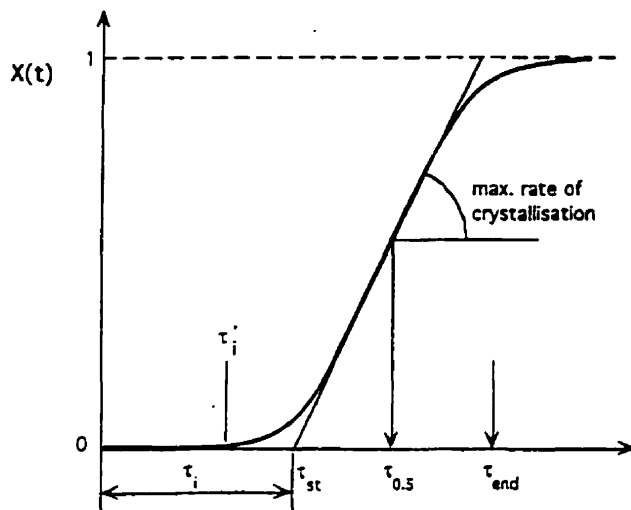


Figure 5.5 Schematic Diagram of the Crystallization Process as a function of time

Another characteristic quantity is the time at the point of inflection in the curve. This is the half time of crystallization, $\tau_{0.5}$, where the resin crystallinity reaches 50%, ($\chi = 0.5$), of its maximum attainable value.

Godovsky and Slonimsky⁸⁵ have formulated the dependence of the induction time on the degree of supercooling and the time required for the creation of stable nuclei as:

$$\tau = P(\Delta T)^{-\epsilon} \quad (5.4)$$

where P and ϵ are fitted parameters.

The experimental induction time was calculated using the data obtained from first and second cooling parts of the experiment. The time of the beginning of crystallization was associated with the deviation from the positive trend of the signal. The time elapsed between the end of cooling and the beginning of crystallization represents the induction time. The end of cooling corresponds to the intersection of the results from first and second cooling sections, as shown in Figure 5.2 and 5.3. The results are provided for both PE and PP samples in Appendix 6.

The large amount of data collected suggested that a new method can be found to help determine in a much easier way the baseline for the cooling step. Different authors define in various ways the upper limit for integration. The method used here,⁶² as previously mentioned, in Chapter 4, worked for high-density polyethylene with very good results, and for Polypropylene. For low-density polyethylene, a much simpler method was formulated.

The period of time elapsed from the on-set of cooling up to the end of the programmed cooling represents the physical time required to attain the experimental isothermal temperature (see Fig.4.5 in Chapter 4). The time elapsed between the end of the programmed cooling and the local minimum of the isothermal plot (see Figure 5.3) represents the induction time. Thus, the crystallization starts at this point, and crystallinity is measured from this point onwards.

5.1.3. Overall Crystallization Rate.

The Avrami equation, Eq. 5.1, describes the overall rate of crystallization incorporating the effects of both nucleation and growth. Different Avrami exponents may be interpreted as indicated in Table 5.1⁸⁶. The non-constant growth rate of the expanding spherulites and associated secondary crystallization processes seems to be the reason for deviation of experimental results from the Avrami equation.

Table 5.1 Different Values of Avrami Exponent and their Interpretation

<i>Avrami Exponent</i>	<i>Nucleation</i>	<i>Growth Habit</i>	<i>Growth control*</i>
[1]	[2]	[3]	[4]
0.5	Instantaneous	Rod	Diffusion
1	Instantaneous	Rod	Interface
1	Instantaneous	Disc	Diffusion
1.5	Instantaneous	Sphere	Diffusion
1.5	Homogeneous	Rod	Diffusion
2	Instantaneous	Disc	Interface
2	Homogeneous	Disc	Diffusion
2	Homogeneous	Rod	Interface
2.5	Homogeneous	Sphere	Diffusion
3	Instantaneous	Sphere	Interface
3	Homogeneous	Disc	Interface
3.5	-	-	-
4	Homogeneous	Sphere	-
5	Instantaneous	Sheaf	Interface
6	Homogeneous	Sheaf	Interface

*The rate-limiting steps can be either the rate of diffusion of molecules to the growth surface, i.e., diffusion control, or the rate of attachment of such molecules to the interface, once they reach it, termed interface control.

5.2 Non-Isothermal Crystallization Experiments.

Conventional polymer processing occurs under non-isothermal conditions. Isothermal conditions are useful when the fundamentals of polymer crystallization such as kinetics and morphology are studied.⁸³ In the present study, the process was simplified by

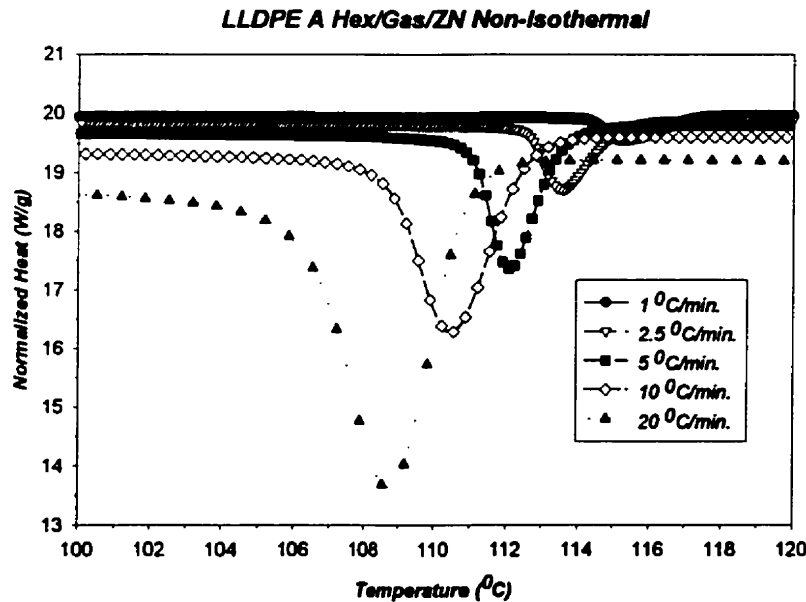


Figure 5.6 Normalized Heat Flow (Endo Up) versus Temperature during Non-Isothermal Crystallization for LLDPE A (HEX/Gas/Z-N) at Different Cooling Rates.

employing a constant rate of cooling. However, in the analysis, it is necessary to deal with information related to the heat transfer, latent heat of crystallization and their relationship with the kinetics of crystallization.⁸¹

The variation of crystallinity during DSC scanning experiments was investigated using Simpson's rule for integration. The parameters $\chi(\infty)$, $k(t)$ and n required by this approach were from the results of isothermal crystallization studies as described in Section 5.1. For all the resins, the non-isothermal results are tabulated in Appendix 4 and Appendix 7 for the simulation.

For a non-isothermal crystallization process, the approximation was made that the entire process may be assumed to consist of infinitesimal small isothermal steps.^{88,89} In the case of crystallization under non-isothermal condition, the process can be modified, keeping in mind that the variation of temperature is linear and represented as follows:

$$T = T_0 + \beta \cdot t \quad (5.5)$$

where T_0 is the on-set temperature, T is the temperature after time t , and β is the heating rate. As required for this case, the cooling cycle requires a negative value for β and Eq. 5.5 can be written as:

$$T = T_0 + (-\beta) \cdot t \quad (5.6)$$

The mathematical interpretation of the peak suggests that at the maximum value of the peak, the derivative of the crystallinity given by Eq. 5.7

$$\chi' = d\chi/dt = nkt^{(n-1)} \cdot (1-\chi) \quad (5.7)$$

should be equal to zero, and also,

$$\chi'' = d\chi'/dt = 0 \quad (5.8)$$

The following mathematical derivation allows the determination of the activation energy E and the Avrami coefficient n from the experimental data of the crystallization exotherm recorded under linearly varying temperature.⁹⁰

Combining Eqs. 5.1, 5.5, and 5.7 and applying the condition specified by Eqs. 5.2 and 5.8 the following relationship is obtained:

$$\frac{\chi'}{(1-\chi)} = nA \cdot e^{-E/RT(T_0+\beta \cdot t)} t^{(n-1)} \quad (5.9)$$

which can be rewritten after differentiation as:

$$\frac{\chi''(1-\chi) + (\chi'')^2}{(1-\chi)^2} = nAe^{[-E/R(T_0+\beta t)]} \left[\frac{-E\beta}{R(T_0+\beta t)^2} t^{(n-1)} + (n-1)t^{(n-2)} \right] \quad (5.10)$$

At the peak maximum $\chi'' = 0$, thus:

$$\frac{\chi'^2}{(1-\chi)^2} = nAe^{E/RT(T_0+\beta t)} t^{(n-1)} \left[-\frac{E\beta}{R(T_0+\beta t)^2} + \frac{n-1}{t} \right] \quad (5.11)$$

Substituting Eq. 5.5 into Eq. 5.9 and after rearrangement, one can obtain the final expression in the form:

$$\frac{\chi' t}{(1-\chi)} = (n-1) - \frac{E\beta t}{RT^2} \quad (5.12)$$

This relationship represents the crystallization behavior at the temperature corresponding to the peak (i.e. maximum) of the non-isothermal exotherm. To denote the peak temperature, the suffix "p" can be used, and the t parameter replaced by the corresponding temperature difference as, $\beta t = T_p - T_0$. From the plot of $\chi'_p [(T_p - T_0)/\beta(1-\chi_p)]$ vs. $[(T_p - T_0)/T_p^2]$ which should be a linear function, the slope equal to E/R , and the intercept equal to $(n-1)$ are thus determined.

We should mention that for this and previous analyses, the χ quantity was evaluated from the ratio of the area under the crystallization exotherm per unit mass of the sample. The χ_p value is considered as the extent of the crystallization process at the peak maximum and is determined as the fractional area under the exotherm (from its onset temperature, T_o , to the peak temperature, T_p) to the total area under the crystallization curve. The T_o value is chosen as the point where the trend of the exotherm starts to decrease, after the induction time, and the peak temperature is the point of intersection of the tangents on the right and left hand side of the exotherm.

CHAPTER 6

RESULTS AND DISCUSSION

The results are presented in two sections, mainly corresponding to the two types of experiments carried out: isothermal and non-isothermal. For each section, a comparative study of the results within the same group and between different groups is given and discussed. Analyses and analogies with previously reported results for similar types of materials are given. Experimental values of the kinetic parameters obtained are tabulated, as well as the fitting of the experimental data using the theoretical models presented in detail in the previous chapters. Due to the large amount of data collected, the bulk of data and the graphs are presented in the Appendices.

6.1. Isothermal Crystallization Kinetics.

The polyethylenes are the most commonly used resins in the thermo-plastic sector, mainly because they are obtained with a variety of molecular architectures. The Ziegler-Natta, Metallocene and now combined Metallocene catalysts are largely responsible for this behavior.⁹¹

Sample films for all 16 resins were prepared by compression molding as described in Appendix 2, following previously recommended procedures.^{62,92-95} The films were 0.2mm thick, free of trapped air (bubbles), uniform and free of defects, from a macroscopic point of view. Circular disks were cut with a final weight between 5 and 7mg. Higher density resins produced samples with a higher weight for the same thickness and diameter. The density range of samples was from 0.907 g/cm³ to 0.961 g/cm³.

6.1.1. Heating and Cooling Experiments.

DSC thermograms recorded during heating of a sample, at a constant rate, before and after crystallization, supply information regarding the enthalpy of fusion, ΔH_f , and the melting temperature, T_m . The experimental values were determined with the Perkin-Elmer Pyris-1 DSC differential scanning calorimeter operated at a heating rate of 10°C/min, and are tabulated for all of the resins in Appendix 5. The area of the melting endotherms (calculated as described in Chapter 5) represents ΔH_f and can be converted to the degree of crystallinity, by considering the enthalpy of fusion of a perfect polyethylene crystal as 69 cal/g.⁹⁰ The melting temperature of the sample was taken as the maximum value at the peak of the trace for the first melting (for compression molded samples) and second melting (after cooling or crystallization) cycles.

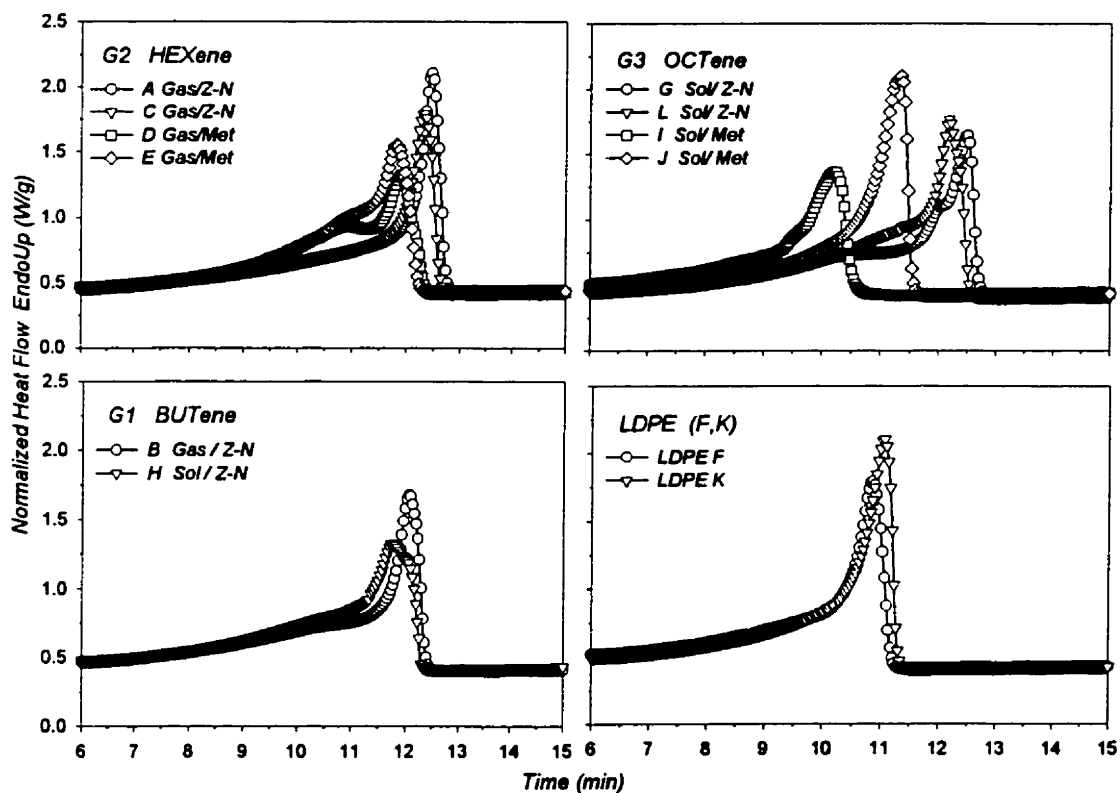


Figure 6.1. DSC Endotherms for Linear/Low Density Polyethylene (First Melting)

Typical endotherms obtained in the first melting of compression molded samples are shown in Figure 6.1. In all these thermograms, the temperature at zero time was 50°C.

Metallocene resins tend to exhibit lower melting points than the Z-N resins having the same co-monomer. Within each co-monomer group, resins based on the same catalyst exhibit similar crystallization profiles. Ziegler-Natta and gas phase metallocene catalyzed resins exhibit a shoulder in the endotherm. While all resins appear to start the on-set of melting at approximately the same temperature, the metallocene resins tend to melt completely before the corresponding Z-N catalyzed resins. As can be seen in Appendix 4 and 5, the heat of fusion of compression molded samples appear to be independent of the cooling rate. Within the same co-monomer group, metallocene catalyzed resins had a lower heat of fusion than the Z-N resins. Resin I had the lowest heat of fusion. It should be noted that resin I had the lowest density and the lowest M_w . Furthermore, it had the highest branching density among all resins. Table 6.1 summarizes the data for all the resins obtained for heating rates of 10°C/min.

Table 6.1. Heat of Fusion and Peak Melting Temperature of Compression Molded Samples. (First Melting; Heating Rate: 10°C/min.)

<i>Resin</i>	<i>Heat of Fusion (J/g)</i> <i>(average)</i>	<i>Peak T_m</i> <i>(°C)</i>	<i>Resin</i>	<i>Heat of Fusion (J/g)</i> <i>(average)</i>	<i>Peak T_m</i> <i>(°C)</i>
<i>B</i>	106.7	120.1	<i>G</i>	108.2	123.4
<i>H</i>	106.2	116.2	<i>I</i>	81.8	98.1
<i>A</i>	109.6	123.5	<i>J</i>	109.9	111.3
<i>C</i>	107.5	122.3	<i>L</i>	114.8	119.5
<i>D</i>	108.1	117	<i>F</i>	106.5	107.5
<i>E</i>	111.7	117	<i>K</i>	114.6	108.7
<i>M</i>	103.2	124.1	<i>PP1</i>	87.5	159.2
<i>HDPE</i>	199.3	133.6	<i>PP2</i>	84.7	158.1

The second heat of fusion followed a similar pattern for all the resins, except that it tended to be somewhat larger than the first heat of fusion. Polypropylene resins, as expected, exhibited lower heats of fusion, while the HDPE resin showed a much higher heat of fusion than LLDPE resins.

The peak melting temperatures of Z-N resins were generally higher than 120°C (except resin L, 119°C), while the metallocene resins showed peak melting temperatures below 120°C, with resin I showing a peak melting temperature of around 98°C. As expected, HDPE has a higher peak melting temperature of around 133°C, while PP showed the highest value at around 158°C. There were small changes in the peak melting temperature

(usually a slight increase) during the second melting. However, the above pattern was maintained. The integral values for the heat of fusion, ΔH_f , for the second melting, after crystallization are not reported for all resins. The on-set of melting (at the end of the isothermal holding) was difficult to assess, and this might be due to the effect of the crystallization temperature (i.e. lower for LLDPE by comparison with HDPE).

The crystallizing regions of each copolymer have different molecular lengths. Haigh and Mandelkern⁹⁷, Fu *et al.*⁹⁸, and Galante *et al.*⁹⁹ suggest that the complex structure and the differences in the crystallization rate of the polyethylene co-monomers with α -olefins, mainly n-butene, n-hexene and n-octene, are primarily related with the activation energy for segmental transport (the non-crystallizable component, i.e. the co-monomer, affects the segmental mobility to different degrees).

It is now generally accepted that the SCB are components of the amorphous region, when a molten polymeric sample undergoes crystallization at a predetermined cooling rate. The absolute percent crystallinity decreases in this case from 60-80% for HDPE, to 30-50% for LLDPE. In the case of short-chain-branched-polyethylene (SCBPE) the chain structure is mainly responsible for the crystal shape, size and distribution, thus dictating the end properties of the final product. Ziegler-Natta catalysts have poor control of co-monomer incorporation, and therefore, a mixture of polymers with great differences in both chain length and co-monomer sequence distribution is obtained.¹⁰⁰⁻¹⁰⁶ On the other hand, metallocene catalysts produce polymers with narrower molecular weight distribution and *very* uniform co-monomer sequence distribution that gives more homogeneity with appended homogeneous chain branches. Mirabella¹⁰⁷ and recently Hill and Barham¹⁰⁸ and Mumby *et al.*¹⁰⁹ have attempted to explain the phase separation in the melt of a SCBPE in a certain range of molecular weights and SCB content.

Multiple peaks, observed during melting for Metallocene LLDPE (i.e. resins D and E) could be explained. Overall, each individual chain has a uniform distribution of the SCB which tends to lead to a "thermal segregation", a non-equilibrium, kinetic process.¹¹⁰ This concept can be explained if we recognize two types of heterogeneity in a SCBPE system,

namely intra- and intermolecular heterogeneity. The first one states that the SCB distribution is not uniform along the chain backbone, while all the molecules have the same SCB distribution. The latter one, instead, states that the SCB distribution is not uniform. The SCB distribution is different in some molecules than in others. The phenomenon is more pronounced in co-monomers obtained via Ziegler-Natta catalysts. Morphological studies could come in support of this theory as well as ^{13}C -nuclear magnetic resonance (NMR) and temperature raising elution fractionation (TREF) experiments.¹¹¹

Thus, upon crystallization and melting, multiple peaks can be observed. Their distribution and appearance might be strongly influenced by the heating/cooling rate. Usually single melting peaks are obtained for high and low undercoolings in the studied range of temperatures, as reported by Tanem and Stori.¹¹²

6.1.2. Isothermal Kinetic Parameters.

DSC thermograms recorded during cooling at a constant rate supply information regarding crystallization rate, $d\chi/dt$, as a function of temperature. During the melting of the sample, the final baseline needed to estimate the heat of fusion can be easily determined. For the crystallization experiments, the method developed by Samara⁶² was employed, taking into account also the methodology suggested by Chu⁴³, citing Hay *et al.*,⁸⁸ and most recently by Turi.¹¹³

In practice, the kinetic parameters are obtained by taking twice the logarithm of the Avrami equation. The following logarithmic form can be written:

$$\log \left\{ -\ln \left[1 - \frac{\chi(t)}{\chi_{\infty}} \right] \right\} = \log k + n \log t . \quad (6.1)$$

By substituting the values obtained for percent crystallinity versus time for each crystallization temperature, a plot of the term on the left of equation 6.1 versus $\log t$ is obtained. The DSC experimental data used in conjunction with Eq. 6.1 are presented in Appendix 3. It is now fairly simple to obtain the values of the Avrami exponent, n , from the slope, and rate constant, k , from the intercept on the abscissa of the straight-line

portion that correlates the data with the exponential relationship. It should be noted that t is the time spent during the process of crystallization measured from the onset of crystallization, the induction time being excluded. One of the major limitations of the Avrami model is that the linear part does not cover all of the data range. The complete sets of results regarding the induction time and isothermal kinetic parameters are tabulated in Appendix 6.

SigmaPlot software was used to obtain the values of the parameters, employing non-linear regression (NLR) for both Avrami and Tobin models, as given in Appendix 6. The tabulated heat of crystallization is expressed in J/g and the values of the induction time are in seconds. The latter is determined as the time elapsed between the programmed end of cooling and the onset of crystallization. The values obtained for n are fractional (theoretical kinetic models use integer values) and, in some cases, they increase with increasing isothermal temperature (resins B/BUT, C/HEX, J/OCT and LDPE F) or follow a pattern that is similar to the changes in the rate constant value (resins B/BUT, A/HEX and G/OCT).

Comparisons were made between resins from the same group (intra-group), and between groups (inter-group). For this purpose the values of the rate constant, k , were recalculated using the non-linear regression for a constant Avrami exponent (i.e. $n = 2$). The values are tabulated in column 8 in Appendix 6. The constant exponent value was chosen as 2, since the experimental values obtained were between 1.5 and 2.5.

The variability of n may be related to the fact that all the experiments were conducted close to a temperature where the highest rate of crystallization can be achieved, while the cooling media used was a mix of ice and water. This temperature value is known to exist between $(0.80-0.85) \times T_m$. The use of ice limited the accessibility of longer isothermal holding times at higher crystallization temperatures. The longest holding period was about 180 minutes. For higher temperatures, the required holding time could reach several hours or days, which cannot be achieved, when cooled with ice. Lower values of the Avrami exponent are observed in this case. Morphological studies could provide a basis for selection of the most appropriate value of n .

Typical plots of DSC isotherms for selected resins are shown in Figure 6.2. It is worth noting, in this case, the characteristic shape of the endotherms for the different polymers.

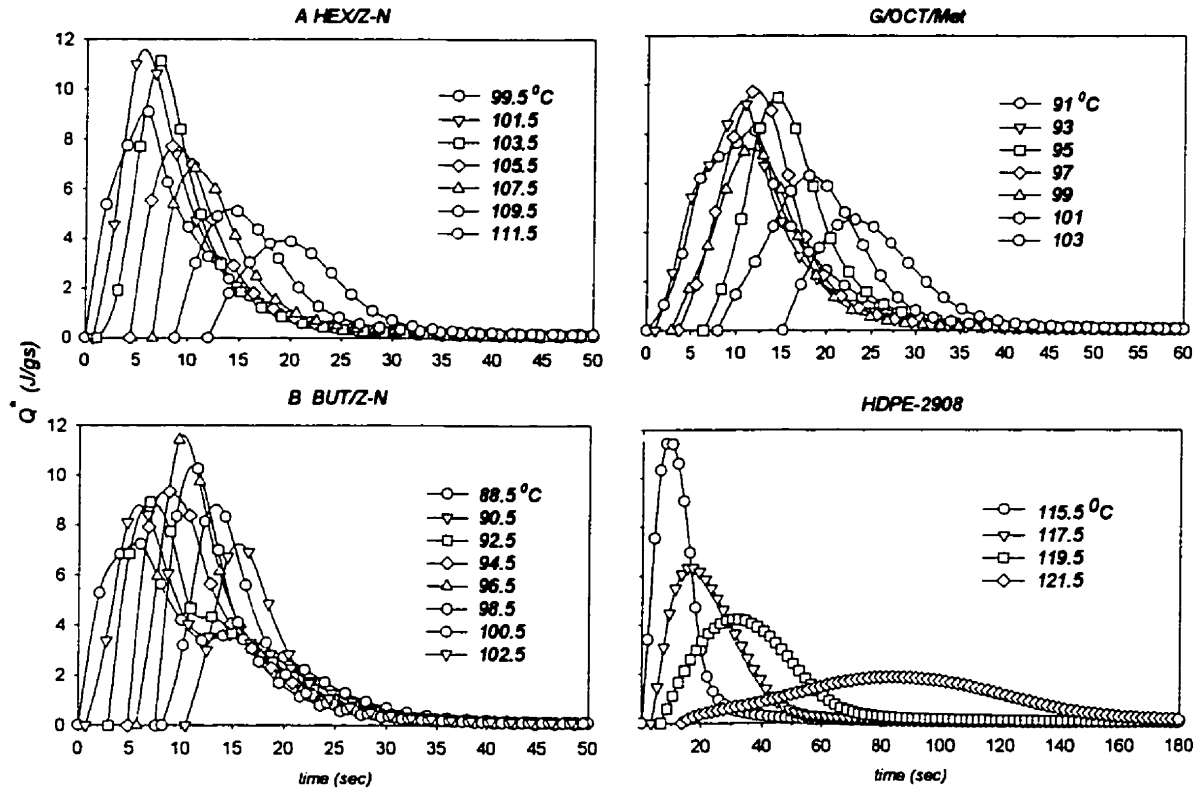


Figure 6.2. DSC Isotherms for Selected Resins at Various Isothermal Crystallization Temperatures ($^{\circ}\text{C}$).

It can be seen that the shape of the curves varies significantly with temperature and resin type. Resins A, B and G exhibit shoulders, over a temperature interval below the temperature at which the maximum crystallization rate occurs.

It is well known that crystallization is a two-step process that occurs mostly heterogeneously, and involves nucleation and growth. Binsbergen¹¹⁴ suggested the type of foreign body that initiates the nucleation in this particular case. For macroscopic nucleation, a large number of spherulites develop at the border and contact surface, and, depending on temperature, different morphologies may develop and form “transcrystalline regions”, in which the crystals grow normal to the surface.¹¹⁵ The

macroscopic surfaces could be metal, such as aluminum or copper¹¹⁶⁻¹¹⁹, other polymers^{116,118-126} (i.e. polymer fibers), and carbon or glass fibers.¹²³⁻¹³⁰ Fitchum and Newman¹¹⁵ explained the morphology of the transcrystalline region by considering the geometrical effects in the proximity of the growing nuclei. Shaner *et al.*¹¹⁷ made the analysis, taking into account the effects on a glass slide. Mechanical stresses were also reported.^{120,131,132}

For sample B, a complex profile is observed after the maximum value is achieved. In the present study, the existing transcrystallinity can be due to the contact between the polymer surface and the aluminum pan. The role of aluminum (Al_2O_3 -alumina) as a nucleation agent has been reported and demonstrated.^{116,118} The effect was reported in the analysis of high-density polyethylene¹²¹ and polypropylene.¹³³ The polypropylenes, both PP-1 and PP-2, exhibit shoulders.

For all samples, the Avrami model over-predicts the experimental values, as observed, at very low temperatures. Similar behavior is observed also if the experimental data are fitted using the Tobin model or polynomials by Non-Linear Regression (NLR) analysis. As reported by others,^{116,121,133} this effect can be attributed to the secondary crystallization that takes places during supercooling.

6.2. Non-Isothermal Crystallization.

Polymer processing operations occur under non-isothermal conditions, which involve a continuous variation of temperature with time. The temperature distribution is a sum of two main effects. The first effect is due to the continuous cooling of the system, whereas the second is due to the crystallization phenomenon itself, a generator of heat, as an exothermic process.¹³¹ Usually complex mathematical models, that are able to combine the heat transfer calculations with crystallization kinetic data and latent heat of fusion, are employed in the study of kinetic data for the observed sample. The mathematical models, explained in detail in Chapter 2, were simplified significantly by Kamal and Chu,⁹⁰ by employing the local isothermal state in non-isothermal DSC experiments when

temperature is decreased at a constant rate. Their assumptions take into account negligible secondary crystallization in the case of non-isothermal operations. For numerical evaluation, the mathematical model proposed by Ziabicki⁵⁰ was used prior to the Nakamura⁴⁹ non-isothermal transformation model, in which the relative crystallinity is expressed as a function of temperature. A computer program developed by Samara *et al.*⁶² was used for the simulation. Using a constant value for the Avrami exponent (i.e. $n = 2$ or 3) at different cooling rates, and setting the temperature range, a series of non-isothermal data were generated (Appendix 7). A comparison between the simulation with the experimental results is shown in Appendix 8. A temperature increment was set at 0.01°C , an interval small enough, to allow convergence to the percent crystallinity. In all cases, the experimental values are well predicted for $n=2$. The rate constant in Nakamura's model, $K(T)$, is a parameter related to the crystallization rate constant of the Avrami equation, $k(t)$, by the following relationship:

$$K(T) = (k)^{1/n} \quad (6.2)$$

where n has the same value and significance as in the isothermal case. The Ziabicki parameters (temperature range length at peak mid-width, D , K_{max} and T_{max}) were estimated using non-linear regression. The final values used for the simulation were the combinations that produced the best fit. With K and T experimental values known from the kinetic models, different procedures were carried out using those values to determine the predicted D , K_{max} and T_{max} , as unknown parameters. Considering the experimental value for K_{max} , at time $t_{1/2}$, D and T_{max} can be found. A different combination involves the use of the T_{max} value at time $t_{1/2}$, to determine D and K_{max} . Final results are tabulated in Appendix 7 for the first algorithm, where D , K_{max} and T_{max} were estimated. The results shown in Appendix 8 suggest that very good agreement between prediction and experimental data is obtained for $n=2$, when the Nakamura method in conjunction with the Ziabicki's approach is employed in the analysis of the non-isothermal experiments.

For selected resins, the DSC exotherms are plotted in Figures 6.3 to 6.6. The values for the heat of fusion, in (J/g), for the first and second melting after crystallization, peak melting temperature ($^{\circ}\text{C}$), heat of crystallization (J/g), and on-set crystallization temperature ($^{\circ}\text{C}$) are tabulated in Appendix 4. Different distributions can be observed,

narrow for LLDPE A, over a range of 6°C, and for LLDPE B, over a range of 10°C. These resins are co-monomers with n-hexene and n-butene, with almost similar densities and melt indices, but narrower MWD for LLDPE A. The percent co-monomer as well as the short chain branch distribution per thousand carbon atoms (SCB/KC) is lower for LLDPE A.

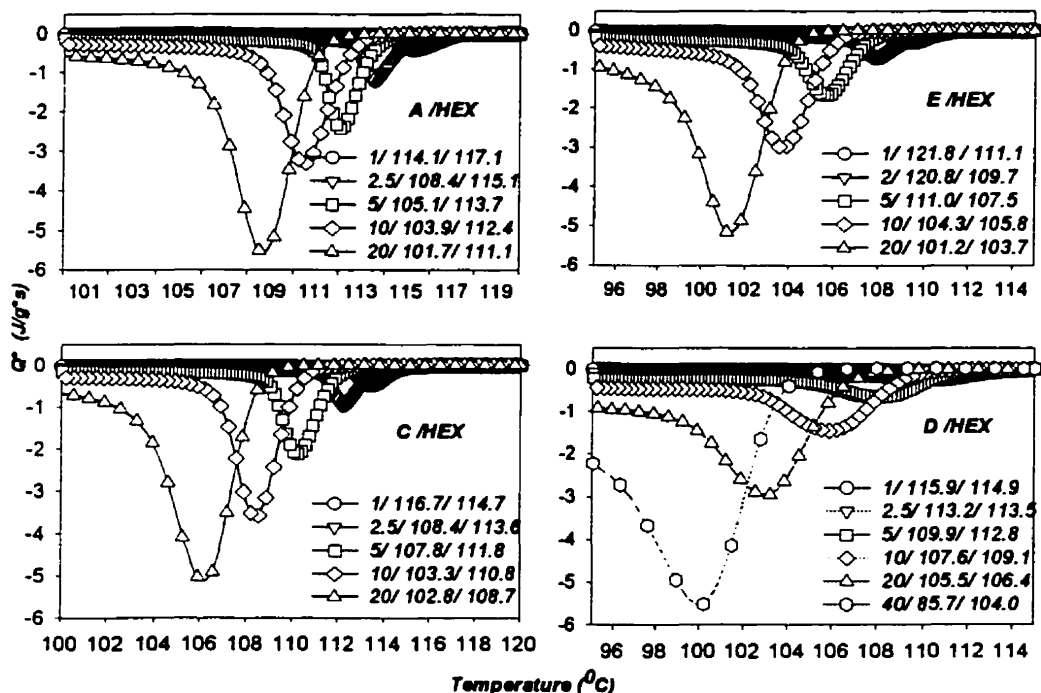


Figure 6.3. Non-Isothermal DSC Thermograms for LLDPE A, C, D, and E at Various Cooling Rates (Legend: (i) Cooling Rate (°C/min), (ii) Heat of Crystallization (J/g), (iii) On-Set Temperature of Crystallization (°C)).

From the remaining results, as expected, higher melting temperatures were obtained for both HDPE and PP samples, with the latter exhibiting a broad crystallization temperature interval (8°C degrees for HDPE and almost 24°C for PP-1). Also, higher on-set crystallization temperatures and heat of crystallization values were obtained. The HDPE sample exhibits the highest density but has similar MWD as some of the LLDPE samples used (i.e. 3.3 for HDPE versus 3.1 for LLDPE resin C or 3.7 for resin A).

The heat of crystallization followed a similar pattern, with regard to the effect of catalyst. In general, the heat of crystallization was equal to or higher than the heat of melting,

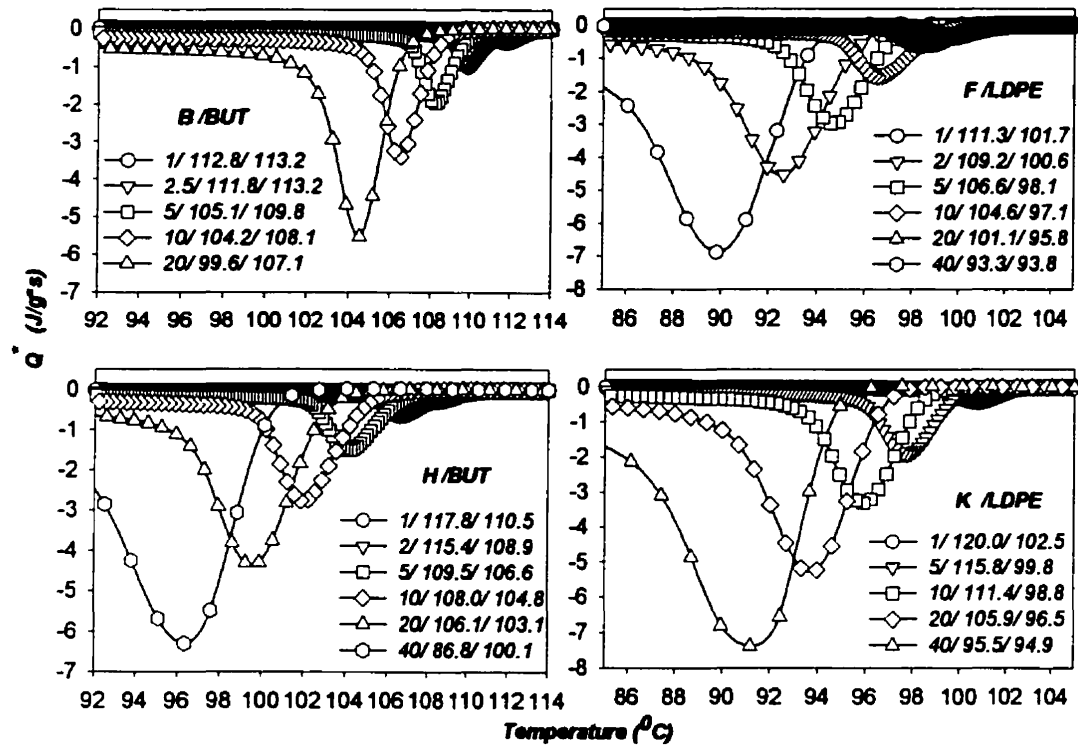


Figure 6.4. Non-Isothermal DSC Thermograms for LLDPE B, and H and LDPE F and K at Various Cooling Rates (Legend: (i) Cooling Rate ($^{\circ}\text{C}/\text{min}$), (ii) Heat of Crystallization (J/g), (iii) On-Set Temperature of Crystallization ($^{\circ}\text{C}$)).

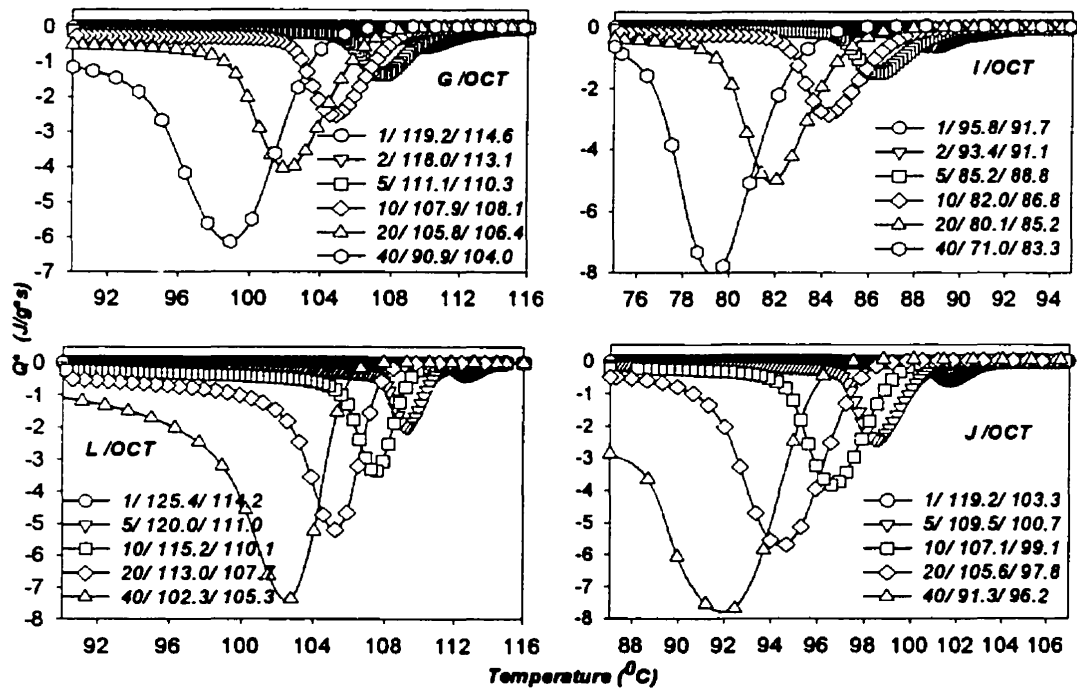


Figure 6.5. Non-Isothermal DSC Thermograms for LLDPE G, I, J, and L at Various Cooling Rates (Legend: (i) Cooling Rate ($^{\circ}\text{C}/\text{min}$), (ii) Heat of Crystallization (J/g), (iii) On-Set Temperature of Crystallization ($^{\circ}\text{C}$)).

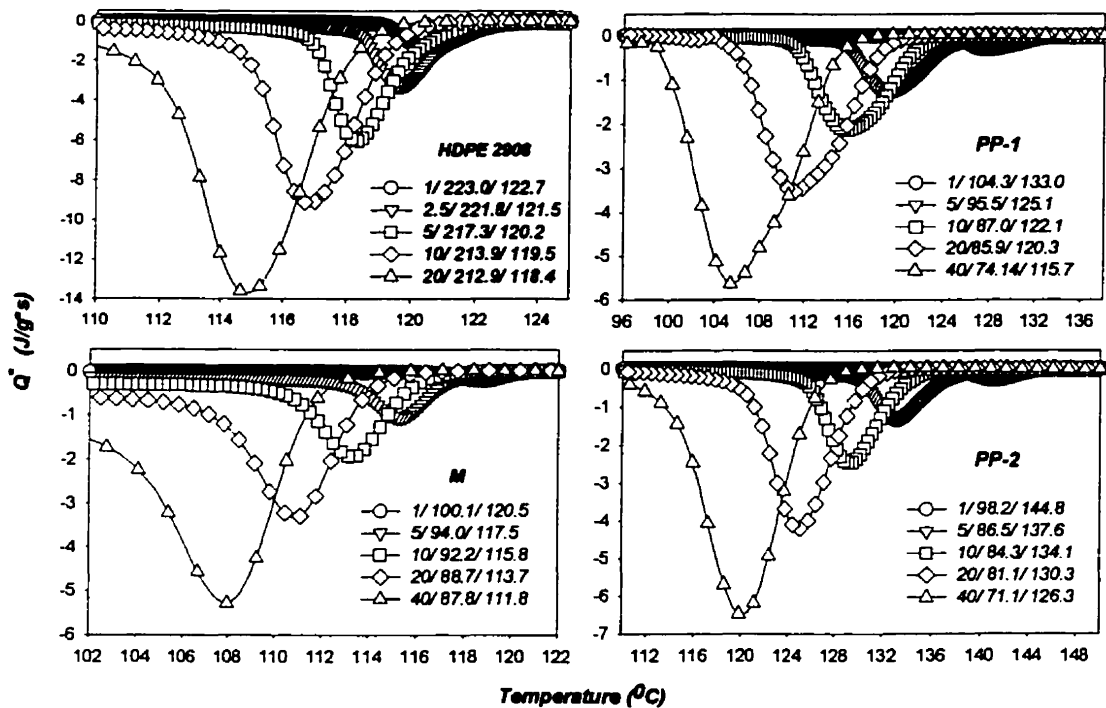


Figure 6.6. Non-Isothermal DSC Thermograms for LLDPE M, HDPE, PP-1 and PP-2 at Various Cooling Rates (Legend: (i) Cooling Rate ($^{\circ}\text{C}/\text{min}$), (ii) Heat of Crystallization (J/g), (iii) On-Set Temperature of Crystallization ($^{\circ}\text{C}$)).

when both heating and cooling rates were low (e.g. $1^{\circ}\text{C}/\text{min}$). However, as the cooling rates increased there was a significant decrease in the heat of crystallization, compared to both heats of fusion, after the first and second melting. This suggests that the sample crystallization was not complete at the end of the cooling cycle. The sample continued to crystallize prior to the second melting.

The on-set of crystallization occurred at low temperatures as the rate of cooling was raised. Generally, the on-set of crystallization was lower than the peak melting temperatures during the first and second melting.

6.2. Intra-Group Isothermal and Non-Isothermal Comparison.

Using the thermograms obtained under isothermal and non-isothermal conditions, various plots were generated to analyze the crystallization behavior for individual groups (i.e. those that contain the same co-monomer). For each group, DSC isotherms were

compared, at the maximum rate and identical temperatures, for the isothermal case. The induction time was excluded, since its value is different from one sample to another. For the non-isothermal case, the thermograms obtained at the same cooling rate (i.e. 20°C/min) were chosen. The results are summarized in Figures 6.7 to 6.12 for isothermal experiments. Figure 6.8 shows a typical non-isothermal thermogram for resin B and H, obtained at a cooling rate of 20°C/min. Complete non-isothermal thermograms at similar rate are shown for all resins in Appendix 9.

For each plot in Figures 6.7 and 6.9 to 6.12, there is a shift on the horizontal time scale equal to 20 seconds, in order to separate isotherms of different samples. The analysis was carried out for each individual group. The plots are given in Appendix 9 for the non-isothermal study. Figure 6.7, for the butene co-monomer LLDPE resins indicates that, at the same temperature (see curves on the left side), significant differences are observed in the isothermal crystallization behavior. However, the isothermal crystallization behavior becomes similar at the same degree of supercooling (see curves on the right side). In this case, the degree of supercooling is based on the peak temperature in the non-isothermal thermograms (MR). Selected properties of resin B and H are given in Table 6.2.

Table 6.2. Physical Properties for LLDPE B and H (Butene)

System	B - Gas/Z-N	H - Sol/Z-N
B/KC	20.2	18.9
%Co-monomer	4.03	3.8
Mn	24.2K	24.9K
Polydispersity (P.D.)	4.1	4.8

In general it appears that resin B crystallizes at a faster rate than H in the early stages of crystallization, while resin H crystallizes at a faster rate in the later stages, i.e. following the peak rate. At the same isothermal crystallization temperatures, the thermograms for resin H tend to be broader than they are for resin B. Also, the peak crystallization rates are higher for resin B. These differences may be attributed to the higher polydispersity of resin H.

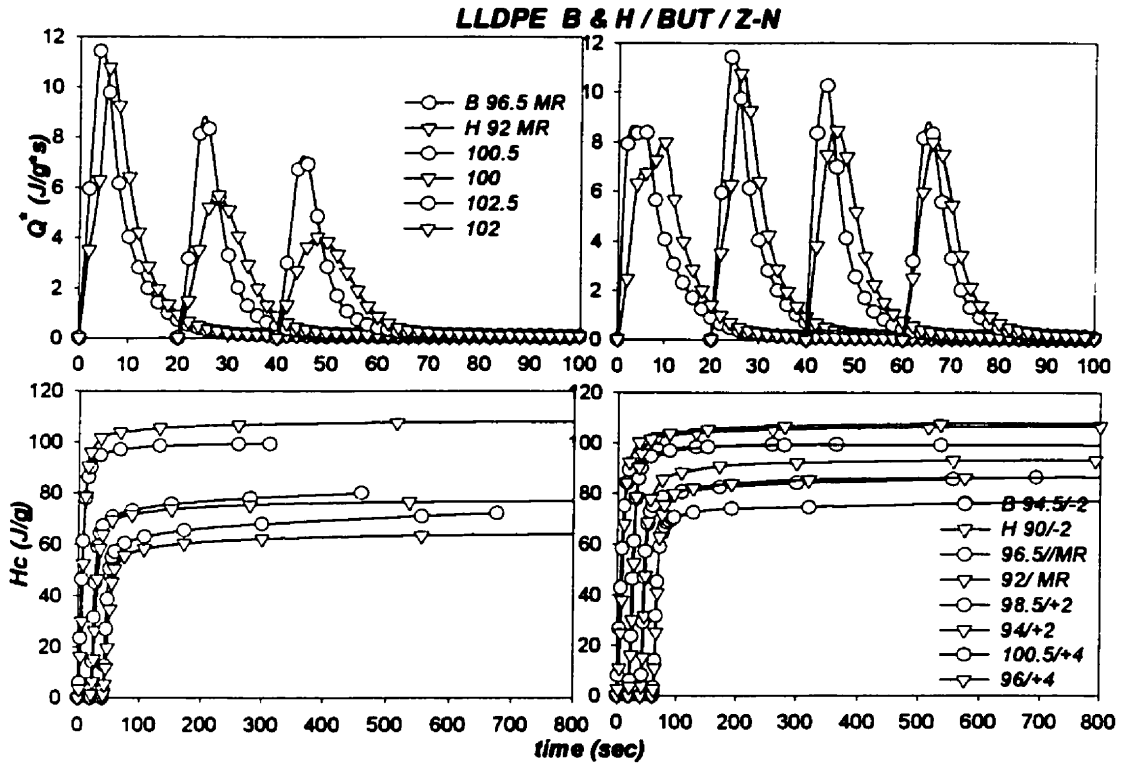


Figure 6.7. Intra-Group Isothermal Study for LLDPE B and H. Left Plots-Rate and Heat of Crystallization vs. Time at the maximum rate (MR) and similar isothermal temperatures. Right Plots-Rate and Heat of Crystallization at the maximum rate and similar supercooling above and below the maximum rate.

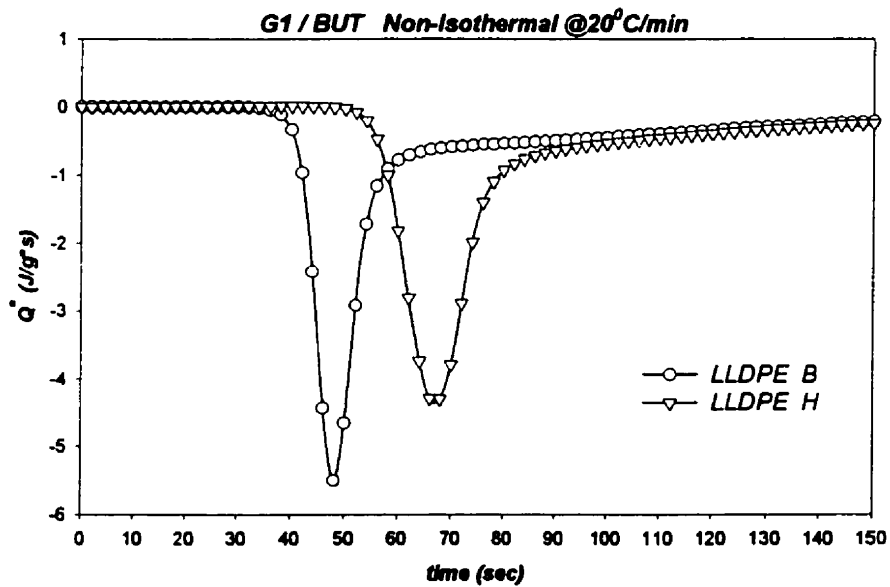


Figure 6.8. Normalized Heat Flow vs. Time for LLDPE B and H. (Intra-Group Non-Isothermal)

For the non-isothermal case (Figure 6.8) at the same cooling rate, narrower peaks and higher on-set crystallization temperatures are associated with LLDPE B. Overall, LLDPE H exhibits a higher percent crystallinity.

For Group 2, with n-hexene co-monomer, the isothermal thermograms are shown in Figure 6.9 and 6.10 and the non-isothermal results are in Appendix 9. Table 6.3 gives some of the relevant properties of the resins.

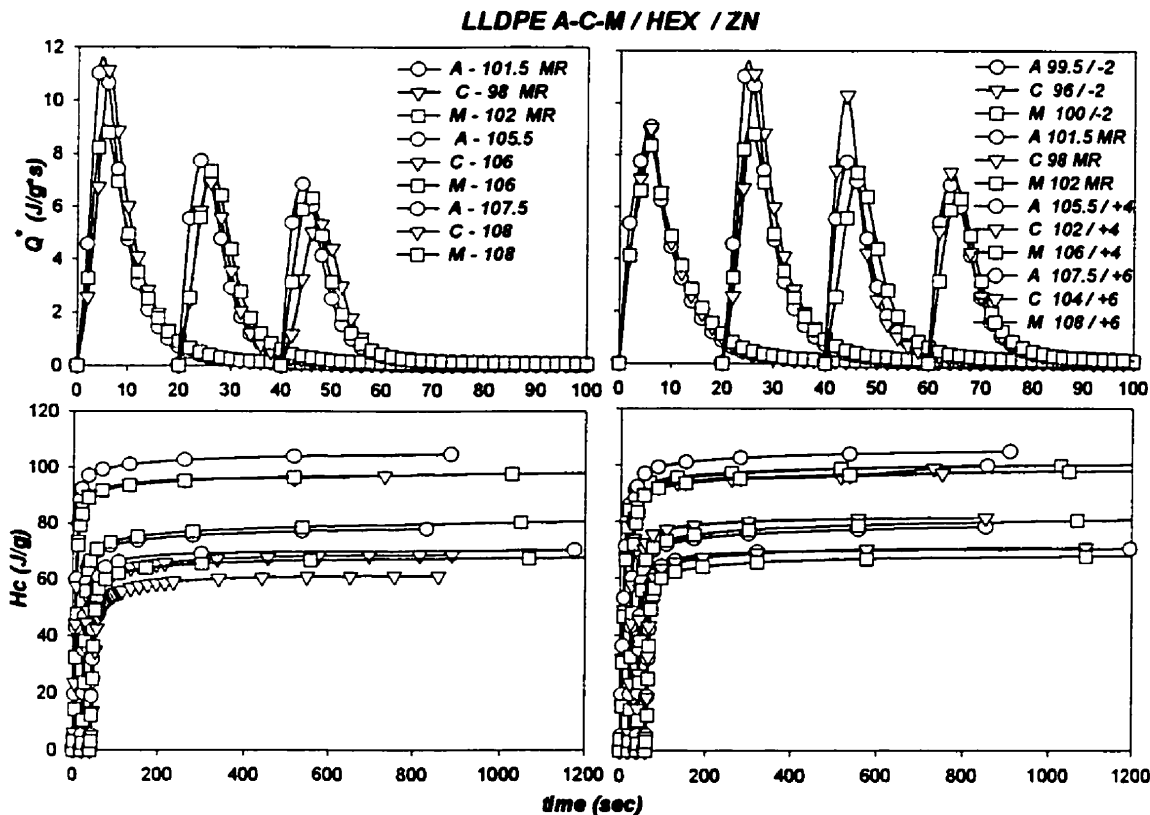


Figure 6.9 Intra-Group Isothermal Study for LLDPE A, C, and M. Left Plots-Rate and Heat of Crystallization vs. Time at the maximum rate (MR) and similar isothermal temperatures. Right plots-Rate and Heat of Crystallization at the maximum rate and similar supercooling above and below the maximum rate.

Table 6.3. Physical Properties of LLDPE A, C, D, E and M (Hexene)

System	A-Gas/Z-N	C-Gas/Z-N	M-Gas/Z-N	D-Gas/Met	M-Gas/Met
B/KC	19.7	18.87	-	15.4	12.8
%Co-mo	3.94	3.77	4.5	3.08	2.56
Mn	30K	36K	20.6K	44K	43K
P.D.	0.9	3.1	3.6	2.2	2.2

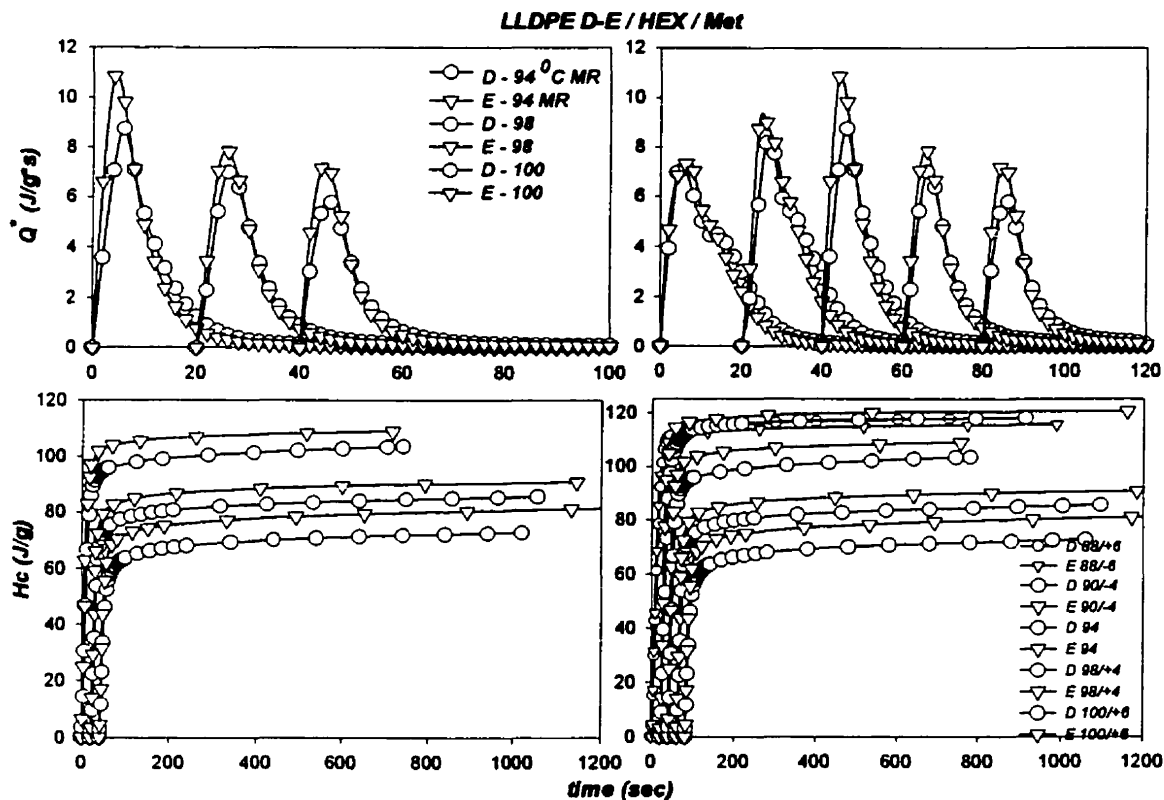


Figure 6.10. Intra-Group Isothermal Study for LLDPE D and E. Left plots-Rate and Heat of Crystallization vs. Time at the maximum rate (MR) and similar isothermal temperatures. Right plots-Rate and Heat of Crystallization at the maximum rate and similar supercooling above and below the maximum rate.

While significant differences are observed between the thermograms of Z-N resins and those of metallocene resins, they tend to be small within each subgroup. For the system in the second group (hexene), the thermograms are similar, irrespective of whether they are compared on the basis of the isothermal temperature or for the same degree of cooling. This is probably due to the fact that, for each subgroup, the peak temperatures for the maximum crystallization rate are almost equal. Thus, the comparison on the basis of temperature and the degree of supercooling should be equivalent.

Similar observations can be made regarding the third group, which has octene as co-monomer (Figures 6.11 and 6.12 and Table 6.4). However, in this case, the improvement achieved by using supercooling as a basis for comparison, rather than temperature, appears to be realized mainly for supercooling and for a lesser degree for superheating (i.e. negative Vs positive $T-T_{MR}$). It should be noted that sample J achieves higher

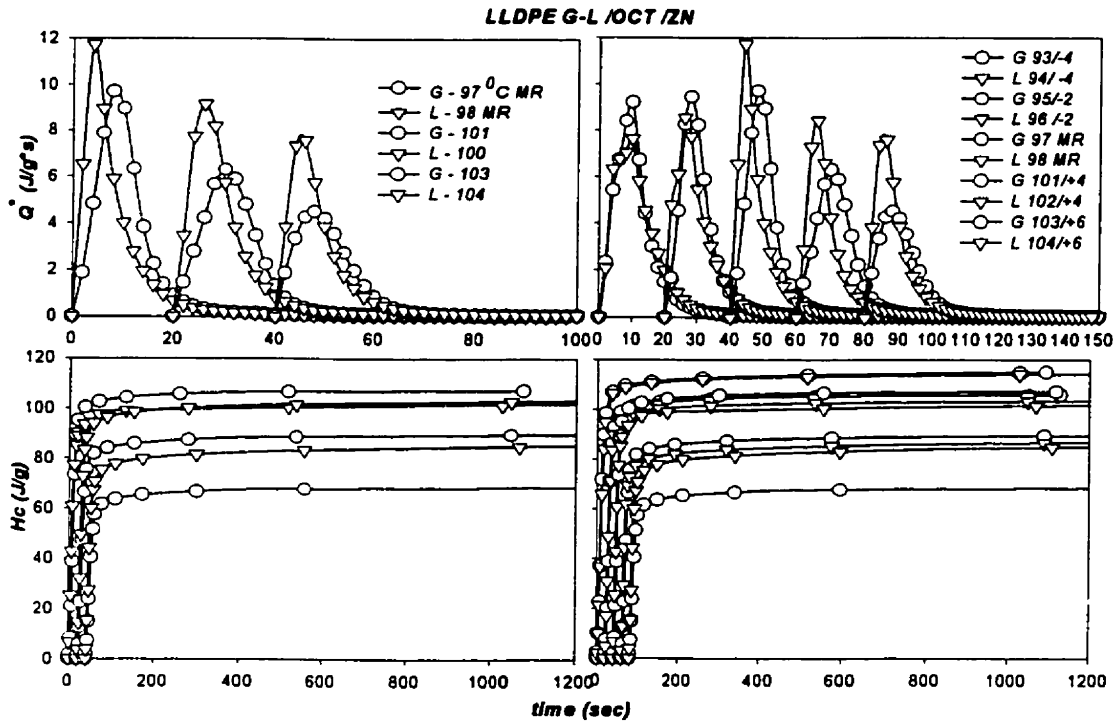


Figure 6.11. Intra-Group Isothermal Study for LLDPE G and L. Left Plots-Rate and Heat of Crystallization vs. Time at the maximum rate (MR) and similar isothermal temperatures. Right Plots-Rate and Heat of Crystallization at the maximum rate and similar supercooling.

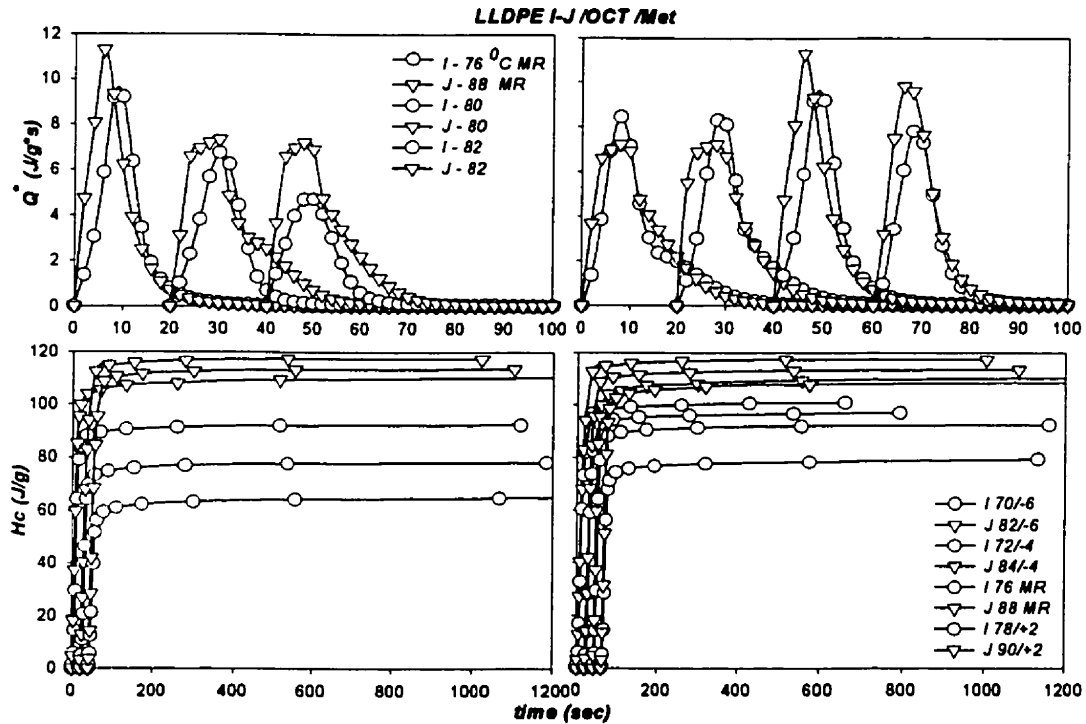


Figure 6.12. Intra-Group Isothermal Study for LLDPE I and J. Left plots-Rate and Heat of Crystallization vs. Time at the maximum rate (MR) and similar isothermal temperatures. Right plots-Rate and Heat of Crystallization at the maximum rate and similar supercooling above and below the maximum rate.

Table 6.4. Physical Properties of LLDPE G, I, J, and L (Octene)

System	G-Sol/Z-N	I-Sol/Met	J-Sol/Met	L-Sol/Z-N
B/KC	15.8	24.8	15.8	-
% Co-mo	3.2	5	3.2	2.8
Mn	17K	22K	38K	25.9K
P.D.	6.2	2.4	1.8	4.4

crystallinity than sample I, both at the same temperatures and at the same values of ($T-T_{MR}$). Sample J has lower polydispersity, which may be an important factor.

Figure 6.8 and the graphs in Appendix 9, for the non-isothermal experiments show that these experiments, at 20°C/min cooling, provide a clear separation of the behavior of the various resins. The thermograms show significant differences, especially with regard to the temperature for the on-set of crystallization, and in many instances for the end of crystallization. The metallocene resins exhibit the lowest on-set and end of crystallization temperatures. The cooling rates employed in this study are very low compared to those encountered in manufacturing processes, such as film blowing or injection molding. The non-isothermal data provide an indication about the differences in crystallization behavior among the various resins in such processes. However, actual comparison for higher cooling rates requires more analysis.

6.4. Inter-Group Isothermal and Non-Isothermal Comparison.

In this case, comparisons were made between the isothermal and non-isothermal thermograms for resins made with different co-monomers (butene, hexene and octene), but similar catalyst (Z-N or Metallocene). Figure 6.13 shows the isothermal and non-isothermal thermograms for resins described in Table 6.5. it is interesting to note that these resins, produced with different reactive media (gas phase or solution) and containing different co-monomers, produce almost identical isothermal thermograms, when the comparison is based on the degree of supercooling or superheating ($T-T_{MR}$). On the other hand, the separation is more pronounced in the case of non-isothermal thermograms. Similar observations may be made with regard to the two metallocene resins E and J, shown in Figure 6.14 and Table 6.6.

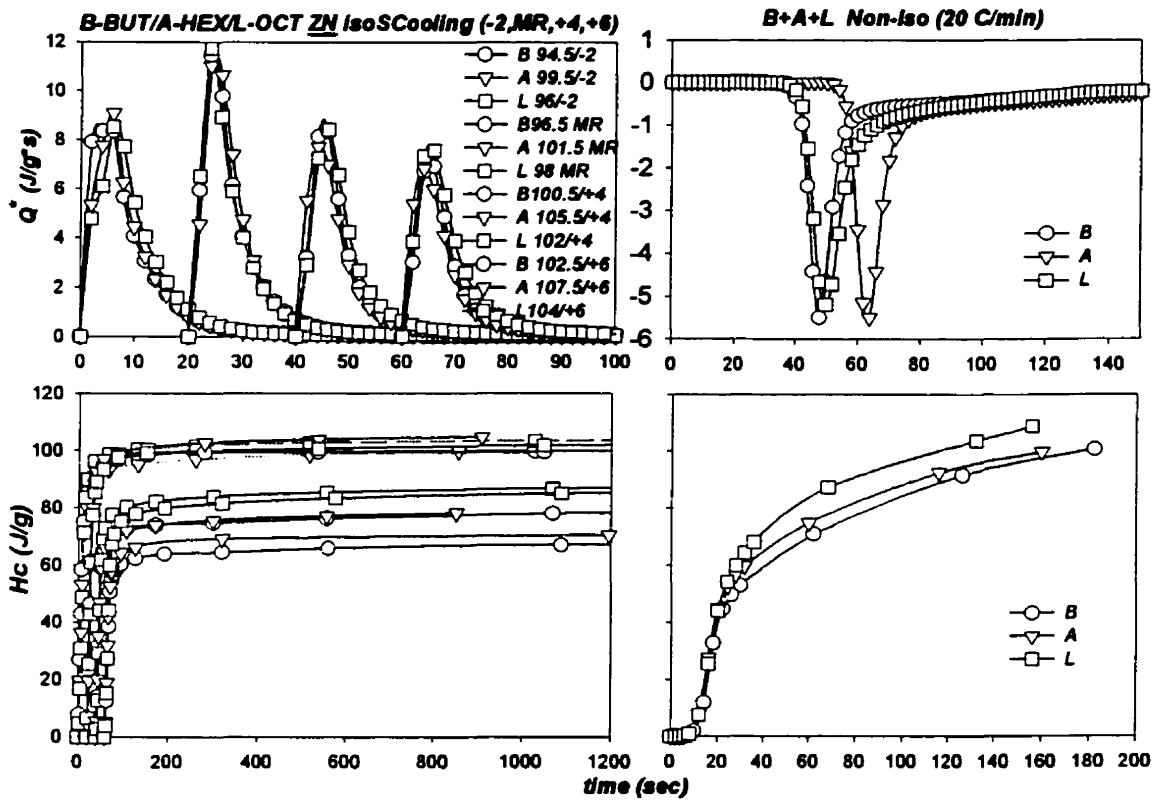


Figure 6.13. Inter-Group Isothermal and Non-Isothermal Analysis. Rate and Heat of Crystallization vs. Time (LLDPE B, A, and L)

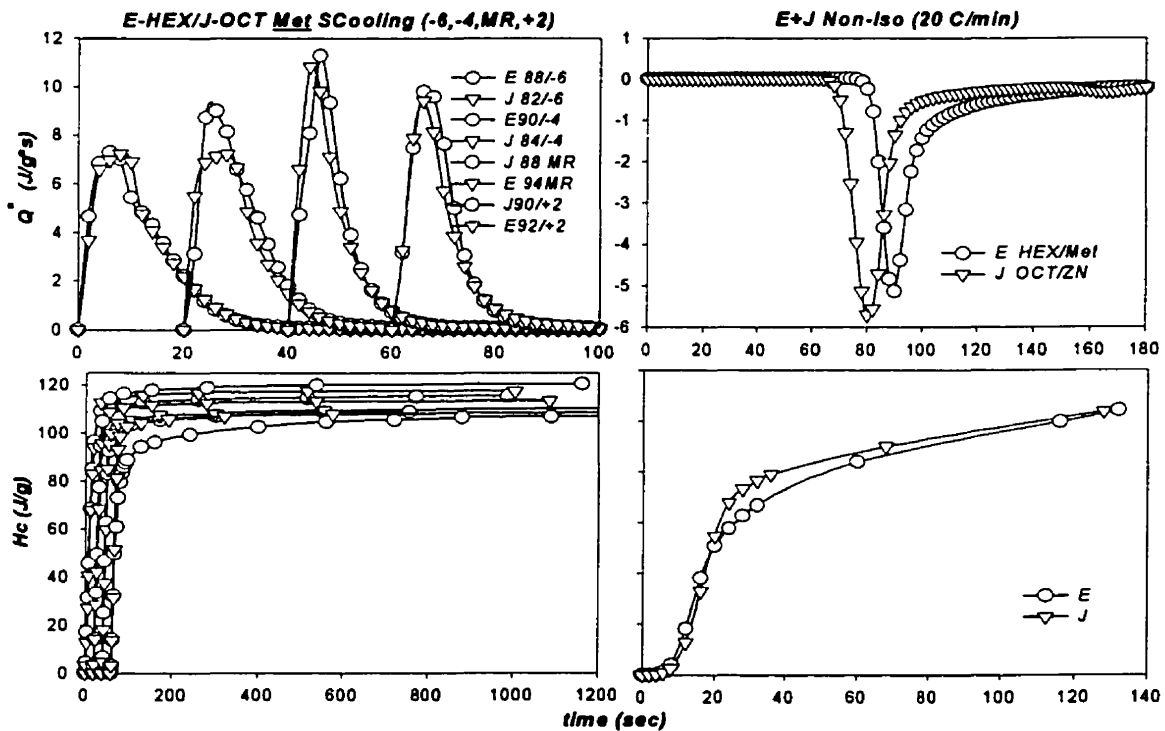


Figure 6.14. Inter-Group Isothermal and Non-Isothermal Analysis. Rate and Heat of Crystallization vs. Time (LLDPE E and J)

Table 6.5. Physical Properties of LLDPE B, A, and L

System	B-BUT/Gas/Z-N	A-HEX/Gas/Z-N	L-OCT/Sol/Z-N
B/KC	20.2	19.7	-
% Co-mo	4.03	3.94	2.8
Mn	24.2K	30K	25.9K
P.D.	4.1	3.7	4.4

Table 6.6. Physical Properties of LLDPE E and J

LLDPE	E- HEX/Gas/Met	J- OCT/Sol/Met
B/KC	12.8	15.8
% Co-mo	2.56	3.2
Mn	43K	38K
P.D.	2.2	1.8

6.5. Melting Behavior and Equilibrium Melting Temperature.

The DSC heating thermograms, which were collected at a heating rate of 10°C/min for all samples and isothermally crystallized at specified temperatures, were analyzed to assess the equilibrium melting temperature (Fig.6.15). The peak melting temperatures tabulated in Appendices 4 to 6 represent the experimental melting temperature, and the values are for both isothermal and non-isothermal cases. Using these values, according to a theory derived by Hoffman and Weeks,¹³⁵ the equilibrium melting temperature T_m^0 , that represents the melting temperature of infinitely extended crystals, can be obtained by linear extrapolation of the (experimental) T_m versus T_c data to the line $T_m=T_c$. The mathematical equation that relates the data is:

$$T_m = \frac{T_c}{2\beta} + T_m^0 \left[1 - \frac{1}{2\beta} \right] \quad (6.3)$$

where β is the “thickening ratio” of the thickness of the mature crystal L_c to that of the initial one L_c^* . It should be noted that β is always greater than or equal to 1. The factor 2 in Eq. (6.3) suggests that the thickness of the crystal undergoing melting is approximately double that of the initial critical thickness.

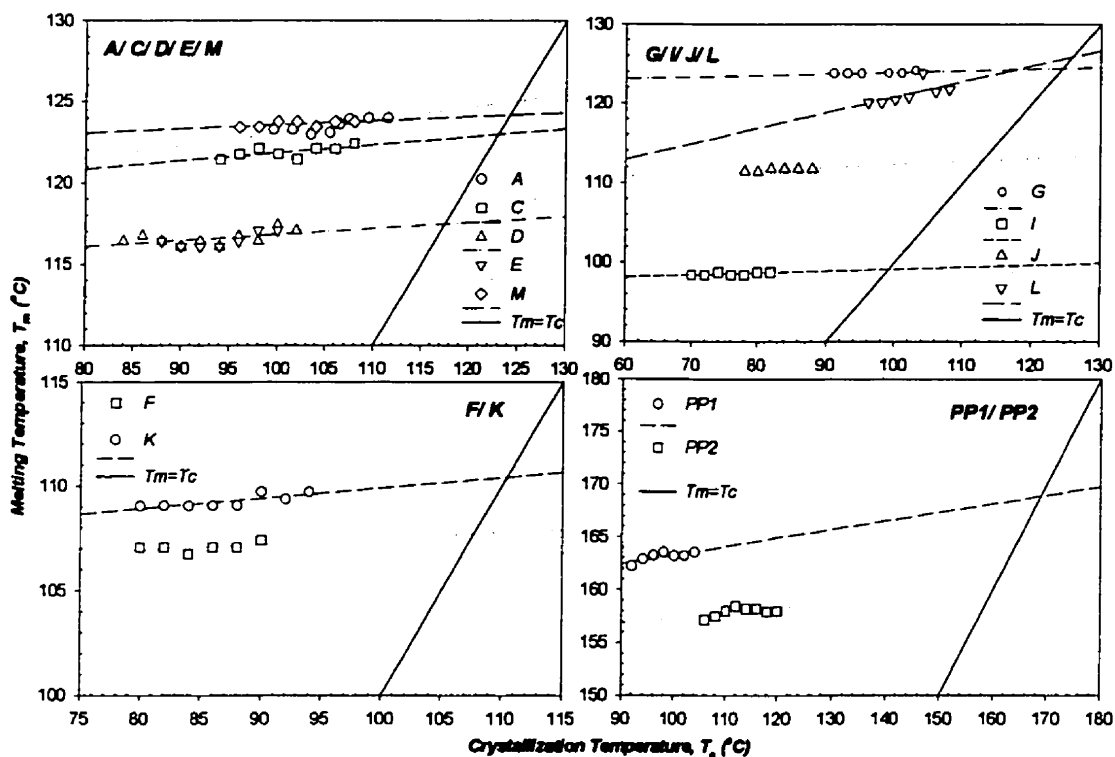


Figure 6.15. Equilibrium Melting Temperatures as a function of Crystallization Temperature.

The T_m values exhibit an almost linear relationship with T_c , at least in the temperature range used. For each sample, the intersection of the least square line fitted to the data set with the line $T_m = T_c$ provides the values of T_m^0 . For individual samples, the slope of the least square line that equals $1/2\beta$, can also be used to calculate the β parameter (i.e., $\beta = 0.5 \times \text{slope}^{-1}$). The values obtained for T_m^0 are reported in Table 6.7.

The results show that the T_m^0 values lie between 121.6°C and 124.5°C, for Group 1, between 117.2°C and 124.9°C for Group 2 and 99.0°C to 125.9°C for Group 3. The LDPE resins F and K are about the same with values of 107.4°C and 110.3°C, respectively. The highest values, as expected, were found for the polypropylenes, 168.2°C for PP-1, and 160.1°C for PP-2.

In general, for the LLDPE resins, the values extend over a wide range, and this might be related to the co-monomer and catalyst type. As previously mentioned, the branches represented by the co-monomer do not participate in the crystallization process, being

rejected by the crystal lamellae. A higher degree of branching along the chain backbone will decrease the crystallization capability of a given polymer. Also the branch size (olefin type, i.e. butene, hexene and higher) will affect the ultimate crystallinity.

Table 6.7. Thermodynamic Equilibrium Melting Points For Polyethylenes and Polypropylenes Samples

Sample	T_m° ($^{\circ}\text{C}$)	T_m° (K°)
B	121.6	394.7
H	124.5	397.6
A	124.9	398.0
C	122.5	395.6
D	117.2	390.3
E	119.4	392.5
M	123.8	396.9
G	124.1	397.2
I	99.0	372.1
J	112.2	385.3
L	125.9	399.0
F	107.4	380.5
K	110.3	383.4
PP1	168.2	441.3
PP2	160.0	433.1
HDPE	141.1	414.2

For the resins obtained using a Ziegler-Natta catalyst (i.e. B, H, A, C, G and L) a higher experimental and equilibrium melting temperature can be observed. The value range is between 121.6 $^{\circ}\text{C}$ and 125.9 $^{\circ}\text{C}$, which is above the 99.1 $^{\circ}\text{C}$ to 119.4 $^{\circ}\text{C}$ interval exhibited by the metallocene polyolefins, resins D, E, J and I.

For the same co-monomer type, i.e. LLDPE H that has a lower degree of branching than LLDPE B, higher melting temperatures were recorded. By analogy, the same behavior is observed for the hexene group. Resins A, C and M show a higher T_m and T_m° by comparison with resins D and E. The last group, that has octene as co-monomer, has the highest and the lowest values. In this case, the size of the co-monomer is balanced by a small number of branches (i.e. 3.2% for LLDPE G and 2.8% for LLDPE L) that gives higher melting temperatures. Both resins have also the highest number-average molecular weight (M_n).

An interesting melting characteristic of LDPE resins observed from their melting endotherms upon re-heating is that the melting starts at a temperature close to the crystallization temperature. This phenomenon was verified and reported recently by Schmidtke et al.¹³⁶ Their observations suggest that the melting starts slightly after T_c , and is followed by a recrystallization in the range of the melting endotherm.^{136, 137} Also, the heating rate used to obtain a melting endotherm, as pointed out by Rodriguez-Arnold and coworkers,¹³⁸ plays a major role in the melting point observed. Thus, the annealing effect contributes to the increase in the melting point at lower heating rates (less than 20°C/min), whereas thermal lag becomes important for higher heating rates.

6.6. Summary.

The crystallization behavior from the melt of HDPE, LDPE and SCB-LLDPE, prepared with heterogeneous Ziegler-Natta and the more homogeneous Metallocene type catalysts was investigated in the present study. The data collected were tabulated in the Appendices and the results obtained were examined and interpreted qualitatively.

Heating rates of 10°C/min to 180°C were employed in each experiment prior to each cooling to erase the thermal history of the sample. The experimental peak melting temperature and heat of fusion were determined. Simpson's rule for step by step integration was used for numerical integration to determine the area under the peak. Single peaks were observed and the cause of this, as reported in the literature, is related to the cooling rate. High rates lead to single peak exotherms.

Resin B has a higher peak temperature melting point compared with resin H (both have n-butene as SCB), under the same crystallization conditions in both isothermal and non-isothermal experiments. Resin B has a narrower MWD, 4.1 compared with 4.8 for resin H.

In the second group, the melting temperatures decrease in the order M>A>C>D>E. As expected, the onset temperature of crystallization increases in the inverse order, 103.7°C (E), 106.4°C (D), 108.7°C (C), 111.1°C (A) and 113.7°C for resin M, at the same cooling

rate of 20°C/min. Resin M has the highest percent co-monomer, as SCB, but has the lowest number-average molecular weight. Its MWD value of 3.6 is between 2.2 (for resins D, E) and 3.7 (for resin A).

In the third group (n-octene), the peak melting temperature decreases in the following order: G>L>J>I. Overall, for intra-group and inter-group analyses, resin I has the highest percent co-monomer content and degree of branching, 5% and 24.8 B/KC, respectively, exhibiting the lowest peak melting temperature (97.95°C to 101.06°C), and lowest onset crystallization temperature. (i.e. 91.7°C at a rate of 1°C/min, and with increasing cooling rate, values as low as 71.05°C at 40°C/min are attained). Also, resin I has the lowest number-average molecular weight in its group.

The two LDPE resins, F and K have almost similar melting temperatures with a slightly higher value for resin K (110.05°C for K versus 109.05°C for F at a rate of 1°C/min). The MWD is 4.1 for resin K and 7.3 for resin F.

As expected, the HDPE and PP have the highest melting temperatures of all the resins in the study, with values of 134.5°C and 159.1°C, respectively.

The Avrami exponent varies between 1.4 to 2.2 for resin B, and increases with increasing temperature, but is nearly constant for resin H at 2.0 to 2.2. Higher crystallization rates were observed for resin B. For the hexene group, a variation around the same value, $n = 2$, was recorded. The limits are 1.7 to 2.6 (A), 1.8 to 2.3 (C), 1.8 to 2.3 (D), 1.8 to 2.1 (E), and 1.9 to 2.1 (M).

The third group, in which the co-monomer is n-octene, provided the highest values for the Avrami index. Resin I produced values between 2 and 2.6, and G between 1.9 and 2.5. On the other hand, resin J produced lower values between 1.7 and 2.1, followed by L with 1.8 to 2.2. The crystallization rates decrease with increasing n , values being highest for resins J and L.

The high density polyethylene exhibited Avrami exponent values that are close to two, i.e. between 1.9 to 2.1; similar behavior was observed for polypropylene.

It should be noted that the parameters obtained (i.e. Avrami exponent n , and crystallization rate k), using different methods of investigation, are subject to interpretation when correlating with the theoretical models and similar results reported in the literature. It is a well known fact that the Avrami model agrees only with the linear region (segment) of the plot of percent crystallinity versus time, after integration. Thus the amount of data collected and the points chosen for the analysis can influence, to a great extent, the values obtained when the double logarithmic plot, $\log\{-\ln(1-X)\}$ versus $\log t$, is used. The slope and the intercept values obtained are sensitive to different manipulations.

Avrami and Tobin models as well as the Non-Linear Regression (NLR) method were used to retrieve the isothermal kinetic parameters. Finally, using the constant value (2.0) for the Avrami index for all the resins, the rate of crystallization was computed using NLR. For the fitting of the non-isothermal model to the experimental data, the same values were used.

Reproducibility was tested for one resin from each group at one isothermal temperature, because of the large number of experiments that are required to analyze all the samples. The results are shown in Appendix 10.

Different studies indicate that during isothermal crystallization of uniformly branched copolymers (i.e. LLDPE), short branches containing from 3 to 10 carbon atoms are excluded from the crystalline phase into an amorphous region, and the lamellar stems are formed from linear chain segments.¹³⁹ Their length cannot exceed the distance between branches. Thus, for a LLDPE with a high content of branched units, a lower crystallization temperature is usually expected. The crystalline phase is “free” of branches and, as a result, the maximum possible lamellar thickness $l_{0, max}$, cannot be exceeded by the uniformly branched copolymer under any temperature regime (i.e., long annealing).¹⁴⁰ For these systems, the equilibrium melting temperature, T_m^0 , for LLDPE, will be below the ideal value of the unbranched chains, T_{HDPE}^0 . It is assumed that, for a low degree of branching, the crystalline structure does not depend on the copolymer content. From the heat of fusion, ΔH_m , and the surface energy, γ , for such a system, the

depression of the equilibrium melting temperature, ΔT_m , in the uniformly branched LLDPE can be estimated:

$$\Delta T_m = T_{HDPE}^{\infty} - T_{m,LLDPE}^0 = \frac{2\gamma T_{HDPE}^{\infty}}{\Delta H_m l_{0,max}(x)} \quad (6.4.)$$

The fact should be mentioned that the LLDPE and HDPE must possess similar molecular weights. The value of ΔH_m and γ , do not differ much from those for HDPE, in this case. For highly branched systems ($x > 6$ mol %), the branching dependence of the melting temperature is much more complicated since the ΔH_m and γ , are significantly different. In such systems, changes from lamellar structure to bundled crystals were reported.¹⁴¹

The deviation of the melting temperature and unique behavior of LLDPE, from the one described in Eq. (6.4.), is attributed to the non-uniformity in inter- and intra-molecular branching distributions. An explanation would be the “blockiness” that strongly changes the dependence between average lamellar thickness and copolymer composition. Branched units will cluster instead of distributing randomly along the chain and in between the molecules.^{142,143}

If the polymeric chain is highly branched, it is less probable that it can contribute to the crystalline phase. The exclusion of branches from the crystalline region determines a decrease in the rate of crystallization. Thus, the amorphous regions in semicrystalline LLDPE should be enriched by more branched chains, whereas the linear chain segments predominate in the crystallites. Morphological studies have revealed the fact that the crystallization of LLDPE starts by the formation of thick primary lamellae, using first the longest linear chain segments. Thinner, less perfect crystals will fill the volume between primary lamellae. Thus, as the branching increases, linear chain segments, capable of fitting into the crystalline lattice become shorter, decreasing the crystallization rate at a given degree of supercooling.

Lambert and Phillips^{144,145} using fractionated ethylene- α -olefin copolymers with a narrow composition distribution showed that the bulk crystallization rate is far slower for branched systems than for linear ones of similar molecular weight at the same degree of supercooling. Kim and Phillips¹⁴⁶ and Wagner *et al.*¹⁴⁷ reported the same observation.

Faster crystallizing, less branched molecules contribute the most to the thicker lamellae determining the properties of the crystalline phase at low degrees of crystallinity near to liquid-to-solid transition. Thus, the branching distribution plays a major role, referring to the system properties near the liquid-to-solid transition and on the morphology of a semi-crystalline copolymer in the case of a low branched fraction of LLDPE that crystallizes first under all temperature regimes.

CHAPTER 7

SUMMARY, CONCLUSIONS AND FURTHER WORK

7.1. Summary and Conclusions.

The resins analyzed in the present study are used widely in most areas of polymer processing, and cover the entire class of polyethylene grades (high, medium and low density). Some of them are commercial grades, and others are experimental ones. Upon cooling, polymeric materials form relatively small crystals compared with the inorganic substances, and are by and large quasi-stable. At specific temperatures, some resins exhibit a broad continuous distribution of non-equilibrium melting points (whereas on cooling the distribution range is narrower). This could be explained as a result of a distribution of lamellar thicknesses and molecular weights within a variety of defective microstructures, each one of them contributing to the overall morphology.

Isothermal crystallization kinetics parameter for both Avrami and Tobin equations were obtained for each of the resins included in the study over the temperature range of interest. The Avrami fit was made over the initial linear region of the crystallization thermograms. The temperatures considered were on both sides of the temperature, T_{MR} , where the maximum rate in the crystallization isotherms was observed. It was found that within one group, and even for comparison of resins with different co-monomers, superposition of thermograms is obtained when the degree of supercooling, $(T-T_{MR})$, was considered rather than temperature (T).

In the case of non-isothermal thermograms, it was found that thermograms obtained at 20°C/min produced clear separation of the non-isothermal crystallization behavior of the various resins. Furthermore, it was found that it is possible to predict non-isothermal thermograms with reasonable accuracy, by application of a combination of Ziabicki's equation and the Nakamura method. A uniform value of 2.0 was used for the Avrami index, n , in these calculations.

The higher rate used for cooling is the main cause for not obtaining the multiple peaks, as reported for rates up to 60°C/min. Also, some observations may be attributed to the trans-crystallization effects generated by the sample holder, and the lower temperatures at which the experiments were recorded. It is also believed that the Metallocene catalyzed polyethylene exhibits potential molecular segregation effects, which are not measured by the DSC, since it crystallizes very fast.

Analysis of the kinetic data, using the Avrami kinetic model, shows very rapid changes in crystallinity for lower temperatures, followed by slow growth periods. For all resins, the maximum degree of crystallinity is achieved at lower crystallization temperatures. In some cases, the general trend in the Avrami exponent fluctuation follows the well-known behavior that high temperature growth leads to greater values, with smaller exponents obtained at lower crystallization temperatures (i.e. resin B). However, resin G exhibits higher values at lower temperatures, where higher crystallization rates are attained.

When the co-monomer content is increased, lower crystallization temperatures are observed. The actual crystallizable fraction is diminished, since the co-monomer does not participate in the formation of growing crystals. Overall, resin I has the lowest crystallization temperature around 70°C. The same pattern can be observed also within each individual group.

Fractional values of n were reported as in the literature and, normally, show better fit to time dependent crystallization than the integer values. For lower temperatures, some difficulties may arise. Overall, the values of n were between 1.9 to 2.4. The values

between 2 to 3 are attributed to simultaneous occurrence of tri-dimensional growth of crystallites from instantaneous nuclei ($n=3$), and two-dimensional growth from instantaneous nucleation.

To establish basic correlations between catalyst and polymer structures, as well as polymer properties of such tailor-made polyethylene grades, the kinetic data should be compared and analyzed with the morphology observed in conjunction with different microscopic techniques.

7.2. Recommendations for Further Work.

Exploratory optical and polarized light microscopy work is recommended to analyze the specific morphology developed during crystallization and for interpreting the kinetic results.

Samples with lower weight between 3-5 mg with liquid nitrogen (LN_2), as the cooling medium, should be tested. The thermal gradients will be reduced within the sample and between sample holder and furnace as well. Higher crystallization temperatures, right below the experimental melting temperature, should also be tested. It is recommended that Intracooler-1 be used as the cooling system. Otherwise, the long period required for complete crystallization becomes unattainable, either with ice or LN_2 .

REFERENCES

1. Strobl, G., in *The Physics of Polymers*, 2nd Ed., Springer, Berlin (1997)
2. Olabisi, O., in *Handbook of Thermoplastics*, Marcel Decker, 1-57 (1997)
3. Robertson, R.E., *J. Phys. Chem.*, **69**, 1575 (1965)
4. Charrier J. M., in *Polymeric Materials & Processing*, Hans Publishing., Munich (1991)
5. Dighton, G. L., in *Polyethylene*, Marcel Decker, N.Y. (1989)
6. Mandelkern, L., in *Crystallization of Polymers*, McGraw-Hill (1964)
7. Kamal, M. R., Lectures Notes, Course 302-681A, McGill University (1998)
8. Faucher, J. A., F. P. Reading, in *Relationships between Structure and Fundamentals Properties, Crystalline Olefin Polymers*, Interscience, N.Y. (1965)
9. Novolin, T. E., *Prog. Polym. Sci.*, **11**, 29-54 (1985)
10. Bohm, L. L., *Polymer*, **19**, 545-553 (1978)
11. Keii, T., E. Suzuki, M. Tamar, Y. Doi, *Makromolek. Chem.*, **180**, 2235 (1979)
12. Ivanchev, S. S., A. A. Baulin, A. O. Rodionov, *J. Polym. Sci., Polym. Chem. Edn*, **18**, 2045-2050 (1980)
13. Shida, M., T. J. Pullukat, R. E. Hoff, *J. Polym. Sci., Polym. Chem. Edn*, **18**, 2857-2895 (1980)
14. Phillips Petroleum Company, U.S. Pat. No.2, 825, 721-1958
15. Groenveld, G., *J.Catal.*, **82**, 77 (1983)
16. Lesnikova, N. P., *Kinet. Katal.*, **20**(6), 1533 (1979)
17. Soga, K., T. Shiono, *Prog. Polym. Sci.*, **22**, 1503-1513 (1997)
18. Fierro, R., J. C. W. Chien, M. D. Rausch, *J. Polym. Sci., Part A. Polym. Chem.*, **32**, 2817 (1994)
19. Arndt, M., in *Handbook of Thermoplastics*, 38-57, Marcel Decker, N.Y. (1997)
20. Hoffman J.D., G.T. Davis, J.I. Lauritzen, in *Treatise on Solid State Chemistry: Crystalline and Non-Crystalline Solids*, vol.3, Plenum, New York (1976)
21. Ward, I.M., in *Structure and Properties of Oriented Polymers 2nd Ed.*, London, New-York, Chapman & Hall (1997)

22. Mandelkern, L., *Prog. Polym. Sci.*, **2**, 165 et seq., Pergamon Press, Oxford (1970)
23. Keller, A., *Prog. Rep. Phys.*, **31**, 623 (1968)
24. Sharples, A., in *Introduction to Polymer Crystallization*, Arnold, London (1966)
25. Anderson, F.R., *J. Appl. Phys.*, **35**, 64 (1964)
26. Wunderlich, B., Arakawa, T., *Makromol. Chem.*, **74**, 174 (1964)
27. Capaccio, G., Ward, I.M., *Nat. Phys. Sci.*, **243**, 143 (1973)
28. Phillips, P.J., *Polymer Crystals*, *Rep. Prog. Physics*, **53**, 549-604 (1990)
29. Kamal, M.R., M.E. Ryan, in *Models of Molecular Behavior*, C:302-602, McGill University (1998)
30. Sharples, A., *Polymer*, **3**, 250 (1962)
31. Christian, J.W., in *The Theory of Transformation in Metals and Alloys*, 2nd edn., Pergamon Press, Oxford (1965)
32. Turnbull, D., J. C. Fisher, *J. Chem. Phys.*, **17**, 71 (1949)
33. Kurz, W., D. J. Fisher, in *Fundamentals of Solidification*, Aedermannsdorf, Switzerland (1976)
34. Wunderlich, B., in *Macromolecular Physics*, Academic Press, New-York (1973)
35. Ishida, H., P. J. Bussi, *J. Mat. Sci.*, **26**, 6373 (1991)
36. Batrzack, Z., A. Galenski, *Polymer*, **31**, 2027 (1990)
37. Yeh, G. S. Y., K. Z. Hong, *Polym. Eng. Sci.*, **19**, 395 (1979)
38. Hill M. J., A. Keller, *Macrom. Sci-Phys.*, **B3**(1), 153 (1969)
39. Moitzi, J., P. Skalicky, *Polymer*, **34**, 3168 (1993)
40. Hoffman, J. D., R. L. Miller, H. Marand, D. B. Roitman, *J. Nat. Bur. Stand.*, **79A**, 671 (1992)
41. Wunderlich, B., in *Macromolecular Physics II*, Academic Press, New-York (1976)
42. Bassett, D.C., in *Principle of Polymer Morphology*, Cambridge University Press, Cambridge (1981)
43. Chu, F.-H.E., in *Crystallization Kinetics and Morphological Studies of High Density Polyethylene*, M.Sc. Thesis, McGill University (1983)
44. Mandelkern, L., in *Relations between Properties and Molecular Morphology of Semicrystalline Polymers*, *Faraday Discuss. R. Soc. Chem.*, **68**, 310 (1979)
45. Avrami, M., *J. Chem. Phys.*, **7**, 1103, 1939; **8**, 212, 1940, **9**, 177 (1941)

46. Tobin, M.C., J. Polym. Sci., Polym. Phys. Ed., **14**, 2253 (1976)
47. Ozawa T., Polymer, **12**, 150, (1971)
48. Malkin A. Y., Beghishev V. P., Keapin I. A., Bolgov S. A., Polym. Eng. Sci., **24**, 18, 1397 & 1402 (1984)
49. Nakamura, K., T. Watanabe, K. Katayama, J. Appl. Polym. Sci., **16**, 1077-1091 (1972)
50. Ziabicki, A., J. Chem. Phys., **85**, 1 (1986)
51. Tobin, M.C., J. Polym. Sci., Polym. Phys., **12**, 399 (1974)
52. Tobin, M.C., J. Polym. Sci., Polym. Phys., **14**, 2253 (1976)
53. Tobin, M.C., J. Polym. Sci., Polym. Phys., **15**, 2269 (1977)
54. Keith, H. D., F. J. Padden, J. Appl. Phys., **35**, 1270 (1964)
55. Verma, R., H. Marand, B. Hsiao, Macromolecules, **29**, 7767 (1996)
56. Kolmogoroff, A. N., Izvestiya Akad. Nauk USSR, Ser. Math., **1**, 355 (1973)
57. Johnson, W. A., K. F. Mehl, Trans. Am. Inst. Mining. Met. Eng., **135**, 416 (1939)
58. Evans, U. R., Trans. Faraday Soc., **41**, 365 (1945)
59. Rabesiaka, J., Kovacs A. J., J. Appl. Phys., **32**, 11 (1961)
60. Spruiell J.E, J.L. White, Polym. Eng. Sci., **15**, 660 (1975)
61. Lopez L. C., G. L. Wilkes, Polymer, **30**, 882 (1989)
62. Samara, M., Ph.D. Thesis, McGill University, Montreal (in print)
63. Hammami A., A.K. Mehrota, Thermochim. Acta., **211**, 137 (1992)
64. Elias H., in *Macromolecules*, vol. 1, Plenum Press, New York (1977)
65. Hoffman J.D., G.T. Davis, J.I. Lauritzen, in *Treatise on Solid State Chemistry: Crystalline and Non-Crystalline Solids*, vol.3, Plenum, New York (1976)
66. Mader, D, J. Heinemann, P. Walter, R. Mulhaupt, Macromolecules, **33**, 1254 (2000)
67. Long Y., R.A. Shanks, Z.H. Stachurski, Prog. Polym. Sci., **20**, 651 (1995)
68. Haines, P. J., in *Thermal Analysis*, Chapman & Hall, Glasgow (1995)
69. Encyclopedia of Polymer Science and Engineering, 2nd Ed. Wiley & Sons, New-York, **17**, 756 (1986)
70. Di Lorenzo M.L., C. Silvestre, Prog. Polym. Sci., **24**, 917 (1999)
71. Krevelen, Van D.W., in *Properties of Polymers*, Elsevier (1990)
72. Long Y., R.A. Shanks, Z. H. Stachurski, Prog. Polym. Sci., **20**, 695 (1995)

73. Kavesh , S., Schultz, J.M., *Polymer Eng. Sci.*, **9**, 5 (1969)
74. Hoffman, J.D., J.J. Weeks, W.M. Murphey, *J. Res. Natl. Bur. Stand.*, **63A**, 67 (1959)
75. Price, F. P., in *Nucleation*, Marcel Dekker, New-York (1969)
76. Price, F. P., *J. Polym. Sci., C*, **3**, 117 (1963)
77. Magill, J.H., P.J. Harris, *Polymer, London*, **3**, 252 (1962)
78. Lauritzen, J.I., J.D. Hoffman, *Theory of Formation of Polymer Crystals with Folded Chains in Dilute Solutions*, *J. Res. Natl. Bur. Stand.*, **64A**, 73 (1960)
79. Hoffman, J.D., *Theoretical Aspects of Polymer Crystallization with Chain Folds: Bulk Polymers*, *SPE Trans*, **4**, 315 (1964)
80. Liu S., Y. Yu, Y. Cui, H. Zang, Z. Mo, *J. Appl. Polym. Sci.*, **70**, 2371 (1998)
81. Gupta A.K., S.K. Rana, B.L. Deopura, *J. Appl. Polym. Sci.*, **51**, 231 (1994)
82. Kim K.G., B.A. Newman, J.I. Scheinbem, *J. Polym Sci., Polym. Phys.*, **23**, 2477 (1985)
83. Collier J.R., J.N. Neal, *Polym. Eng. Sci.*, **9**, 182 (1969)
84. Long Y., R.A. Shanks, Z.H. Stachurski, *Prog. Polym. Sci.*, **20**, 651 (1995)
85. Godovky, Y.K., G.L. Slonimsky, *J. Polym. Sci., Polym. Phys. Ed.*, **12**, 1053 (1974)
86. Flory P.J., A.C. McIntyre, *J. Polym. Sci.*, **18**, 592 (1955)
87. Khanna Y.P., T.J. Taylor, *Polym. Eng. Sci.*, **27**, 764 (1989)
88. Hay J.N., P.J. Millis, *Polymer*, **23**, 1380 (1982)
89. Ziabicki A., *Appl. Polym. Symp.*, **6**, 1 (1967)
90. Kamal M.R., E. Chu., *Polym. Eng. Sci.*, **23**, 27 (1983)
91. Beigzadeh D., J.P.B. Soares, T.A. Duever, *Macrom. Rapid Commun.*, **20**, 541 (1999)
92. Wunderlich, B., in *Thermal Analysis*, Academic Press, New York (1990)
93. Alamo, R.G., L. Mandelkern L., *Macromolecules*, **24**, 6480 (1991)
94. Alamo R.G., E.K.M. Chan, L. Mandelkern, I.G.Voight-Martin, *Macromolecules*, **25**, 6381 (1992)
95. Billon, N., C. Magnet, J. M. Haudin, D. Lefebvre, *Colloid. Poym. Sci.*, **272**, 654 (1994)
96. Quinn, F. A., L. Mandelkern, *J. Am. Chem. Soc.*, **80**, 3178 (1958)
97. Haigh, J. A., C. Nguyen, R. G. Alamo, L. Mandelkern, *J. Therm. Anal. Cal.*, **59**, 435 (2000)

98. Fu, Q et al., M. Y. Keating, E.T. Hsieh, P. J. DesLauries, J. Macrom. Sci.-Phys., B., **36**, 41 (1997)
99. Galante, M. J., L. Mandelkern, R.G. Alamo, et al., J. Therm. Anal., **47**, 913 (1996)
100. Sinn, H., Adv. Organomet. Chem., **18**, 99 (1980)
101. Nocolin T.E., Progr. Polym. Sci., **11**,29 (1985)
102. Choi, K. Y., W. H. Ray, J. Macrom. Sci.-Rev. Macrom. Chem.Phys., **C25**, 1 (1985)
103. Soga, K., T. Shiono, Makromol. Chem., **189**, 1531 (1988)
104. Barbe P. C.,G. Cecchin, L. Noristi, Adv. Polym. Sci., **81**, 1 (1987)
105. Soga, K., Makromol. Chem., **191**, 2853 (1990)
106. Mathot, V., M. Pijpers, J. Appl. Polym. Sci., **39**, 979 (1990)
107. Mirabella F.M., J. Polym. Sci. Polym. Phys. Ed., **26**, 1995 (1988)
108. Hill, M. J., P. Barham., Polymer, **36**, 1523 (1995)
109. Mumby, S. J., P. Sher, J. van Ruiten, Polymer, **36**, 2921 (1995)
110. Ref. 97.
111. Wild, L., T. Ryle. D. Knobelock, and I. Peat, J. Polym. Sci Polym. Phys. Ed., **20**, 441 (1992)
112. Tanem, B.S., A. Stori, Thermochim. Acta, **345**, 73 (2000)
113. Turi, E., in *Thermal Characterization of Polymeric Materials*, San Diego, Academic Press (1997)
114. Binsbergen, F. L., J. Polym. Sci. - Polym. Phys. Ed., **11**, 117 (1973)
115. Fitchmun, D. R., S. Newman, J. Polym. Sci. A., **8**, 1545 (1970)
116. Chatterjee, A. M., F. P. Price, J. Polym. Sci. - Polym. Phys. Ed., **13**, 2369 (1975)
117. Shaner, J. R., R. D. Corneliussen, J. Polym. Sci. - Polym. Phys. Ed., **10**, 1611 (1972)
118. Chatterjee, A. M., F. P. Price, J. Polym. Sci. - Polym. Phys. Ed., **13**, 2391 (1975)
119. Kantz, M.R., R. D. Corneliussen, J. Polym. Sci., Polym. Lett. Ed., **11**, 279 (1973)
120. Gray, D. G., J. Polym. Sci., Polym. Lett. Ed., **12**, 509 (1974)
121. Ref. 90.
122. Huson, M. G., W. J. McGill, J. Polym. Sci. - Polym. Chem. Ed., **22**, 3571 (1984)
123. He, T., R. S. Porter, J. Appl. Polym. Sci., **35**, 1945 (1988)

124. Yu, Z., A. Ait-Kadi, J. Brisson, *Polym. Eng. Sci.*, **31**, 122 (1991)
125. Campbell, D., N. M. Qayyum, *J. Polym. Sci. - Polym. Phys. Ed.*, **18**, 83 (1980)
126. Thomason, J. L., A. A. vanRooyen, *J. Mat. Sci.*, **27**, 889 (1992)
127. Lee, Y.C., R.S. Porter, *Polym. Eng. Sci.*, **26**, 633 (1986)
128. Caramaro, L., B. Chabert, J. Chauchard, *Polym. Eng. Sci.*, **31**, 1279 (1991)
129. Hsiao, B.S., E.J.H. Chen, *Mat. Res. Soc. Symp. Proc.*, 170 (1990)
130. Chabert, B., J. Chauchard., *Ann. Chim. Fr.*, **16**, 173 (1991)
131. Thomason, J. L., A.A. van Rooyen, *J. Mater. Sci.*, **27**, 897 (1992)
132. Monasse, B., *J. Mater. Sci.*, **27**, 6947 (1992)
133. Janeschitz-Kriegl, H., *Progr. Colloid Polym. Sci.*, **87**, 117 (1992)
134. Nakamura, K. et al, *J. Appl. Polym. Sci.*, **16**, 1077 (1972)
135. Hoffman, J. D., J. J. Weeks, *J. Res. Nat. Bur. Stand.*, **A66**, 13 (1962)
136. Schmidtke, J., G. Stroble, T. Thurn-Albrecht, *Macromolecules*, **30**, 5804 (1997)
137. Marigo, A., C. Marega, R. Zanetti, A. Celli, G. Paganetto, *Macromol. Rapid commun.*, **15**, 225 (1994)
138. Rodriguez-Arnold, J., A. Zhang. S. Z. D. Cheng, A. J. Lovinger, E. T. Hseih. P. Chu, T. W. Johnson, K. G. honnell, R. G. Gerts, S. J. Palackal, G. R. Hawley, M. B. Welch, *Polymer*, **35**, 1884 (1994)
139. Flory, P. J., *Trans. Faraday. Soc.*, **51**, 848 (1955)
140. Gelfer M. Y., H. H. Winter, *Macromolecules*, **32**, 8974 (1999)
141. Besanson, S., J. Minick, A. Moet, S. Chum, A. Hiltner, E. Baer, *J. Polym. Sci., Phys. Ed.*, **34**, 1301 (1996)
142. Kimura, K., S. Yuassa, Y. Maru, *Polymer*, **25**, 441 (1984)
143. Deffieux, A., M. Ribeiro, E. Addison, M. Fontanille, *Polymer*, **33**, 4337 (1992)
144. Lambert, W. S., P. J. Phillips, *Polymer*, **3**, 3585 (1996)
145. Lambert, W. S., P. J. Phillips, *Macromolecules*, **27**, 3537 (1994)
146. Kim, M.-H., P. J. Phillips, *J. Appl. Polym. Sci.*, **70**, 1893 (1998)
147. Wagner, J., S. Abu-Iqyas, K. Monar, P. J. Phillips, *J. Poly.*, **40**, 4717 (1999)

APPENDIX 1

RESINS PHYSICAL PROPERTIES

Resins Physical Properties

Resin	Como	Mod/Cat	Co-me %	Branc B/KC	Term Unsat	Side Unsat	Internal Unsat	Total Unsat	Mn (g/mol)	Mw (g/mol)	Mw/Mn	Density (g/cm ³)	Melt Index
1-B	BUT	Gas/ZN	4.03	20.20	0.01631	0.00619	0.00910	0.02860	24200	98700	4.1	0.9194	0.94
2-H	BUT	Sol/ZN	3.80	18.90	0.04681	0.00866	0.00724	0.06451	24900	120000	4.8	0.9190	0.75
3-A	HEX	Gas/ZN	3.94	19.72	1.01890	0.01248	0.00655	0.03792	30000	111000	3.7	0.9208	0.9
4-C	HEX	Sol/ZN	3.77	18.87	1.01821	0.01617	0.00459	0.03896	36000	111300	3.1	0.9234	0.85
5-D	HEX	Gas/Met	3.08	15.41	1.01903	0.02139	0.00433	0.04474	44000	98000	2.2	0.9192	1
6-E	HEX	Gas/Met	2.56	12.80	1.01231	0.01203	0.00810	0.03245	43000	94000	2.2	0.9194	1.03
7-M	HEX		4.50						20600	74200	3.64	0.9192	
8-G	OCT	Sol/ZN	3.20	15.80	0.05452	0.00805	0.01178	0.07435	17000	106000	6.2	0.9200	1
9-I	OCT	Sol/Met	5.00	24.80	0.03945	0.01016	0.02764	0.07725	22000	53000	2.4	0.9070	6.5
10-J	OCT	Sol/Met	3.20	15.80	0.03801	0.00583	0.02140	0.06524	38000	70000	1.8	0.9180	1.8
11-L	OCT	Sol/ZN	2.80						25900	114000	4.4	0.9212	0.63
12-F	LDPE	Gas							12000	88000	7.3	0.9190	2.3
13-K	LDPE	Gas							16000	66200	4.1	0.9203	2.31
14	HDPE								22300	74500	3.3	0.961	7.4

APPENDIX 2

COMPRESSION MOLDING EXPERIMENTAL PROCEDURE

In the preparation of samples for the DSC studies, some important steps must be followed. First of all, the resin, even if it is not highly hygroscopic, should be dried to eliminate any source of error that can arise and interfere with measurements on the DSC apparatus. Using a Fischer vacuum oven, all resins were dried at a constant temperature 90°C for two hours and a vacuum of 25mmHg pressure. After the drying period, the resins were removed from the oven and placed immediately into a desiccator to keep dry before compression molding into sample sheets.

For the compression molding, a Carver Laboratory Press (maximum load 50,000 lbs, or approximately pressure 4.3MPa) was used. The press is first preheated to the required operating temperature, with the upper and lower heated compression plates pressed together by applying a small pressure (using a load of about 1,000-1,500 lbs., or a reading on the pressure gauge of 85-128kPa). For precise control, the heater dial for each plate should be adjusted (by trial and error) to obtain the desired temperature. In the mean time, the flat rectangular sheet mold “sandwiched” between plates can be prepared. The arrangement consisted of the following layers: (i) the first thick aluminum plate (1cm) is placed at the bottom, (ii) then a square stainless steel plate (flat and smooth to produce good sample surface finish), and a Mylar (high temperature) foil / sheet to cover the plate (to prevent the molding surface from sticking to the plate on cooling), (iii) the sheet mold (its thickness dimension dictated by the sample requirements for the type of DSC procedure), and then the resin to completely fill the mold cavity and to allow for the density change and the compressibility as a melt, (iv) the second steel plate with Mylar foil/ sheet cover, and (v) finally, the second aluminum plate at the top.

The resin quantity necessary to fill the molding can be calculated from the mold cavity dimensions and resin melt density. To avoid empty air spaces, and ensure complete filling during compression molding, an extra 30-50% of the resin is added. Since the thickness of the mold is small, the excess material wasted is not significant.

The next step involves carefully placing the cold mold arrangement between the heated plates. The pressure is released until the distance between the plates is enough for the mold to be inserted. For safety, lab coat, suitable glasses for eye protection, and high

temperature gloves should be worn for this operation. Time is monitored using a timer located on the press.

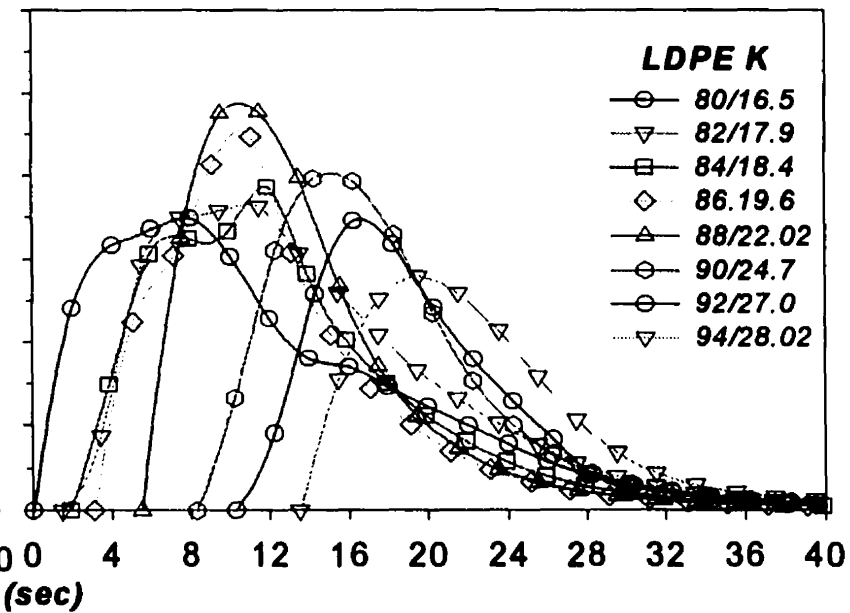
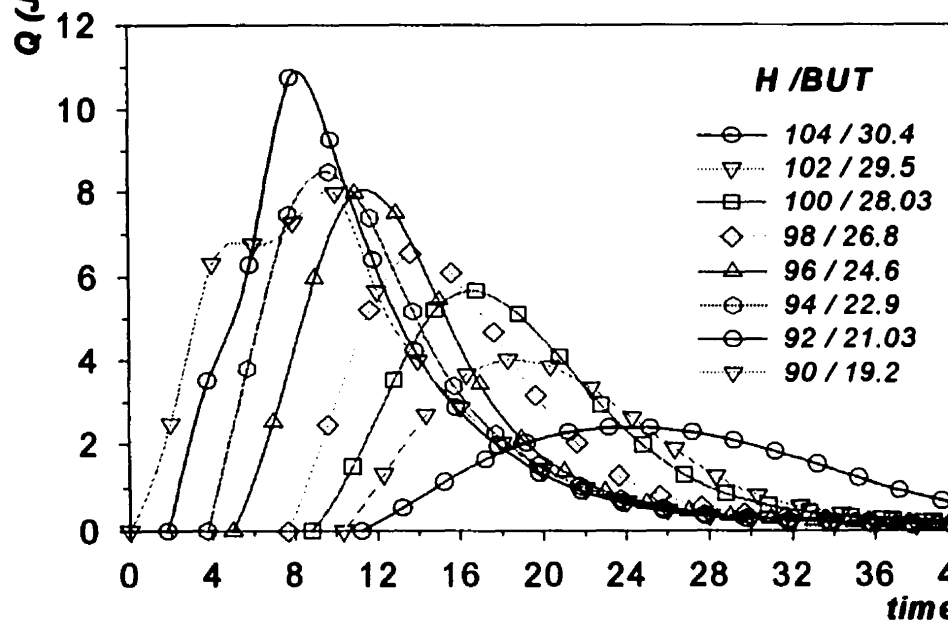
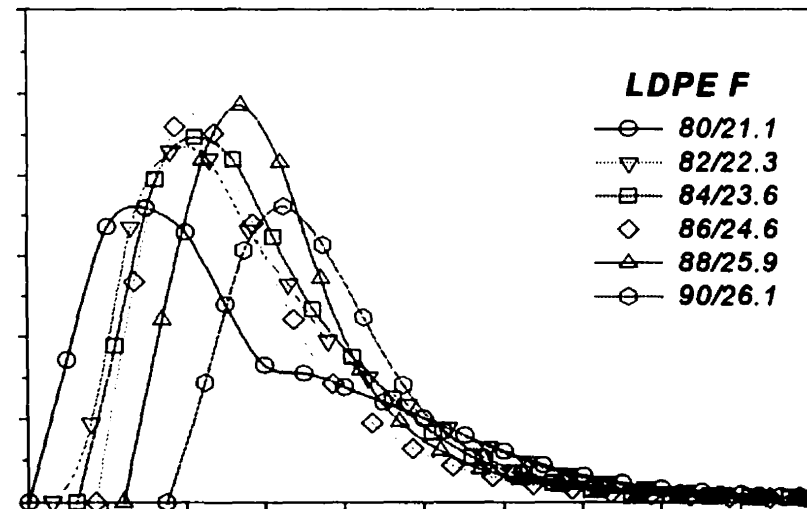
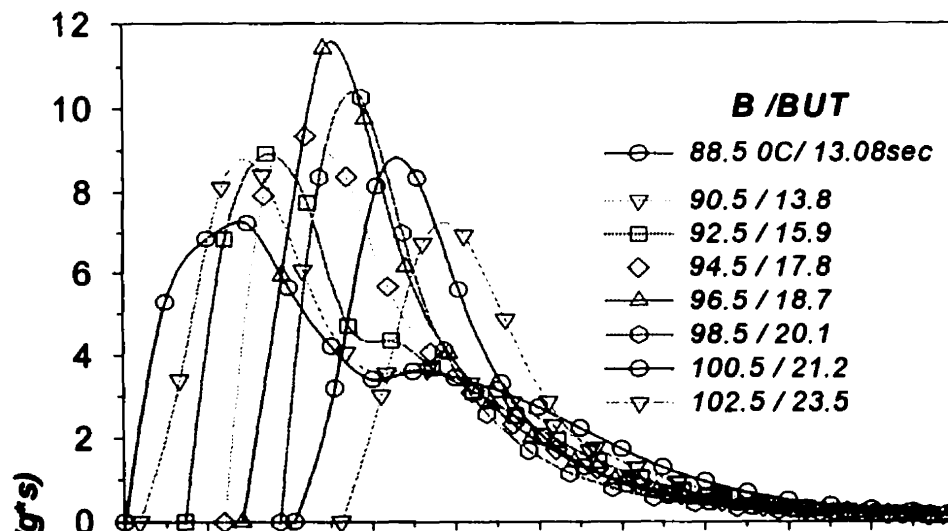
To avoid air entrapment in the molding, compression was performed using the following procedure: (i) pressurize the material at a load of 12,000 lbs (or pressure 1MPa) using the press pump lever, and maintain for about 3 minutes. During this period, small variations in temperature of $\pm 5^{\circ}\text{C}$ were observed, and slight adjustments to the pressure were required, (ii) release the pressure and wait for 30 seconds, (iii) repeat step 1, (iv) repeat step 2, (v) pressurize the instrument at a load of 15,000 lbs (or pressure 1.27MPa), and keep at this level for 10 minutes. In this case, small adjustments to the pressure are required, (vi) now, the press heaters are switched off, and the valve for water cooling fully opened until the temperature reduces to room temperature. This period of cooling down can take between 12-15 minutes, (vii) any remaining pressure is released, and the mold is removed. The molding is handled with care to avoid perforation or breakage when the Mylar plastic foils in contact with the sheet surfaces are removed. To avoid moisture absorption, the plastic sheet is placed in a desiccator.

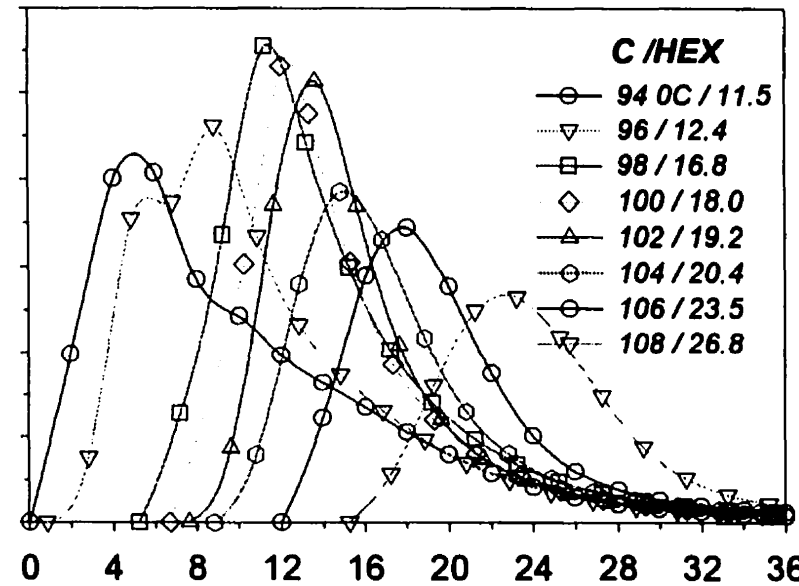
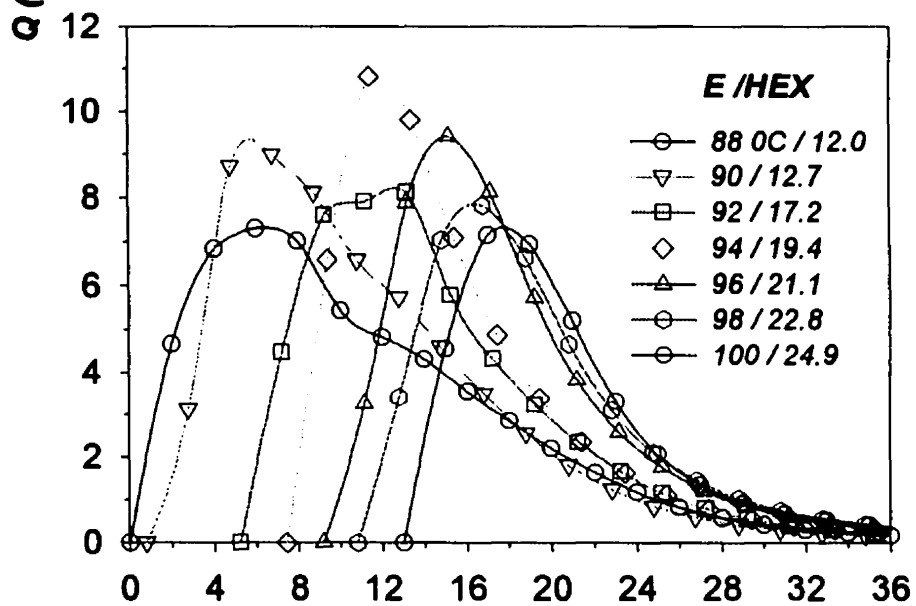
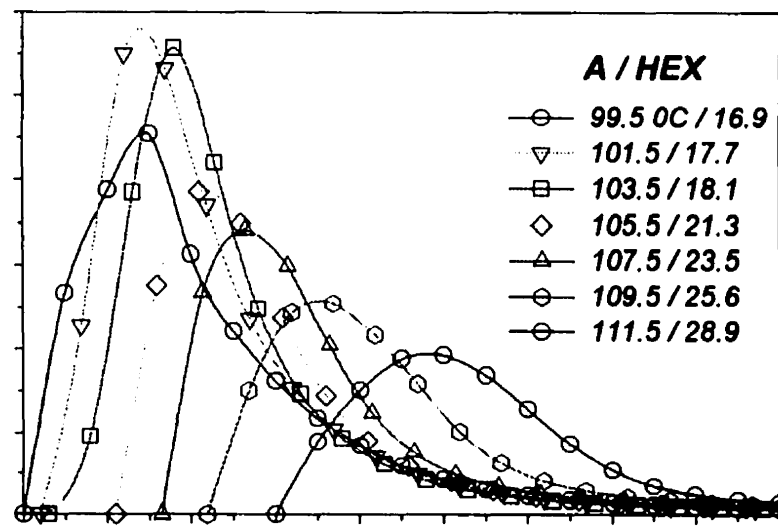
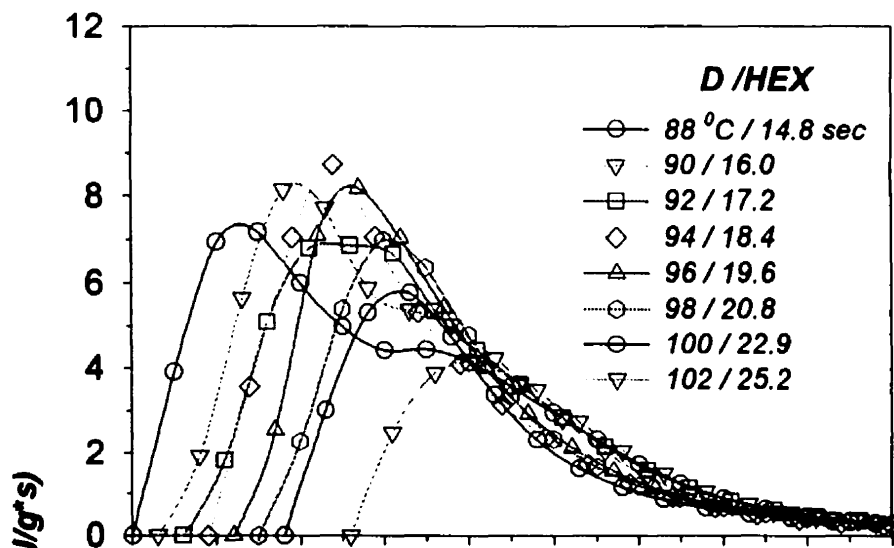
To obtain samples that fit into the circular-shaped aluminum pans, a steel hole-punch of diameter 3/16 inch (4.76mm) was used. To avoid any contamination of the samples, the puncher must be cleaned before use.

APPENDIX 3

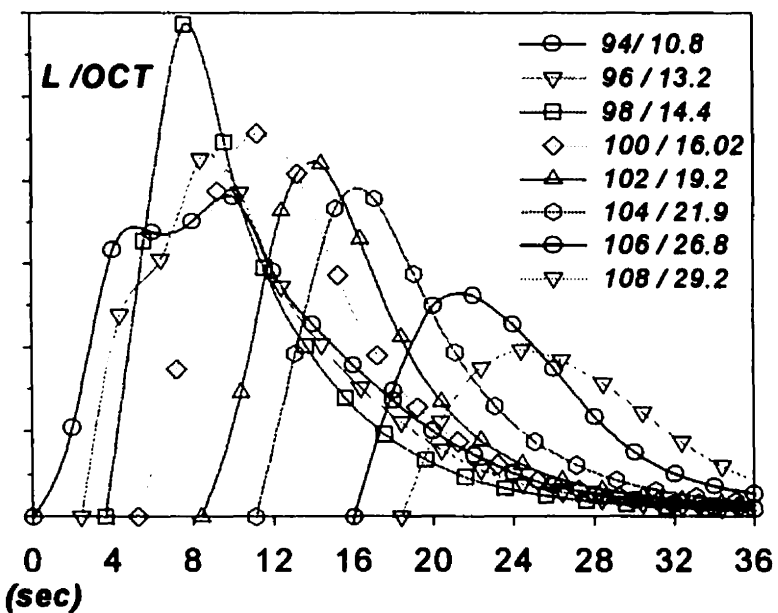
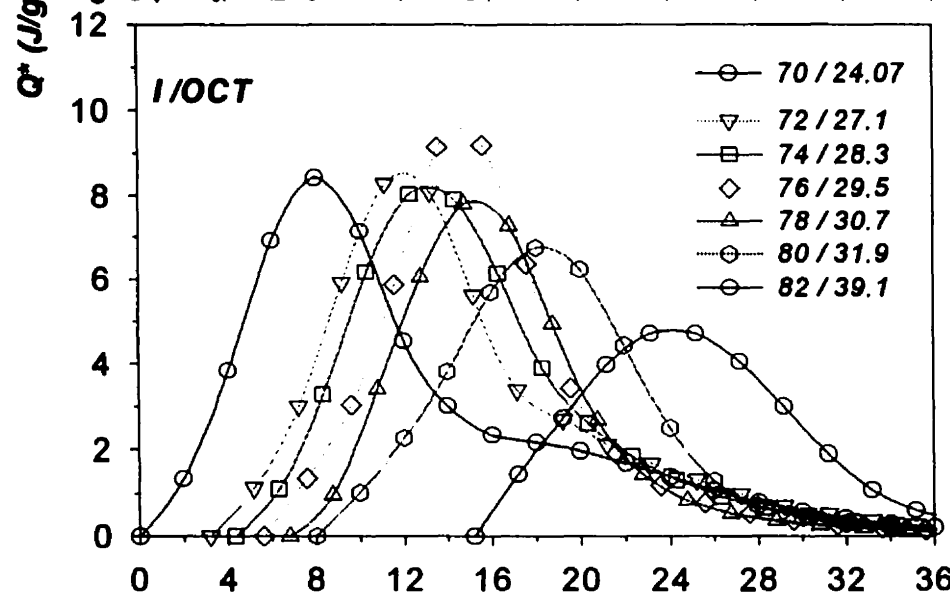
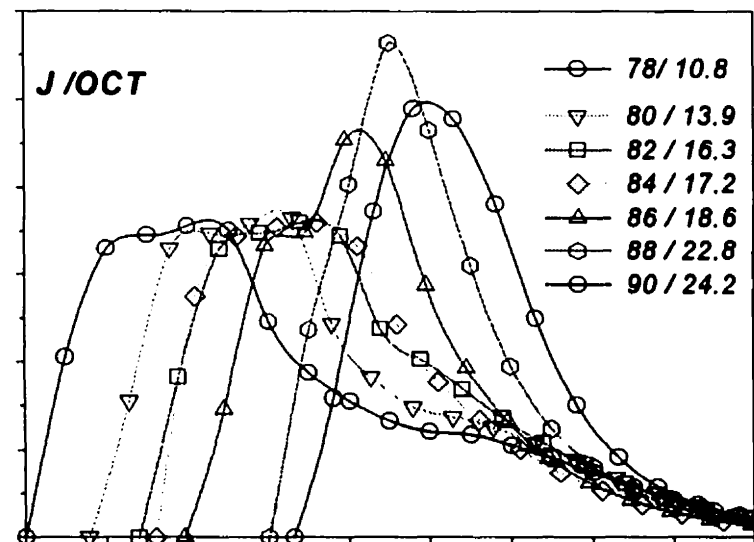
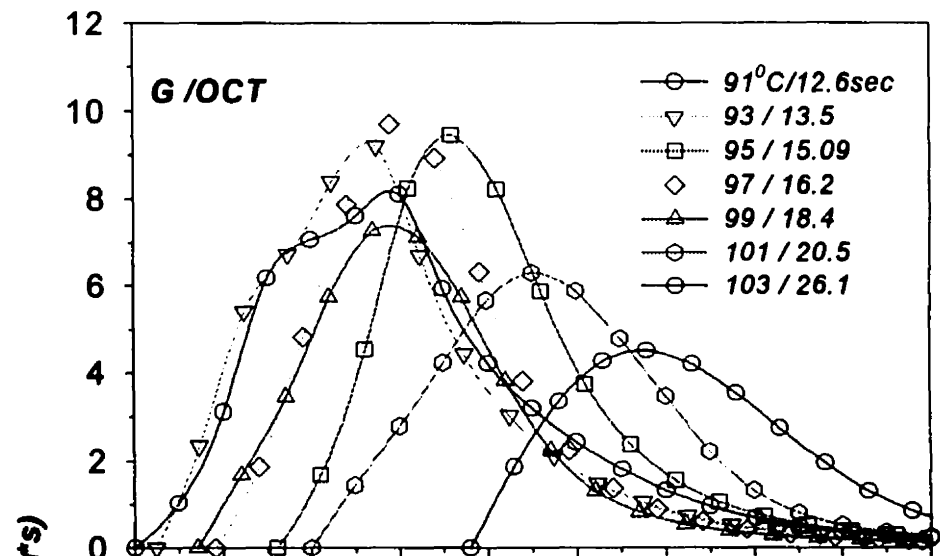
PLOTS OF ISOTHERMAL DSC EXOTHERMS.

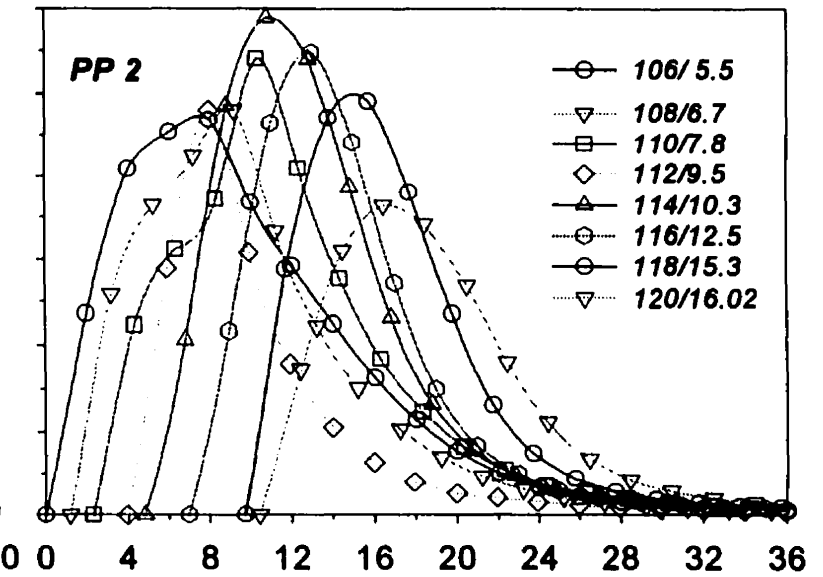
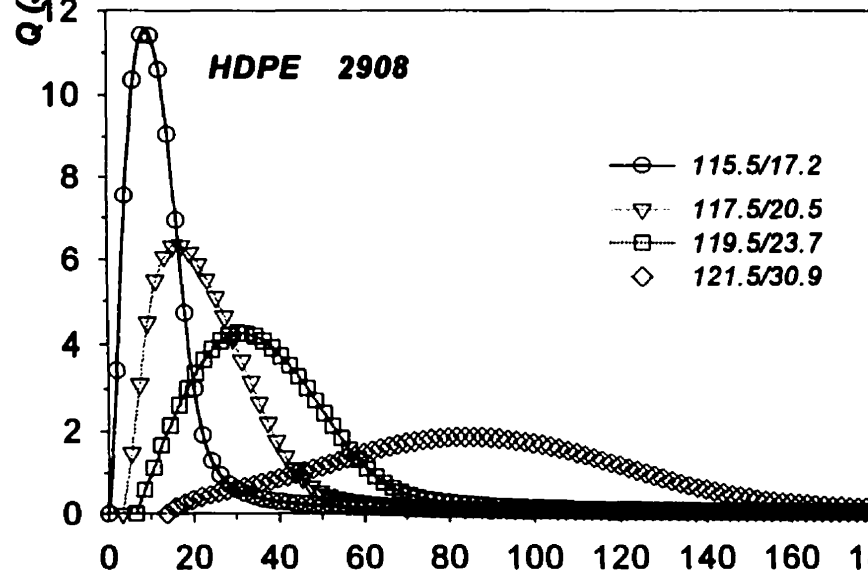
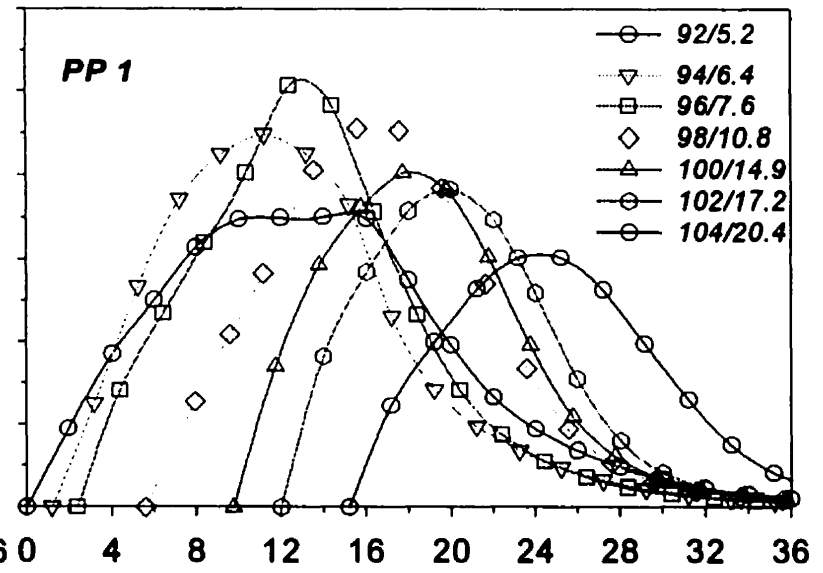
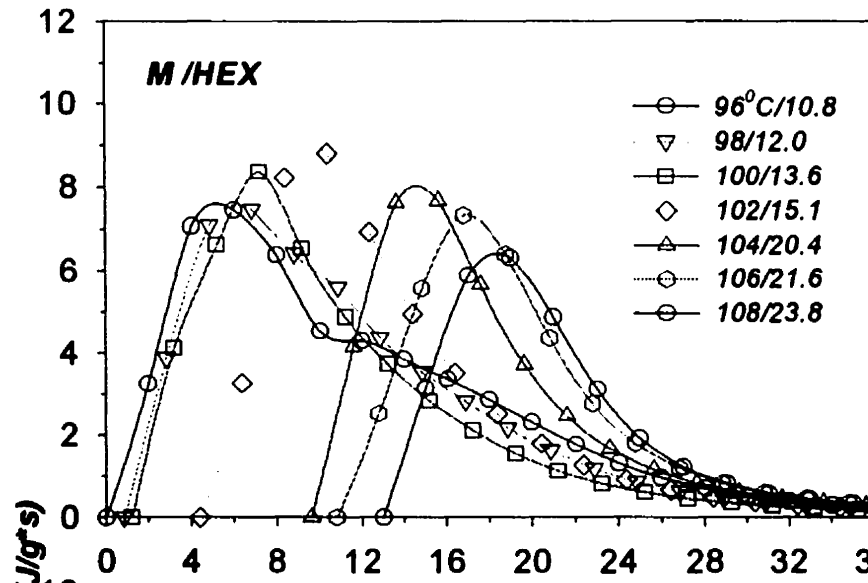
**(Legend: Experimental Isothermal Temperature (°C),
Induction Time (sec.))**





time (sec)





time (sec)

APPENDIX 4

HEAT OF FUSION, HEAT OF CRYSTALLIZATION AND PEAK MELTING TEMPERATURE VALUES AT DIFFERENT COOLING RATES (NON-ISOTHERMAL EXPERIMENTS)

B / BUT/Gas/ZN

Rate of Cooling (C/min)	Heat fus CM (J/g)	T melt CM-Peak (C)	Heat fus SM (J/g)	T melt SM-Peak (C)	Heat of Cryst. (J/g)	On-Set Cryst (C)
[1]	[2]	[3]	[4]	[5]	[6]	[7]
1	105.039	120.097	107.104	122.734	112.825	113.29
2.5	105.045	120.436	108.343	121.77	108.858	111.411
5	109.473	120.082	106.726	121.084	105.109	109.863
10	106.577	120.087	106.21	120.42	103.292	108.159
20	107.803	120.083	107.583	119.761	99.627	107.106

H / BUT/Sol/ZN

[1]	[2]	[3]	[4]	[5]	[6]	[7]
1	106.39	116.403	115.356	120.750	117.809	110.542
2	106.001	116.158	114.045	119.750	115.4	108.957
5	107.897	116.087	113.665	118.748	109.573	106.696
10	105.489	116.023	111.011	117.748	108.027	104.834
20	105.924	116.947	109.738	117.089	106.187	103.141
40	105.756	115.978	107.678	116.419	86.866	100.112

A / HEX/Gas/ZN

[1]	[2]	[3]	[4]	[5]	[6]	[7]
1	110.216	123.432	113.754	125.1	114.01	117.158
2.5	110.307	123.752	112.237	124.555	108.438	115.154
5	108.251	123.423	111.759	124.093	105.138	113.703
10	109.177	123.756	111.14	124.086	103.546	112.493
20	110.265	123.438	109.798	123.441	101.705	111.109

C / HEX/Gas/ZN

[1]	[2]	[3]	[4]	[5]	[6]	[7]
1	108.387	122.401	108.998	123.75	116.846	114.784
2.5	107.228	122.072	110.427	123.415	110.485	113.635
5	105.721	122.08	108.273	123.079	107.8	111.879
10	109.118	122.428	108.00	122.415	104.391	110.833
20	107.525	122.42	107.12	122.418	102.877	108.747
40	107.226	122.409	107.221	121.42	87.207	106.657

D / HEX/Gas/Met

[1]	[2]	[3]	[4]	[5]	[6]	[7]
1	108.533	117.087	111.647	120.094	118.921	114.998
2.5	108.018	117.418	110.968	119.76	113.258	113.52
5	107.126	117.405	108.750	118.754	109.983	111.88
10	109.072	117.406	109.730	118.417	107.672	109.164
20	108.363	116.743	107.376	116.745	105.588	106.48
40	107.637	116.074	107.763	116.074	85.715	104.047

E / HEX/Gas/Met

[1]	[2]	[3]	[4]	[5]	[6]	[7]
1	112.739	116.752	115.918	119.427	122.166	111.184
2	111.008	117.088	115.774	119.09	120.365	109.708
5	112.722	117.077	113.456	118.408	111.08	107.531
10	110.258	117.082	112.125	117.413	104.325	105.829
20	112.213	117.064	110.85	116.741	101.258	103.778

G / OCT/Sol/ZN

[1]	[2]	[3]	[4]	[5]	[6]	[7]
1	108.883	123.76	115.570	123.423	119.279	114.613
2	108.589	123.454	114.906	123.095	118.022	113.166
5	108.054	123.501	114.677	122.089	111.1	110.37
10	108.026	123.476	110.622	123.763	107.998	108.16
20	107.984	123.187	111.162	124.083	105.831	106.432
40	107.855	123.182	109.027	123.759	90.923	104.009

I / OCT/Sol/Met

[1]	[2]	[3]	[4]	[5]	[6]	[7]
1	82.876	98.028	87.196	100.709	95.899	91.772
2	81.598	98.578	86.826	100.380	93.451	91.1
5	80.978	98.654	86.068	99.37	85.285	88.873
10	80.217	97.957	84.041	98.709	82.002	86.887
20	83.158	98.005	83.938	98.377	80.105	85.283
40	82.567	97.966	82.724	98.044	71.056	83.351

J / OCT/Sol/Met

[1]	[2]	[3]	[4]	[5]	[6]	[7]
1	109.458	111.598	116.739	112.385	119.212	103.305
5	109.987	111.122	114.300	111.820	109.587	100.709
10	109.859	111.45	112.314	111.725	107.12	99.183
20	110.159	111.251	109.480	111.392	105.613	97.842
40	110.258	111.354	108.359	111.027	91.332	96.208

L / OCT/Sol/ZN

[1]	[2]	[3]	[4]	[5]	[6]	[7]
1	114.684	119.759	121.972	123.098	125.459	114.224
5	115.019	119.658	120.381	121.761	120.026	111.042
10	114.279	119.211	117.687	121.43	115.289	109.856
20	114.359	119.448	117.52	120.762	113.071	107.77
40	116.025	119.451	115.394	120.091	102.3	105.305

LDPE F / Gas

[1]	[2]	[3]	[4]	[5]	[6]	[7]
1	106.763	107.708	108.634	109.05	111.364	101.771
2	107.448	107.38	108.232	108.721	109.283	100.63
5	106.573	107.721	106.801	108.055	106.664	98.187
10	105.198	107.389	105.452	107.72	104.612	97.183
20	106.687	107.384	104.812	107.386	101.198	95.847
40	106.657	108.052	103.657	107.055	93.313	93.801

LDPE K / Gas

[1]	[2]	[3]	[4]	[5]	[6]	[7]
1	114.655	108.711	118.222	110.052	120.02	102.571
5	115.258	108.521	117.466	109.721	115.891	99.878
10	115.189	108.089	113.539	109.385	111.437	98.878
20	113.957	109.258	113.339	109.053	105.951	96.526
40	114.085	109.012	112.439	108.721	95.518	94.922

PP-1 / Montell

[1]	[2]	[3]	[4]	[5]	[6]	[7]
1	87.558	159.17	99.462	163.849	104.327	133.062
5	87.523	159.593	93.332	161.180	95.531	125.195
10	87.549	158.948	90.989	160.514	87.021	122.135
20	87.537	158.99	88.800	159.849	84.919	120.37
40	87.541	159.544	87.133	159.183	74.118	115.772

PP-2 / Montell

[1]	[2]	[3]	[4]	[5]	[6]	[7]
1	84.516	158.178	93.800	162.191	98.249	144.873
5	84.624	158.193	89.754	159.851	86.581	137.687
10	84.669	158.201	87.260	159.522	84.323	134.123
20	84.981	158.151	85.865	158.517	81.122	130.337
40	84.858	158.215	84.152	157.848	71.112	126.287

M

[1]	[2]	[3]	[4]	[5]	[6]	[7]
1	103.628	124.419	108.704	126.768	100.139	120.518
5	102.988	124.022	107.904	124.763	94.037	117.529
10	103.225	124.384	107.233	124.423	91.295	115.804
20	103.581	124.125	106.715	124.086	88.782	113.727
40	102.852	123.858	103.186	123.417	87.835	111.821

HDPE 2908

[1]	[2]	[3]	[4]	[5]	[6]	[7]
1	200.666	133.105	219.311	134.572	223.021	122.769
2.5	198.642	134.405	215.317	133.720	221.857	121.593
5	198.893	134.401	211.444	132.716	217.382	120.231
10	200.013	132.408	208.445	131.061	213.964	119.524
20	198.538	133.729	205.654	132.729	212.968	118.413

APPENDIX 5

HEAT OF FUSION AND PEAK MELTING TEMPERATURE VALUES AT DIFFERENT COOLING RATES (ISOTHERMAL EXPERIMENTS)

LLDPE B

<i>T</i> cryst (C)	<i>H</i> fus/CW/J/g	<i>T</i> melt/CW(C)	<i>H</i> fus/SW/J/g	<i>T</i> melt/SW(C)
[1]	[2]	[3]	[4]	[5]
88.5	110.182	120.085	116.5	119.607
90.5	109.167	120.098	105.81	118.953
92.5	107.993	120.106	91.05	118.957
94.5	107.08	120.115	98.25	119.299
96.5	108.311	120.087	-	119.286
98.5	108.532	119.76	-	119.278
100.5	110.484	120.402	-	119.935
102.5	109.727	119.75	-	120.27
104.5	107.126	119.445	-	120.936

LLDPE H

[1]	[2]	[3]	[4]	[5]
90	112.201	117.77	105.53	117.11
92	110.646	117.777	105.9	117.105
94	110.686	118.106	91.05	117.439
96	111.16	117.433	-	117.776
98	109.013	117.767	-	118.444
100	109.433	117.441	-	119.448
102	108.866	117.778	-	98.386
104	110.706	118.779	-	98.405

LLDPE A

[1]	[2]	[3]	[4]	[5]
99.5	108.871	123.749	-	123.276
101.5	110.541	123.754	103.2	123.278
103.5	109.026	123.756	91.7	122.946
105.5	109.491	123.753	-	123.067
106.5	109.756	123.405	-	123.599
107.5	111.012	123.739	-	123.931
109.5	108.294	123.758	-	123.947
111.5	108.155	123.782	-	123.968

LLDPE C

[1]	[2]	[3]	[4]	[5]
94	108.894	122.429	102.61	121.428
96	107.021	122.090	97.230	121.762
98	109.503	122.422	96.09	122.097
100	109.298	122.435	89.1	121.767
102	106.674	121.768	-	121.438
104	108.198	122.764	-	122.099
106	109.218	122.081	-	122.088
108	108.560	122.088	-	122.422

LLDPE D

[1]	[2]	[3]	[4]	[5]
84	108.531	117.421	-	116.425
86	110.893	117.418	-	116.755
88	110.547	117.746	115.9	116.418
90	109.957	116.742	110.7	116.076
92	108.203	117.076	106.51	116.408
94	107.718	115.743	99.02	116.084
96	109.806	117.738	-	116.743
98	108.550	117.408	-	116.414
100	108.480	118.081	-	117.419
102	108.579	116.737	-	117.072

LLDPE E

[1]	[2]	[3]	[4]	[5]
88	112.81	117.082	112.2	116.421
90	112.76	117.409	118.75	116.083
92	114.94	117.087	-	116.085
94	113.62	117.08	106.6	116.086
96	109.76	117.069	-	116.413
98	112.31	117.059	-	117.081
100	112.02	117.082	-	117.087

LLDPE M

[1]	[2]	[3]	[4]	[5]
96	106.88	124.048	108.45	123.42
98	106.35	124.085	105.4	123.422
100	106.33	124.425	97.2	123.759
102	103.71	124.413	-	123.753
104	107.58	124.107	-	123.447
106	107.07	124.107	-	123.763
108	102.77	124.091	-	123.761

LLDPE G

[1]	[2]	[3]	[4]	[5]
91	109.89	124.092	117.3	123.761
93	114.39	123.744	112.15	123.763
95	112.87	123.754	106.2	123.764
97	113.17	123.772	-	123.439
99	110.22	123.768	-	123.772
101	109.61	124.117	-	123.788
103	110.03	124.12	-	124.126

LLDPE I

[1]	[2]	[3]	[4]	[5]
70	84.28	101.062	97.58	98.386
72	85.061	100.399	87.6	98.405
74	85.121	100.073	-	98.739
76	83.635	99.74	-	98.407
78	85.939	100.067	-	98.403
80	84.647	100.406	-	98.738
82	85.946	99.736	-	98.738

LLDPE J

[1]	[2]	[3]	[4]	[5]
78	109.71	112.425	123.1	111.425
80	107.57	112.089	115.7	111.422
82	108.09	112.421	108.8	111.759
84	111.31	112.423	99.89	111.755
86	111.69	112.485	-	111.756
88	110.17	112.417	-	111.754
90	109.89	112.071	-	111.088

LLDPE L

[1]	[2]	[3]	[4]	[5]
94	118.12	120.086	110.2	121.028
96	118.54	120.757	-	120.092
98	119.13	120.748	98.4	120.08
100	118.07	121.418	98.2	120.422
102	115.53	120.765	-	120.77
104	111.65	121.443	-	123.784
106	112.3	121.074	-	121.415
108	118.03	121.072	-	121.751

LDPE F

[1]	[2]	[3]	[4]	[5]
80	108.23	107.711	-	107.058
82	106.91	107.723	108.31	107.061
84	104.2	107.389	103.2	106.729
86	108.41	107.715	-	107.055
88	110.46	107.397	-	107.058
90	106.69	107.785	-	107.388

LDPE K

[1]	[2]	[3]	[4]	[5]
80	116.02	109.701	113.82	109.04
82	115.06	109.717	118.9	109.051
84	114.84	109.713	106.5	109.043
86	112.07	109.379	103.2	109.05
88	113.29	109.394	-	109.054
90	116.4	109.706	-	109.713
92	114.19	109.697	-	109.378
94	115.25	109.709	-	109.717

PP-1

[1]	[2]	[3]	[4]	[5]
92	87.82	160.866	129.4	162.208
94	93.666	161.208	128.89	162.878
96	88.473	160.203	128.1	163.21
98	89.058	159.862	125.2	163.54
100	87.34	160.515	100.01	163.19
102	87.415	161.19	94.9	163.199
104	87.039	160.514	-	163.521

PP-2

[1]	[2]	[3]	[4]	[5]
106	85.766	158.176	122.09	157.176
108	82.674	157.851	-	157.517
110	83.541	158.512	113.28	158.022
112	84.399	157.323	-	158.45
114	84.52	157.909	118.5	158.192
116	86.258	158.171	98.7	158.217
118	87.021	158.173	92.15	157.934
120	86.011	158.064	89.8	157.998

HDPE 2908

[1]	[2]	[3]	[4]	[5]
115.5	199.85	134.41	189.8	133.24
117.5	200.11	134.41	187.91	134.59
119.5	199.79	133.74	184.2	134.57
121.5	200.35	133.74	182.1	135.24

APPENDIX 6

EXPERIMENTAL VALUES OF THE AVRAMI & TOBIN PARAMETERS (n, k), HEAT OF CRYSTALLIZATION AND INDUCTION TIME (LINEAR AND NON-LINEAR REGRESSION)

NLR – r^2 –PARAMETER VALUES FOR SELECTED ISOTHERMAL TEMPERATURES.

LLDPE B

isoT (C)	n/LR Avrami	k/LR E+03	n/LR Tobin	k/LR E+03	n/NLR	k/NLR E+03	k/NLR E+03		QCryst (J/g)	IndTime (sec)
[1]	[2]	[3]	[4]	[5]	[6]	[7]	[8]		[9]	[10]
88.5	1.727	14.588	1.793	14.723	1.597	18.370	22.01/8.4	1.52	117.240	13.08
90.5	2.095	7.780	2.195	7.730	1.928	10.549	9.191	2.0	107.346	13.87
92.5	1.425	22.130	1.980	17.864	1.556	29.137	32.31/12.6	1.52	102.880	15.98
94.5	1.701	26.791	1.983	22.387	1.590	32.623	38.4/15.2	1.52	99.680	17.88
96.5	2.102	14.554	2.232	14.421	2.103	14.535	17.228	2.0	97.360	18.72
98.5	1.878	28.379	2.122	25.468	1.766	33.756	23.133	2.0	86.465	20.13
100.5	2.271	8.433	2.495	7.211	2.368	7.224	5.7/13.3	2.52	80.033	21.28
102.5	2.173	9.462	2.374	8.279	2.224	8.734	12.722	2.0	72.091	23.52

LLDPE H

[1]	[2]	[3]	[4]	[5]	[6]	[7]	[8]		[9]	[10]
90	2.092	5.871	2.442	3.980	1.991	7.123	7.002	2.00	106.920	19.21
92	2.056	8.531	2.416	6.081	2.176	7.113	9.962	2.00	107.940	21.03
94	2.060	10.115	2.323	8.204	2.109	9.486	11.382	2.00	93.244	22.94
96	2.221	6.310	2.427	5.458	2.320	5.350	3.99/1	2.52	86.568	24.69
98	2.117	7.534	2.306	6.637	2.109	7.664	9.442	2.00	79.924	26.84
100	2.208	4.169	2.433	3.357	2.297	3.561	2.5/5.9	2.52	77.285	28.03
102	2.026	5.212	2.265	4.093	2.068	4.934	5.626	2.00	64.568	29.54
104	2.000	2.421	2.197	1.914	1.958	2.725	2.444	2.00	59.165	30.41

LLDPE A

[1]	[2]	[3]	[4]	[5]	[6]	[7]	[8]		[9]	[10]
99.5	1.892	15.170	2.094	13.520	1.869	15.953	12.815	2.0	99.753	16.92
101.5	2.160	10.232	2.325	9.638	2.307	8.442	6.0/14.1	2.52	104.740	17.70
103.5	2.645	3.177	2.865	2.685	3.219	2.645	4.2/11.0	2.52	94.106	18.15
105.5	1.832	21.677	2.082	18.836	1.705	27.236	15.761	2.0	77.970	21.30
107.5	1.772	24.547	2.007	21.877	1.635	31.404	40.04/15.9	1.52	70.340	23.50
109.5	1.894	13.304	2.097	11.587	1.791	15.985	10.759	2.0	64.786	25.68
111.5	1.909	8.810	2.176	6.855	1.811	10.812	7.127	2.0	56.280	28.92

LLDPE C

[1]	[2]	[3]	[4]	[5]	[6]	[7]	[8]		[9]	[10]
94	1.993	10.139	2.111	9.705	1.839	13.407	9.858	2.0	104.102	11.59
96	2.011	10.471	2.144	10.023	1.999	10.719	10.696	2.0	98.76	12.43
98	2.034	16.069	2.111	16.904	1.996	17.054	16.949	2.0	97.050	16.81
100	1.993	10.139	2.111	9.705	1.839	13.407	9.858	2.0	92.102	18.01
104	1.854	21.522	2.099	18.923	1.863	22.191	17.709	2.0	70.580	20.42
106	2.192	8.035	2.447	6.592	2.308	6.755	4.8/11.3	2.52	68.820	23.59
108	2.370	3.555	2.536	3.105	2.531	2.689	2.8/6.6	2.52	61.200	26.83

LLDPE D

[1]	[2]	[3]	[4]	[5]	[6]	[7]	[8]	[9]	[10]	
88	1.888	9.484	1.946	11.324	1.914	9.492	8.207	2.0	117.750	14.82
90	2.319	3.304	2.454	2.965	2.490	2.522	2.4/5.8	2.5/2	112.964	16.02
92	2.256	3.565	2.370	3.273	2.396	2.879	2.4/5.6	2.5/2	108.667	17.21
94	2.057	8.531	2.179	8.110	2.110	7.947	9.561	2.0	103.577	18.45
96	2.235	5.495	2.271	5.741	2.402	4.337	3.6/8.5	2.5/2	101.335	19.64
98	2.159	6.124	2.319	5.458	2.281	5.121	3.5/8.2	2.5/2	85.541	20.82
100	1.946	11.324	2.081	10.665	1.971	11.206	10.674	2.0	72.678	22.94
102	1.854	12.217	1.980	11.580	1.848	12.696	9.841	2.0	59.575	25.20

LLDPE E

[1]	[2]	[3]	[4]	[5]	[6]	[7]	[8]	[9]	[10]	
88	1.808	12.217	1.969	10.964	1.775	13.231	8.348	2.0	115.546	12.01
90	2.191	15.929	2.357	5.248	2.346	4.841	3.71/8.7	2.5/2	120.520	12.78
92	1.921	11.967	2.130	10.280	1.921	12.237	10.725	2.0	104.386	17.22
94	1.910	17.378	2.159	14.927	1.944	17.196	15.670	2.0	108.853	19.42
96	2.177	6.871	2.385	5.834	2.290	5.829	4.07/9.5	2.5/2	107.925	21.16
98	2.060	9.419	2.282	7.962	2.127	8.662	10.719	2.0	90.765	22.80
100	1.878	16.330	2.137	13.614	1.889	16.662	13.844	2.0	81.578	24.99

LLDPE M

[1]	[2]	[3]	[4]	[5]	[6]	[7]	[8]	[9]	[10]	
96	2.024	7.568	2.055	7.943	2.103	6.952	8.269	2.00	110.886	10.80
98	1.932	9.931	2.088	8.954	1.963	9.783	9.188	2.00	107.880	12.00
100	1.945	11.066	2.103	10.162	1.936	11.290	10.146	2.00	100.163	13.62
102	2.172	7.656	2.433	6.166	2.309	6.366	4.5/10.7	2.5/2	98.582	15.18
104	1.946	13.427	2.057	13.551	1.787	17.057	11.946	2.00	84.332	20.40
106	2.157	6.966	2.281	6.620	2.238	6.121	3.9/9.1	2.5/2	82.559	21.60
108	2.017	11.939	2.239	10.280	2.064	11.334	12.621	2.00	68.106	23.80

LLDPE G

[1]	[2]	[3]	[4]	[5]	[6]	[7]	[8]	[9]	[10]	
91	2.463	1.517	2.641	1.262	2.395	1.787	1.3/4.4	2.5/2	118.660	12.60
93	2.143	4.645	2.252	4.305	2.187	4.230	6.426	2.0	115.080	13.55
95	2.390	2.951	2.548	2.576	2.649	1.825	2.4/6.5	2.5/2	109.953	15.09
97	2.342	3.335	2.470	3.048	2.507	2.456	2.4/6.5	2.5/2	107.246	16.22
99	2.215	3.882	2.296	3.715	2.369	2.851	2.2/5.8	2.5/2	89.930	18.44
101	2.117	3.656	2.155	3.639	2.174	3.184	4.472	2.0	81.593	20.58
103	1.939	7.499	2.109	6.516	1.947	7.517	6.787	2.0	68.426	27.78

LLDPE I

[1]	[2]	[3]	[4]	[5]	[6]	[7]	[8]	[9]	[10]	
70	2.392	2.500	2.576	2.118	2.656	1.578	2.14/5.6	2.5/2	100.800	24.000
72	2.467	1.945	2.700	1.560	2.778	1.072	0.68/4.92	3.0/2	97.023	27.181
74	2.498	1.950	2.868	1.282	2.748	1.218	7.3/5.2	3.0/2	94.687	28.313
76	2.443	2.410	2.911	1.406	2.726	1.323	2.07/5.4	2.5/2	92.348	29.585
78	2.581	2.004	2.994	1.271	2.774	1.400	0.89/6.3	3.0/2	79.320	30.768
80	2.237	3.192	2.750	1.706	2.557	1.557	1.7/5.5	2.5/2	78.181	31.988
82	2.071	5.272	2.511	3.184	2.143	4.607	6.348	2.000	64.809	39.180

LLDFE J

[1]	[2]	[3]	[4]	[5]	[6]	[7]	[8]	[9]	[10]	
78	1.780	10.399	1.984	8.750	1.716	12.049	8.104/6.968	1.52	125.221	10.81
80	1.942	7.430	2.167	6.063	1.870	8.799	6.847	2.00	117.333	13.98
82	1.862	9.594	2.183	6.918	1.805	10.974	7.546	2.00	113.465	16.38
84	1.701	16.982	2.133	10.889	1.628	19.649	24.964	2.00	108.844	17.22
86	2.074	6.622	2.516	4.083	1.984	7.833	7.594	2.00	109.050	18.62
88	2.061	10.423	2.384	7.943	2.080	10.245	11.327	2.00	110.694	22.80
90	2.160	6.761	2.561	4.539	2.280	5.836	3.66/9.6	2.52	109.032	24.02

LLDFE L

[1]	[2]	[3]	[4]	[5]	[6]	[7]	[8]	[9]	[10]	
94	2.137	7.834	2.416	3.304	2.159	4.358	5.934	2.00	114.514	10.80
96	1.854	7.386	2.154	10.139	1.771	15.854	10.211	2.00	103.594	13.20
98	1.879	13.323	2.011	19.230	1.762	23.020	16.822	2.00	102.284	14.40
100	2.137	7.295	2.173	7.447	2.225	6.886	10.010	2.00	103.483	16.02
102	2.208	6.194	2.402	6.501	2.332	6.212	4.6/10.8	2.52	87.470	19.20
104	1.961	12.022	2.180	10.303	1.797	15.201	11.625	2.00	86.199	21.90
106	1.896	11.587	2.084	10.568	1.906	12.000	10.055	2.00	72.990	26.82
108	1.817	9.571	1.912	9.141	1.799	10.000	7.166	2.00	71.999	29.20

LDPE F

[1]	[2]	[3]	[4]	[5]	[6]	[7]	[8]	[9]	[10]	
80	1.979	8.933	2.056	8.810	2.020	8.633	8.926	2.0	102.483	21.18
82	1.854	14.233	2.064	12.331	1.740	17.466	10.667	2.0	110.006	22.38
84	1.970	9.862	2.254	7.674	2.110	8.336	10.026	2.0	106.680	23.62
86	1.957	15.170	2.246	12.302	1.993	14.829	14.668	2.0	96.553	24.60
88	2.073	11.271	2.354	9.099	2.113	10.644	12.866	2.0	92.600	25.98
90	2.114	8.851	2.132	7.379	2.188	7.969	10.927	2.0	77.720	26.15

LDPE K

[1]	[2]	[3]	[4]	[5]	[6]	[7]	[8]	[9]	[10]	
80	1.681	14.028	1.916	11.534	1.636	16.000	207.812	1.52	117.901	16.52
82	2.230	3.296	2.452	2.636	2.163	3.993	5.479	2.00	121.176	17.99
84	1.915	8.017	2.324	5.117	1.898	8.612	6.863	2.00	107.931	18.42
86	1.864	12.473	2.248	8.610	1.945	11.250	10.020	2.00	106.562	19.62
88	1.383	43.752	1.603	39.627	1.566	32.812	36.03/13.9	1.52	102.930	22.02
90	2.106	6.486	2.396	4.956	2.161	6.100	8.315	2.00	100.071	24.78
92	2.274	6.081	2.499	5.105	2.460	4.668	4.3/10.1	2.52	63.524	27.00
94	1.915	11.886	2.190	9.419	1.909	12.924	10.010	2.00	72.396	28.02

PP-1

[1]	[2]	[3]	[4]	[5]	[6]	[7]	[8]	[9]	[10]	
92	2.040	3.508	2.084	3.459	2.067	3.249	3.846	2.00	130.548	5.22
94	2.108	4.487	2.219	4.140	2.119	4.396	5.752	2.00	130.231	6.42
96	2.047	5.035	2.042	5.358	2.156	3.843	5.475	2.00	129.845	7.62
98	2.062	4.550	2.025	5.012	2.221	3.109	5.137	2.00	126.375	10.80
100	1.972	8.570	2.131	7.656	1.959	8.731	8.085	2.00	103.990	14.98
102	1.928	10.000	2.107	8.974	1.931	10.000	8.861	2.00	96.792	17.22
104	1.960	7.568	2.081	6.982	1.955	7.528	6.905	2.00	84.381	20.40

PP-2

[1]	[2]	[3]	[4]	[5]	[6]	[7]	[8]	[9]	[10]	
106	1.887	11.091	2.197	8.356	1.630	1.879	9.230	2.00	123.540	5.58
108	1.843	14.190	2.291	8.670	1.929	11.555	10.092	2.00	108.900	6.78
110	1.884	10.739	2.343	6.577	1.875	10.717	8.437	2.00	114.750	7.89
112	2.055	21.232	2.162	22.387	2.096	20.487	23.284	2.00	69.476	9.52
114	2.164	7.798	2.529	5.585	2.027	9.316	9.757	2.00	119.873	10.38
116	2.167	9.705	2.496	7.430	2.257	8.439	5.580	2.00	101.619	12.54
118	1.938	16.218	2.320	4.786	1.991	16.254	16.017	2.00	94.906	15.31
120	1.985	9.727	2.189	8.356	2.001	9.592	9.604	2.00	92.986	16.02

HDPE-2908

[1]	[2]	[3]	[4]	[5]	[6]	[7]	[8]	[9]	[10]	
115.5	2.041	4.571	2.337	3.304	1.998	5.166	5.138	2.00	191.137	17.28
117.5	1.966	2.113	2.186	1.581	1.832	2.986	1.871	2.00	189.337	20.52
119.5	1.974	0.804	2.125	0.644	1.966	0.825	0.741	2.00	186.946	23.70
121.5	1.756	0.258	1.780	0.252	1.783	0.230	0.108	2.00	184.515	30.90

Note: Iso T - Experimental Isothermal Temperature (C degree)

LR - Linear Regression

NLR - Non-Linear Regression

Q Cryst - Total Heat of Crystallization (J/g)

Ind Time - Induction Time (sec)

Avrami's Isokinetic Model - $X(t) = 1 - \exp(-k \cdot t^n)$

Tobin's Isokinetic Model - $X(t) / 1 - X(t) = k \cdot t^n$

NLR - r2 - Parameter Values for Selected Isothermal Temperatures							
Iso Temp	NLR	Iso Temp	NLR	Iso Temp	NLR	Iso Temp	NLR
Resin B	r2	Resin H	r2	Resin A	r2	Resin C	r2
88.5	0.984	90	0.998	99.5	0.998	94	0.995
90.5	0.996	92	0.994	101.5	0.994	96	0.999
92.5	0.979	94	0.999	103.5	0.974	98	0.999
94.5	0.984	96	0.993	105.5	0.991	100	0.999
96.5	0.999	98	0.998	107.5	0.986	102	0.998
98.5	0.993	100	0.994	109.5	0.995	104	0.998
100.5	0.991	102	0.999	111.5	0.995	106	0.994
102.5	0.996	104	0.999			108	0.985
Iso Temp	NLR	Iso Temp	NLR	Iso Temp	NLR	Iso Temp	NLR
Resin D	r2	Resin E	r2	Resin M	r2	HDPE	r2
88	0.999	88	0.991	96	0.999	115.5	0.998
90	0.987	90	0.993	98	0.999	117.5	0.99
92	0.991	92	0.999	100	0.999	119.5	0.989
94	0.999	94	0.999	102	0.994	121.5	0.999
96	0.99	96	0.994	104	0.994		
98	0.995	98	0.993	106	0.996		
100	0.999	100	0.998	108	0.999		
102	0.998						
Iso Temp	NLR	Iso Temp	NLR	Iso Temp	NLR	Iso Temp	NLR
Resin G	r2	Resin I	r2	Resin J	r2	Resin L	r2
91	0.985	70	0.976	78	0.992	94	0.998
93	0.996	72	0.968	80	0.997	96	0.995
95	0.976	74	0.97	82	0.996	98	0.992
97	0.984	76	0.971	84	0.997	100	0.996
99	0.991	78	0.968	86	0.999	102	0.993
101	0.997	80	0.975	88	0.999	104	0.995
103	0.999	82	0.998	90	0.995	106	0.999
						108	0.996
Iso Temp	NLR	Iso Temp	NLR	Iso Temp	NLR	Iso Temp	NLR
Resin F	r2	Resin K	r2	PP-1	r2	PP-2	r2
80	0.999	80	0.987	92	0.999	106	0.998
82	0.993	82	0.995	94	0.998	108	0.992
84	0.999	84	0.998	96	0.997	110	0.998
86	0.999	86	0.998	98	0.994	112	0.999
88	0.999	88	0.978	100	0.999	114	0.999
90	0.997	90	0.997	102	0.999	116	0.997
		92	0.988	104	0.999	118	0.999
		94	0.999			120	0.999

APPENDIX 7

NON-ISOTHERMAL SIMULATION.

KINETIC DATA

Kinetic Data / Non-isothermal Simulation/Ziabicki Equation

Resin	T _{exp} , [C]	K _{exp}		T, [C]	K _{max}	D	T _{max}	
								(experimental)
B - ZN	96.5	0.017228		B	94-100	2.3	19.7	97.57
H - ZN	92	0.009962		H	90-96	2.08	18.18	94.79
A - ZN	101.5	0.014111		A	103-109	1.99	30.34	104.25
C - ZN	98	0.016949		C	98-105	2.19	32.6	101.25
M - ZN	102	0.010723		D	90-102	1.8	32.93	99.14
D - Met	94	0.009561		E	90-102	1.5	36.38	95.2
E - Met	94	0.01567		M	100-108	2.2	33.74	106.29
G - ZN	97	0.006588		G	93-99	0.94	44.29	97.4
L - ZN	98	0.016822		I	74-80	1.25	41.57	76.43
I - Met	76	0.005479		J	82-90	2.49	35.07	82.1
J - Met	88	0.011327		L	96-104	1.8	38.9	100.37
F	88	0.012856		F	82-90	1.46	28.8	86.82
K	88	0.013997		K	84-94	1.01	28.2	89.97
				PP-1	94-104	2.02	32.41	102.9
				PP-2	110-115	2.32	22.27	113.91
				HDPE	100-125	2.95	16.47	107.33

K_{exp} - value at the experimental temperature (T_{exp}) when the maximum rate was recorded

K_{max}, D, T_{max} - predicted Ziabicki parameters

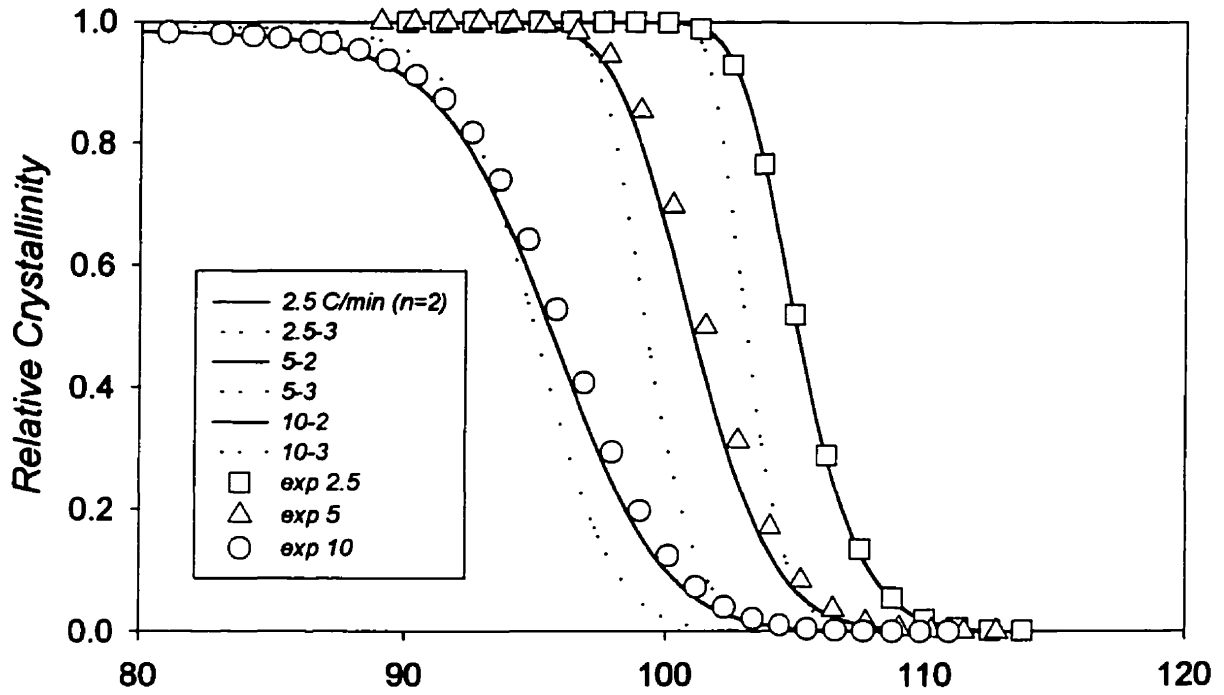
T [C] - temperature range of validity

APPENDIX 8

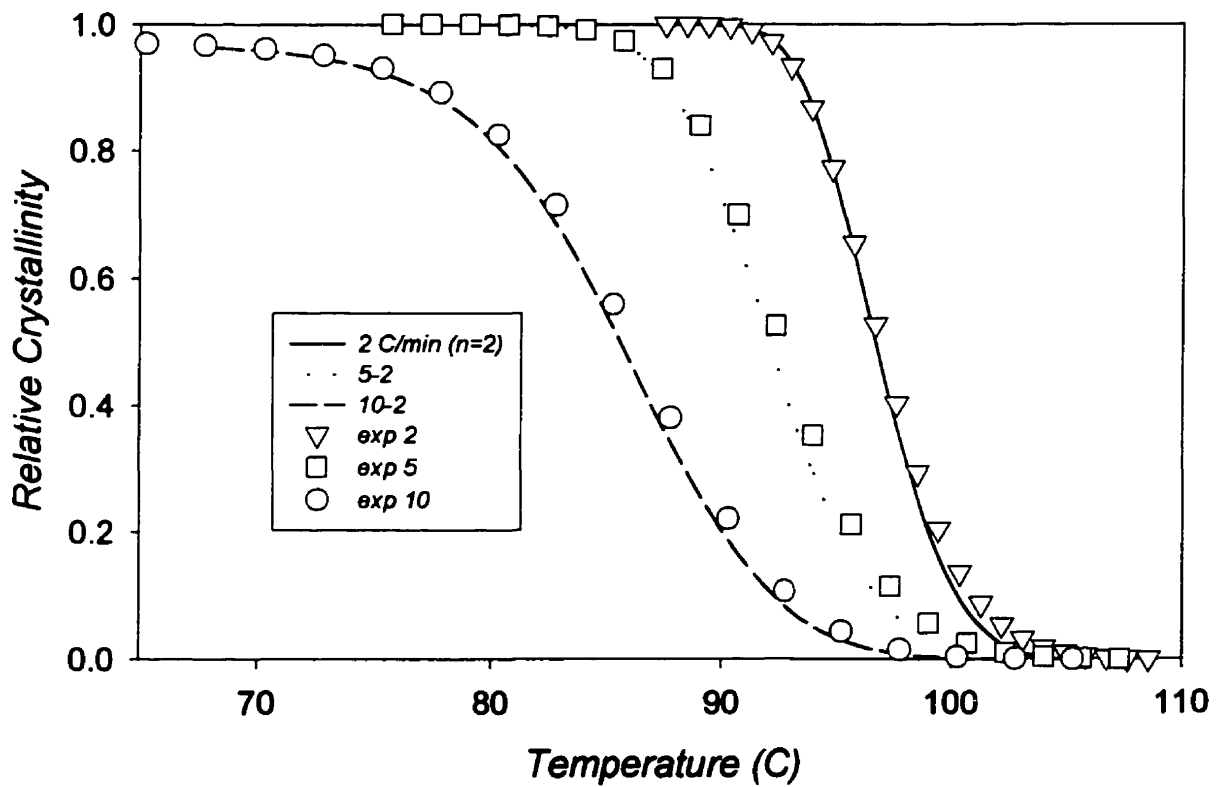
**PLOTS OF RELATIVE CRYSTALLINITY AS A
FUNCTION OF TEMPERATURE.**

**NON-ISOTHERMAL SIMULATION FOR
SELECTED RESINS.**

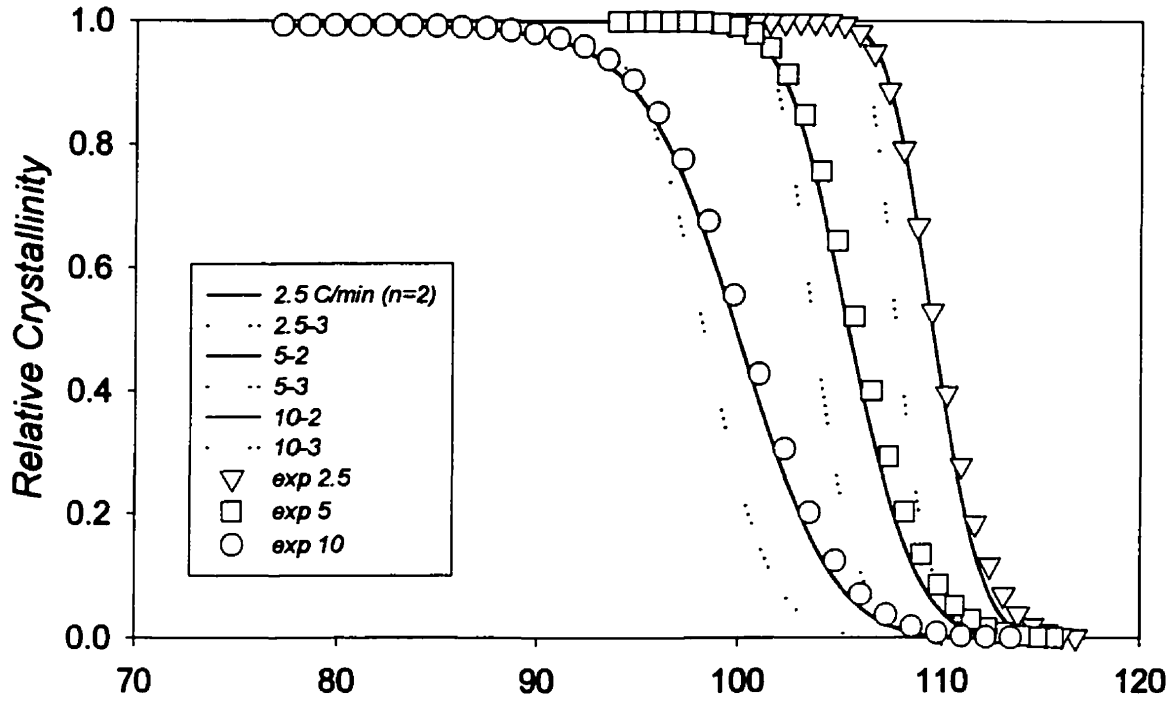
B - BUT/ZN/Gas $K_{max}=2.3e-2/T_{max}=97.57/D=19.7$



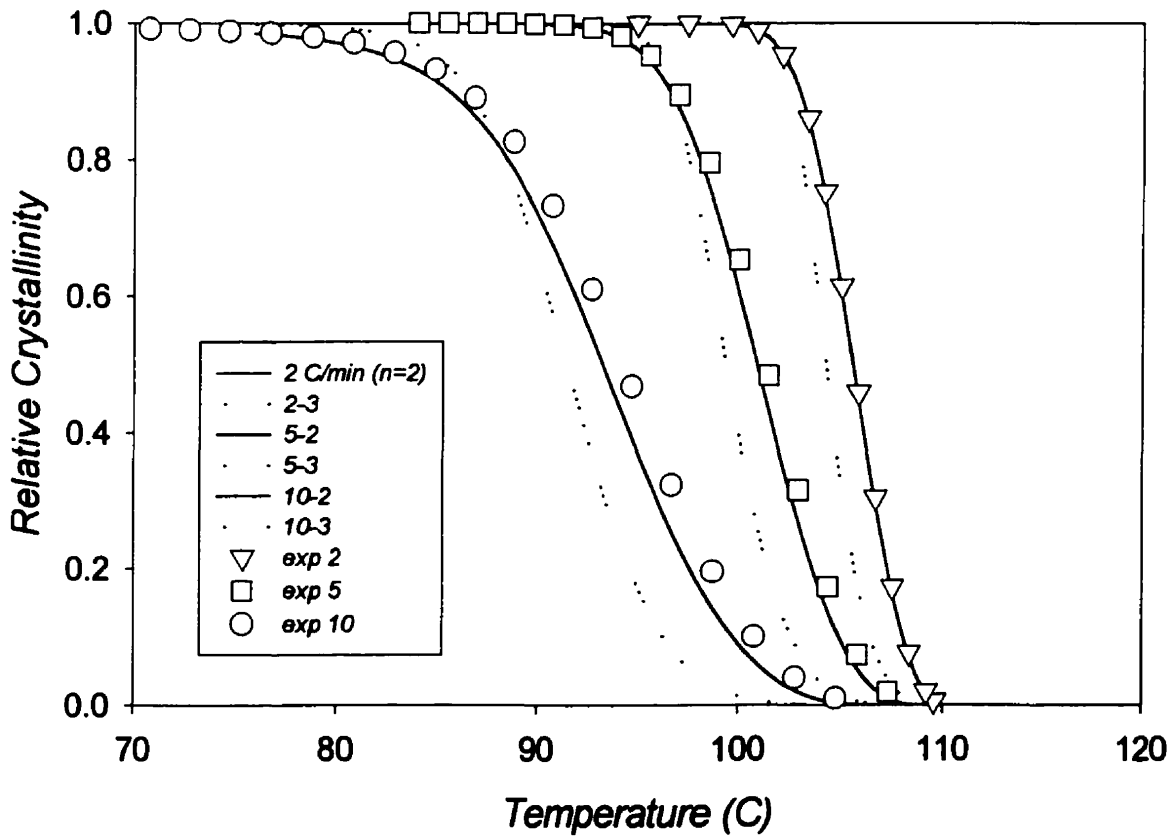
F - LDPE $K_{max}=1.46e-2/T_{max}=86.8/D=28.8$



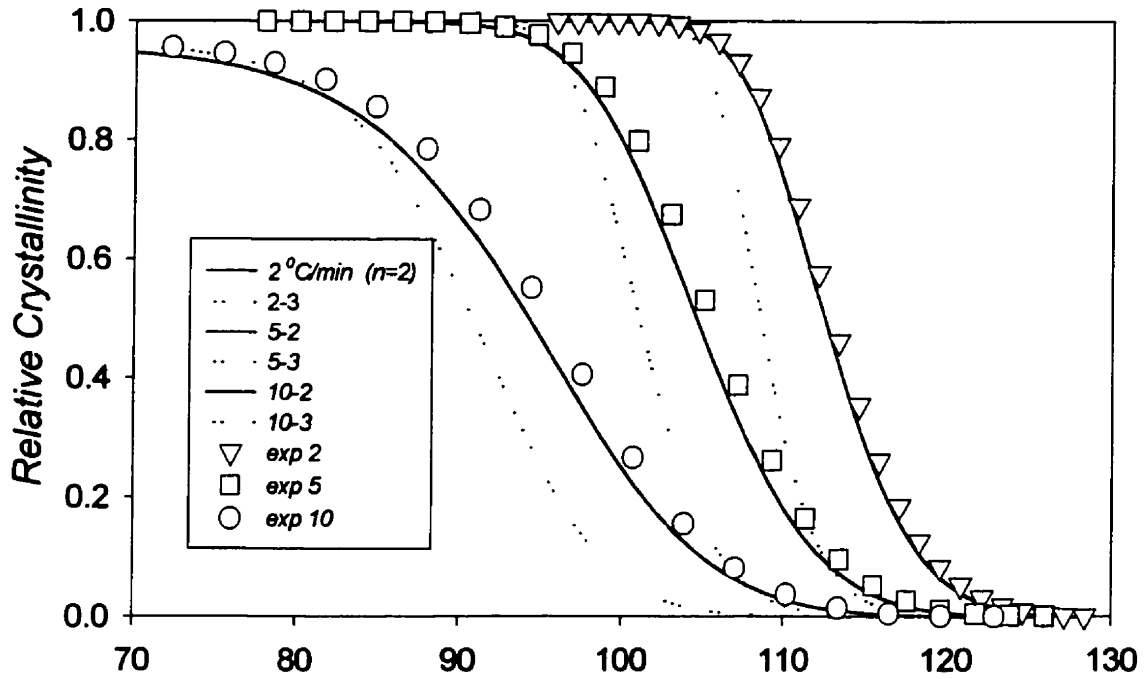
C - HEX/ZN/Gas $K_{max}=2.19e-2/T_{max}=101.2/D=22.9$



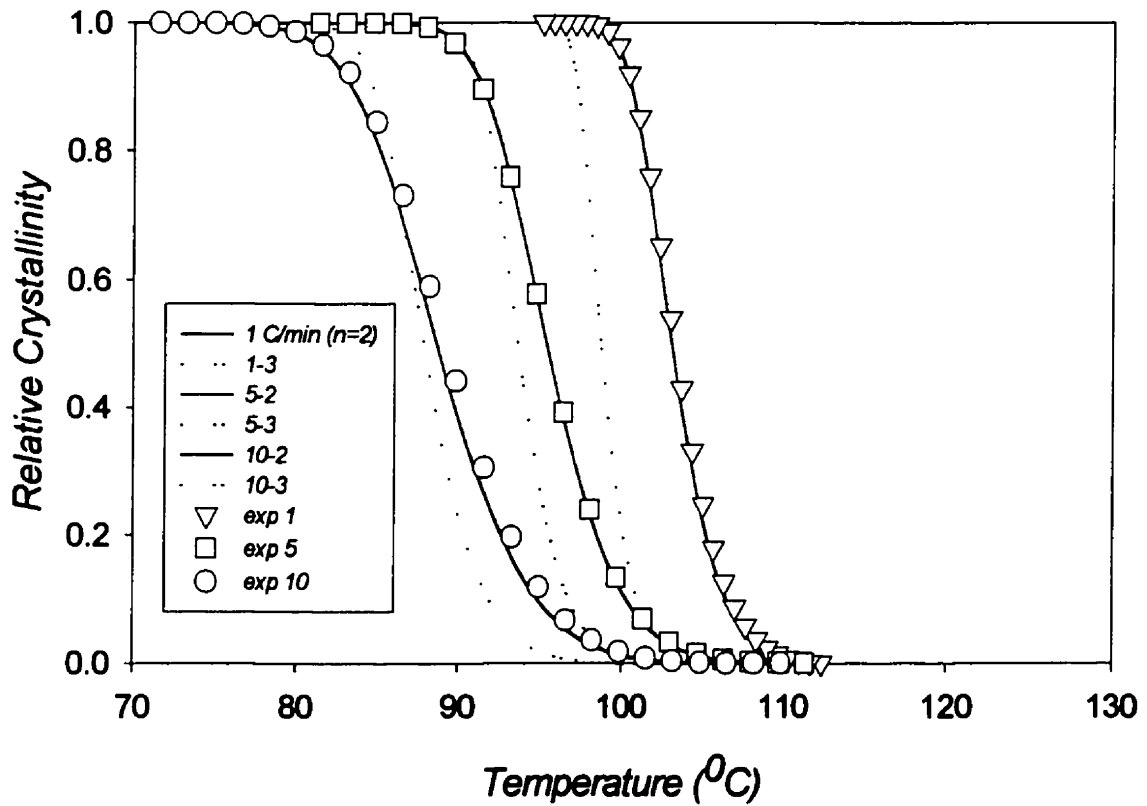
E - HEX/Met/Gas $K_{max}=1.5e-2/T_{max}=95.2/D=36.38$



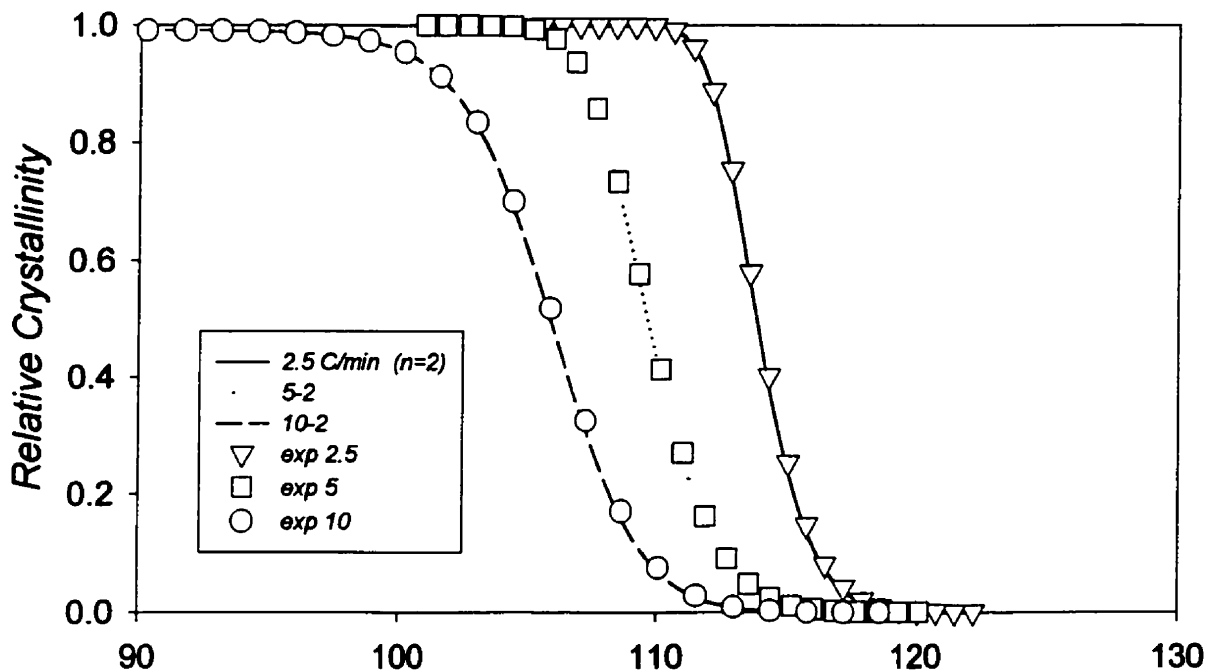
G - OCT/ZN/Sol $K_{max}=0.94e-2/T_{max}=97.4/D=44.29$



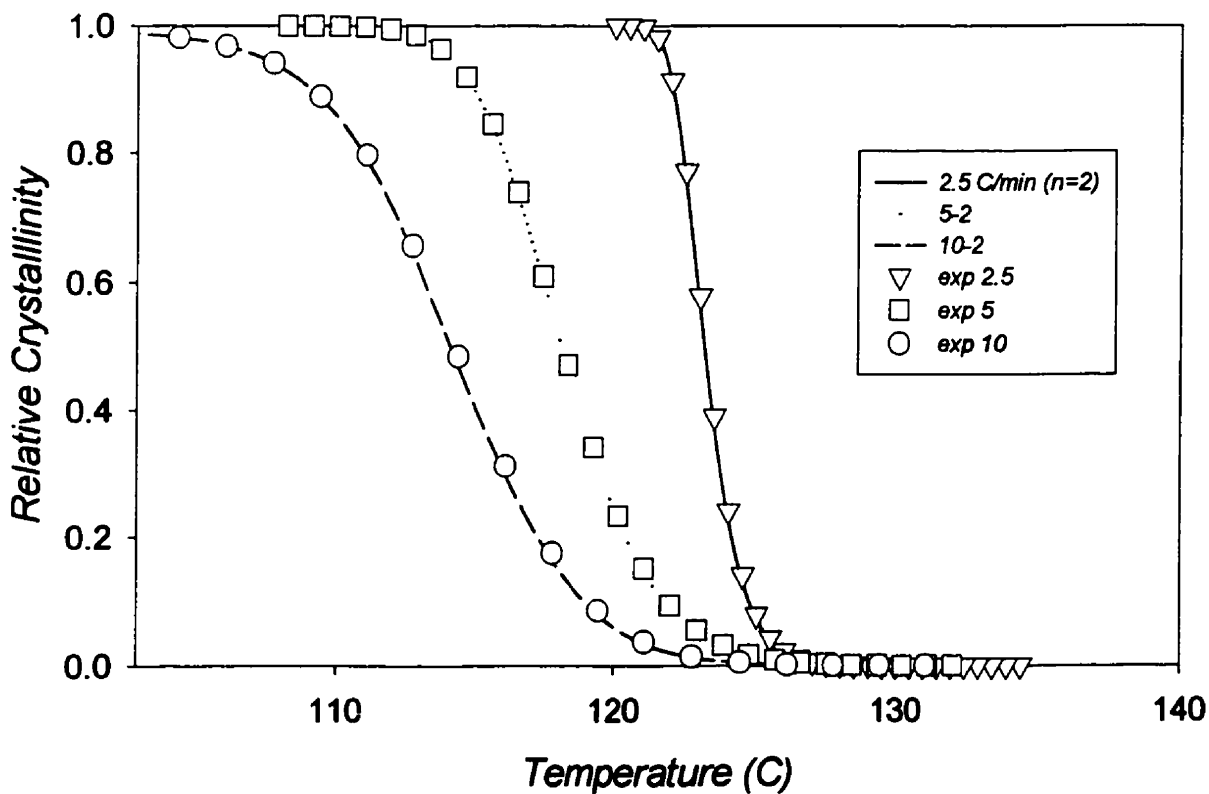
J - OCT/Met/Sol $K_{max}=2.49e-2/T_{max}=82.1/D=35.07$



HDPE 2908 Sclair $K_{max}=2.95e-2/T_{max}=107.3/D=16.47$

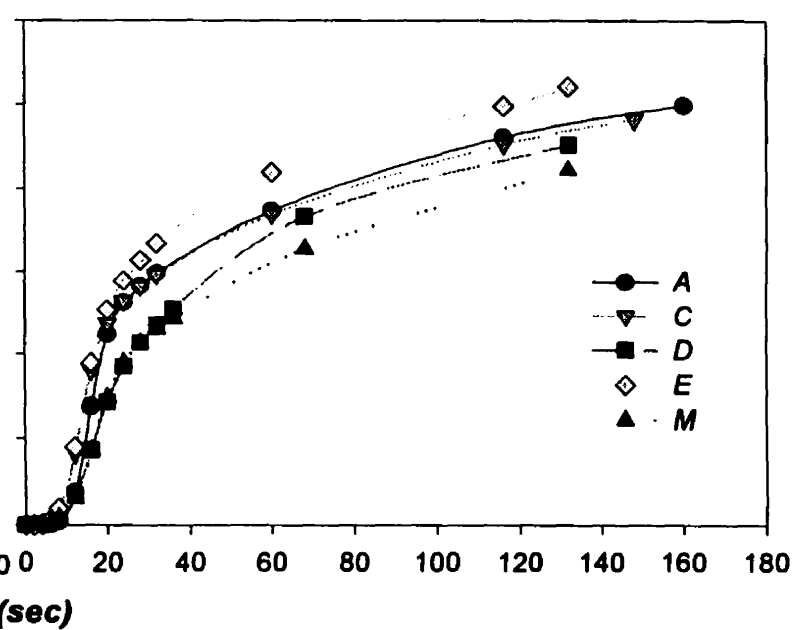
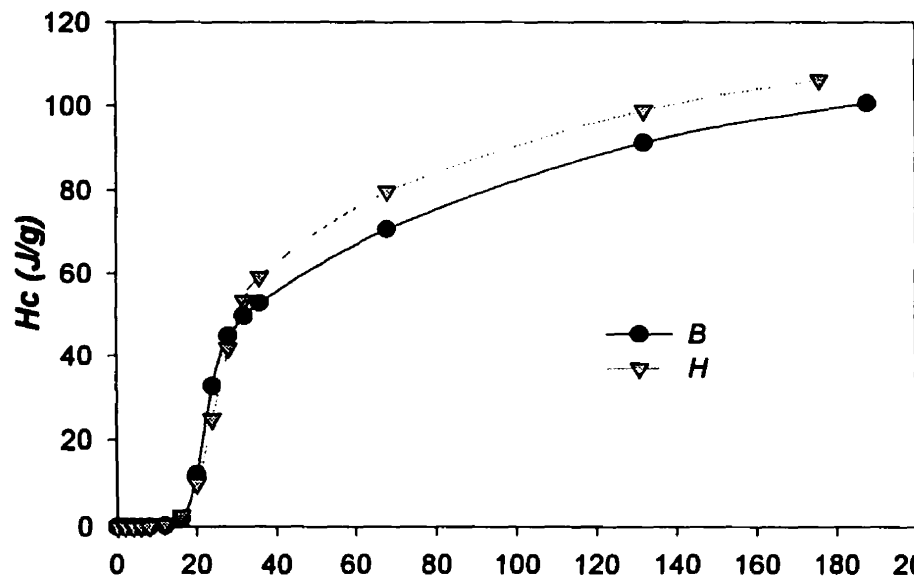
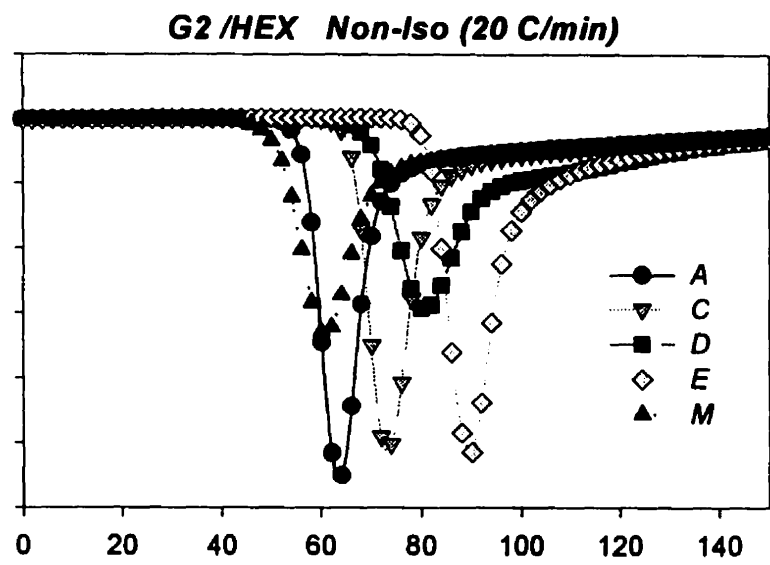
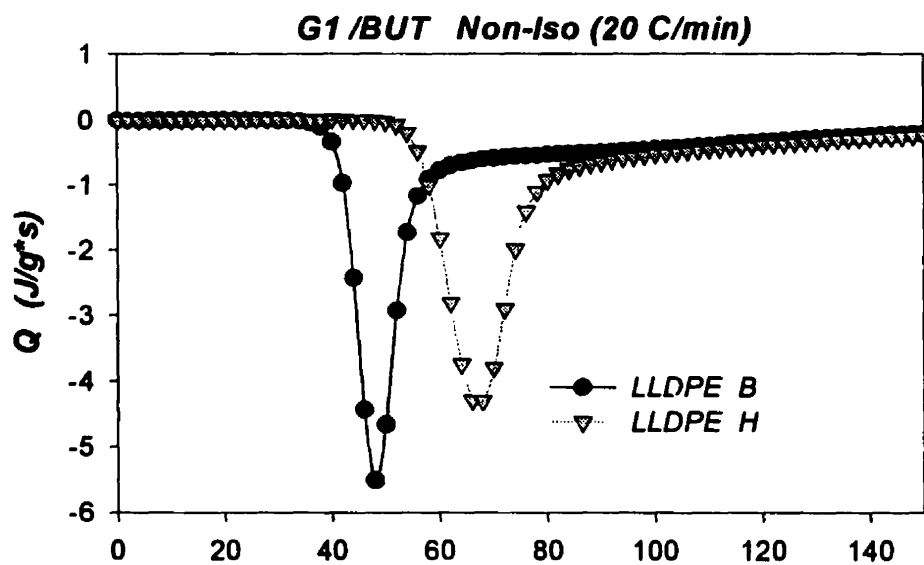


PP - 2 Montell $K_{max}=2.32e-2/T_{max}=113.9/D=22.27$



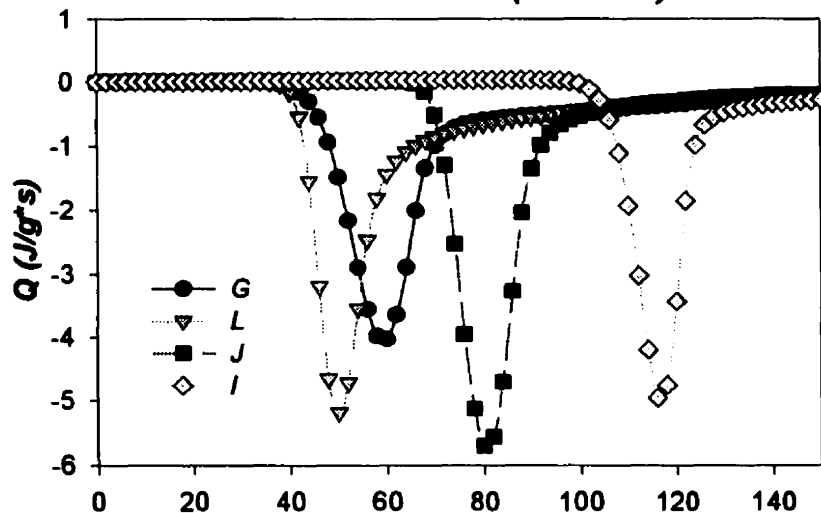
APPENDIX 9

PLOTS OF NORMALIZED HEAT FLOW (Q^*) AND HEAT OF CRYSTALLIZATION (H_C) vs. TIME (INTRA-GROUP STUDY)

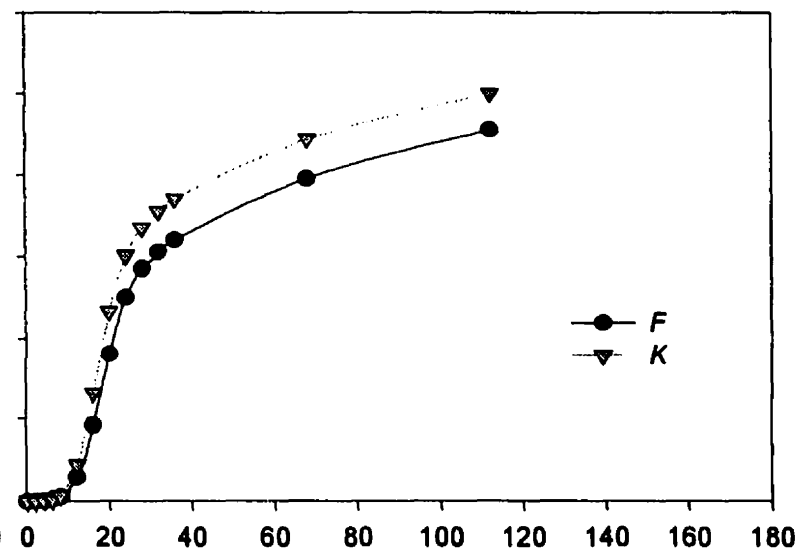
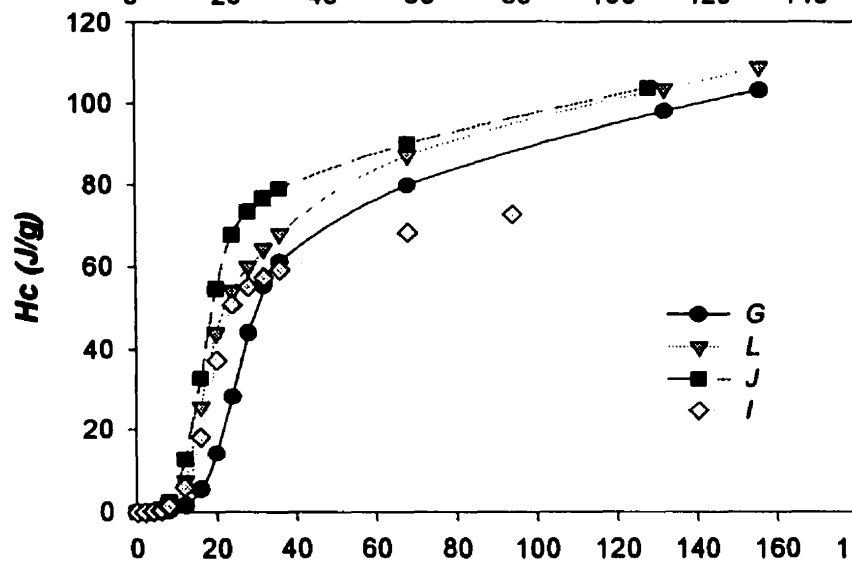
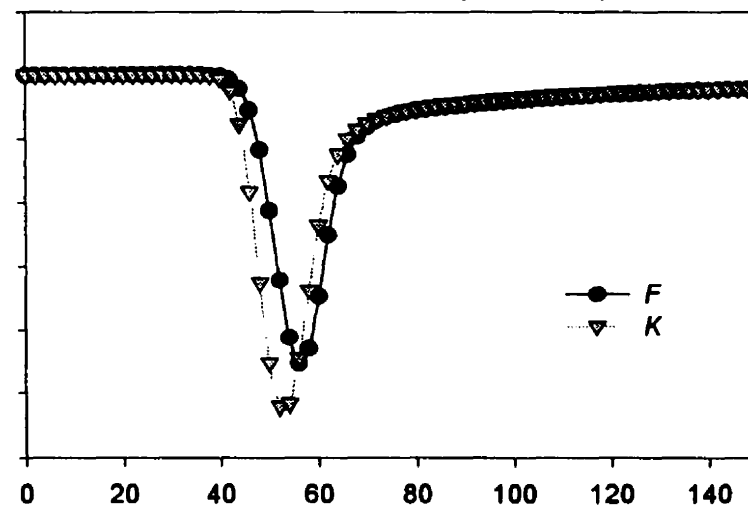


time (sec)

G3 /OCT Non-Iso (20 C/min)



G4 /LDPE Non-Iso (20 C/min)



time (sec)

APPENDIX 10

PLOTS OF $\log\{-\ln(1-X)\}$ vs. $\log t$ FOR SELECTED RESINS E, G, H, F (FIRST AND SECOND RUN AT THE SAME ISOTHERMAL TEMPERATURE)

